Light Matter Interaction in Nanostructured Materials

Christian Kremers

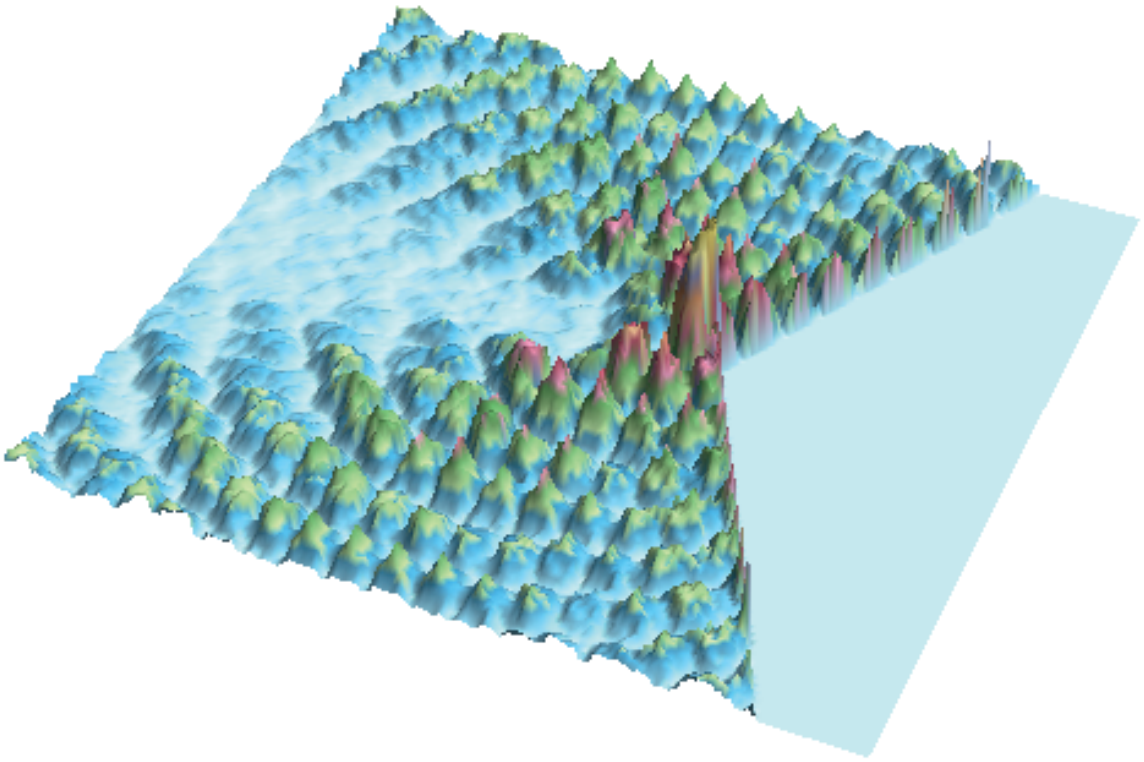

Light Matter Interaction in Nanostructured Materials

Vom Fachbereich Elektrotechnik,
Informationstechnik, Medientechnik der
Bergischen Universität Wuppertal
genehmigte Dissertation zur Erlangung
des akademischen Grades
Doktor der Ingenieurwissenschaften

vorgelegt von
Christian Kremers
Diplom Physiker

Wuppertal 2011

Referent:	Prof. Dr. rer. nat. U. Pfeiffer
Korreferent:	Prof. Dr. rer. nat. M. Clemens

Tag der mündlichen Prüfung: 08.07.2011

Abstract

In this thesis two aspects of electromagnetic wave interaction with nano structured material are studied.

First, two alternative semi-analytical methods to solve the scattering problem on optical nanowire antenna are introduced. In order to reduce the general three dimensional volume integral equation describing the scattering problem to a simple semi-analytical one dimensional integro-differential equation, both methods utilize solutions of the problem of plane wave scattering on infinite cylinder. A regularization and discretization scheme is proposed in order to transform the integro-differential equations into solely integral equation. This transformation enables to solve the original problem without the necessity to impose additional boundary conditions at the nanowire edges. Numerical evaluation of the proposed methods and their comparison with different numerically rigorous methods is presented for scattering cross-section calculations. Gold nanowires are analyzed at optical and near-infrared spectral range. The introduced one-dimensional semi-analytical methods demonstrate good agreement and superior numerical performance in comparison with rigorous numerical methods.

Second, the radiation of a uniformly moving charge (Cherenkov radiation) inside a general three dimensional (3D) and two dimensional (2D) periodic dielectric medium is studied. In particular analytical expressions for the emission spectrum and for the field distribution in the far-field zone are derived. The obtained formula for the Cherenkov power emitted per unit length (emission spectrum) of the charge trajectory involves the calculations of Bloch modes and corresponding group velocities at limited points of the reciprocal space only. The analysis reveals (i) that the Cherenkov effect exists for every charge velocity (ii) that the radiation can be suppressed if the coupling of the current density produced by a moving charge with a Bloch mode is poor and (iii) that an enhancement of radiated energy is possible if only the component of the group velocity orthogonal to the trajectory of the charge is small. Additional inside in the Cherenkov radiation process is gained from the analytical expression for the field distribution in the far-field zone. It is shown that the far-field radiation can be calculated in a 3D photonic crystal by a surface integral and in a 2D one by a contour integral over just a small

fraction of the first Brillouin zone. The spatial variation in the far-field intensity is due to (i) interference of just a few Bloch eigenmodes and (ii) the topological properties of the k-space surface (3D) or contour (2D). The obtained expressions both for the emission spectrum and the field distribution are confirmed by comparison with rigorous numerical calculations. The agreement in both cases is very good where the analytical expressions are faster and much less demanding on computational resources.

Acknowledgments

First of all I would like to thank Prof. Ullrich Pfeiffer for giving me the opportunity to continue my research on nano photonics in his laboratory at the University of Wuppertal and for being my supervisor over these years. I also thank him for his encouragement.

I am particular grateful to Dr. Dmitry N. Chigrin for being my supervisor, teacher, colleague and friend since I wrote my Diploma thesis at the University of Bonn and further at the University of Wuppertal. I also thank Dmitry for many stimulating and encouraging discussions and his continuos interest in my work.

I would like to thank all my colleagues working in the High-Frequency and Communication Technology institut at the University of Wuppertal for their help and patience. I am particular grateful to Dr. Sergei Zhukovsky and Evaristus Fuhchuo for many fruitful discussions.

And last but not least, this thesis would not be possible without strong support from Alexandra Leo. Thank you very much for your support and love.

The work presented in this thesis was partially supported by the DFG-Forschergruppe 557 „Light Confinement and Control with Structured Dielectrics and Metals“.

Contents

Introduction

A light wave causes charges (electrons and nuclei), the constituents of matter, to oscillate. These charges emit secondary light waves which interfere with each other and with the original one. By appropriate spatial averaging over the fields at atomic level the collective response of all constituents can be derived at a macroscopic lengthscale. The macroscopic response depends strongly on the type of material. However, to engineer materials with properties not found in nature, one can build artificial structures out of building blocks ("meta-atoms") with feature sizes smaller than the wavelength of light. These artificial structures are called metamaterials. In this case a spatial averaging over the fields at "meta-atom" level can still be performed yielding also a macroscopic response. The ability to design the "meta-atoms" in a largely arbitrary fashion adds a new degree of freedom in engineering material. The potential of this approach shows promise for a wide range of unusual physical phenomena rare or absent in nature. Examples include negative refraction [1, 2], cloaking [3, 4, 5] and planar chiral metamaterials [6].

The fabrication of metamaterials is in themselves a challenging topic because of the small feature sizes especially in the optical spectral range (about 10 to 100nm). In the same time the analysis of artificial materials is a complex theoretical and computational problem. The theoretical research in the field of metamaterials can be roughly divided into two branches. On one hand there is the active research field concerning with the derivation of macroscopic material parameters (in particular susceptibility and permeability tensors) out of the electromagnetic properties of the single "meta-atom" [7, 8] and on the other hand a lot of efforts are invested in the study of light interaction with single nano particles. Here, especially metallic (plasmonic) nano particles attract attention [9] because they can exhibit strong resonances in the visible spectrum possessing though feature sizes much smaller than the wavelength.

Because of their close relationship to antennas in microwave and RF regime plasmonic particles are often called 'optical antennas' [10]. As their counterparts in the microwave and RF spectral regime, they are used as a bridge between propagating radiation and localized fields. In the microwave and RF spectral regime semi-analytical models exist [11], offering insight into interaction processes and guiding engineers in antenna design.

In the same time, for practical antenna design and optimization well established numerical tools are typically used [12]. At optical frequencies however metal can no longer be treated as perfect electric conductor. Because of this fundamental difference the semi-analytical models used in microwave regime can not be used in the visible and near infrared spectral regime and in the same time the demands in computational resources increase tremendously. Irrespectively of these difficulties recent progresses in nanotechnology have enabled the fabrication of optical antennas (nano-antennas) [10, 13] and opened already many exciting possibilities towards nano-antenna applications. For example, it has been recently demonstrated that nano-antennas can enhance [14] and direct the emission of single molecules [15] and that they can play a key role in sensing application [16]. Great potential in improving the efficiency of solar-cells should also be mentioned [17].

Another class of artificial material which bears great potential in controlling the propagation of light are photonic crystals. As many metamaterials they are periodic structures but with the difference that the lattice period as well as the feature sizes of the constituents are comparable to the wavelength. In this case an averaging approach to derive macroscopic material parameters is no longer possible. One of the most interesting peculiarity achievable with photonic crystals is a photonic bandgap, a frequency range where light propagation is forbidden. Back in 1972 Bykov pointed out [18] the possibility to realize a complete photonic band gap in a periodic medium but his work does not attract great interest. The idea of control light by means of a periodic medium became popular after 1987. In this year Yablonovich [19] proposed to use a three-dimensional periodic medium, which he called photonic crystal, to enhance the spontaneous emission of atoms. In the same year it was proposed by John [20] that a disordered periodic medium could be used to localize electromagnetic waves. Since then many interesting phenomena were predicted. Summaries of them can be found in [21, 22]. Popular application using predominantly the band gap of photonic crystals are for example photonic crystal fibers [23], omnidirectional reflectors [24, 25], and high-Q cavities in defects of the crystal [26]. Not only the band gap attract interest but also the effect of the nontrivial dispersion relation in non-forbidden frequency ranges on the emission and diffraction of light. The combination of anisotropy and spatial dispersion leads to many peculiar effects including superprism [27], and self-collimating phenomena [28] as well as self-guiding [29].

Organization

The focus of the work presented in this thesis, is the theoretical study of the peculiarities of electromagnetic wave propagation in nano structured materials. Two distinct goals should be achieved. One of them was to develop a semi-analytical approach to the problem of light interacting with plasmonic nano wire antennas in the optical spectral range. And the other was to derive simple analytical formulas for both the emission spectrum and the electric field distribution due to an uniformly moving charge inside a photonic crystal.

The dissertation is organized in three parts. The first part (chapters 1 to 4) provides an introduction to the basic theoretical concepts required for the subsequent parts. Part two and three contain the main results of this work. In particular, in part two (chapter 5) light scattering on plasmonic nano wires and in part three (chapters 6 to 8) Cherenkov radiation in photonic crystals is analyzed.

The fundamental basics of electromagnetism in macroscopic media are presented and discussed in chapter 1. In chapter 2, Maxwell's equations are formally solved by means of a Green's function approach. It is also discussed how one can deal in an appropriate manner with the arising singularities. In the subsequent chapter 3, the self-consistent volume integral equation which determines the electric field in scattering problems is derived and the scattering cross section is defined. Additionally the problem of plane wave scattering on infinitely long cylinders is formally solved. In chapter 4, electrodynamics in periodic dielectric media is discussed. The main result of this chapter is the general solution for the electric field inside two and three-dimensional photonic crystals due to currents both in time and frequency domain.

Chapter 5 presents the derivation of two alternative simple one dimensional integral equations for the case of nanowire antennas, starting from the original three dimensional volume integral equation presented in chapter 3 using the solution for plane wave scattering problems on infinite cylinders also presented in chapter 3. The resulting integral equations are solved by means of a method of moments approach and are compared with each other as well as with rigorous numerical tools with respect to computational demands and accuracy.

Chapter 6 presents the introduction to the subsequent two chapters dealing with Cherenkov radiation in photonic crystals. In chapter 7 an exact expression for the emission spectrum is derived starting from the general solution in frequency domain presented in chapter 4. The influence of topological properties of the dispersion relation on the emitted power is discussed. As example the emission spectra of moving electrons with

different velocities in a 2D photonic crystal are calculated and compared with rigorous numerical calculation. The starting point for chapter 8 is the general solution in time domain presented in chapter 4. An approximate electric field solution in time domain valid in the far field regime is derived by means of a stationary phase approximation. Main features of the field and their relation to topological properties of the band structure are discussed. The obtained results are confirmed by comparison with rigorous numerical calculations for a 2D photonic crystal case.

References

[1] T. Mackay and A. Lakhtakia. Negative refraction, negative phase velocity, and counterposition in bianisotropic materials and metamaterials. *Physical Review B*, 79(23), June 2009.

[2] M. McCall. A covariant theory of negative phase velocity propagation. *Metamaterials*, 2(2-3):92–100, September 2008.

[3] D. Schurig, J. J. Mock, B. J. Justice, S. A. Cummer, J. B. Pendry, A. F. Starr, and D. R. Smith. Metamaterial electromagnetic cloak at microwave frequencies. *Science (New York, N.Y.)*, 314(5801):977–80, November 2006.

[4] F. Bilotti, S. Tricarico, and L. Vegni. Plasmonic Metamaterial Cloaking at Optical Frequencies. *IEEE Transactions on Nanotechnology*, 9(1):55–61, January 2010.

[5] U. Leonhardt. To invisibility and beyond. *Nature*, 471(7338):292–3, March 2011.

[6] A. Potts, A. Papakostasa, D. M. Bagnalla, and N. I. Zheludev. Planar chiral metamaterials for optical applications. *Microelectronic Engineering*, 73-74(1):367–371, June 2004.

[7] D. R. Smith and J. B. B. Pendry. Homogenization of metamaterials by field averaging. *Journal of the Optical Society of America B*, 23(3):391, March 2006.

[8] D. Smith, S. Schultz, P. Markoš, and C. Soukoulis. Determination of effective permittivity and permeability of metamaterials from reflection and transmission coefficients. *Physical Review B*, 65(19), April 2002.

[9] F. J. Romero, I.and García De Abajo. Anisotropy and particle-size effects in nanostructured plasmonic metamaterials. *Optics Express*, 17(24):22012, November 2009.

[10] P. Bharadwaj, B. Deutsch, and L. Novotny. Optical Antennas. *Advances in Optics and Photonics*, 1(3):438, August 2009.

[11] C. A. Balanis. *Advanced engineering electromagnetics*. Wiley, 1989.

[12] J. Volakis. *Antenna Engineering Handbook, Fourth Edition*. McGraw-Hill Professional, 2007.

[13] P. Mühlschlegel, H. J. Eisler, O. J. F. Martin, B. Hecht, and D. W. Pohl. Resonant optical antennas. *Science (New York, N.Y.)*, 308(5728):1607–9, June 2005.

[14] L. Rogobete, F. Kaminski, M. Agio, and V. Sandoghdar. Design of plasmonic nanoantennae for enhancing spontaneous emission. *Optics Letters*, 32(12):1623, June 2007.

[15] T. H. Taminiau, F. D. Stefani, F. B. Segerink, and N. F. van Hulst. Optical antennas direct single-molecule emission. *Nature Photonics*, 2(4):234–237, March 2008.

[16] G. Raschke, S Kowarik, T. Franzl, C. Sönnichsen, T. A. Klar, J. Feldmann, A Nichtl, and K. Kürzinger. Biomolecular Recognition Based on Single Gold Nanoparticle Light Scattering, May 2003.

[17] H. A. Atwater and A. Polman. Plasmonics for improved photovoltaic devices. *Nature materials*, 9(3):205–13, March 2010.

[18] V. P. Bykov. Spontaneous emission in a periodic structure. *Sov. Phys. JETP*, 35:269, 1972.

[19] E. Yablonovitch. Inhibited Spontaneous Emission in Solid-State Physics and Electronics. *Physical Review Letters*, 58(20):2059–2062, May 1987.

[20] S. John. Strong localization of photons in certain disordered dielectric superlattices. *Physical Review Letters*, 58(23):2486–2489, June 1987.

[21] C. M. Soukoulis. *Photonic crystals and light localization in the 21st century*. Springer, 2001.

[22] K. Sakoda. *Optical properties of photonic crystals*. Springer, 2005.

[23] P. Russell. Photonic crystal fibers. *Science (New York, N.Y.)*, 299(5605):358–62, January 2003.

[24] D.N. Chigrin, A.V. Lavrinenko, D.A. Yarotsky, and S.V. Gaponenko. All-dielectric one-dimensional periodic structures for total omnidirectional reflection and partial spontaneous emission control. *Journal of Lightwave Technology*, 17(11):2018–2024, 1999.

[25] Y. Fink. A Dielectric Omnidirectional Reflector. *Science*, 282(5394):1679–1682, November 1998.

[26] Y. Akahane, T. Asano, B. S. Song, and S. Noda. High-Q photonic nanocavity in a two-dimensional photonic crystal. *Nature*, 425(6961):944–7, October 2003.

[27] H. Kosaka, T. Kawashima, A. Tomita, M. Notomi, T. Tamamura, T. Sato, and S. Kawakami. Superprism phenomena in photonic crystals. *Physical Review B*, 58(16):R10096–R10099, October 1998.

[28] H. Kosaka, T. Kawashima, A. Tomita, M. Notomi, T. Tamamura, T. Sato, and S. Kawakami. Self-collimating phenomena in photonic crystals. *Applied Physics Letters*, 74(9):1212, 1999.

[29] D. N. Chigrin, S. Enoch, C. Sotomayor Torres, and G. Tayeb. Self-guiding in two-dimensional photonic crystals. *Optics Express*, 11(10):1203, May 2003.

Part I

Theoretical Foundations

1 Macroscopic Electromagnetism

The goal of the present chapter is to introduce the fundamental sets of equations and physical ideas used in the subsequent chapters.

First, *Maxwell's equations in macroscopic media* both in time and frequency domain are reviewed and supplemented with *constitutive relations* relating the electromagnetic field to the response of the medium. In section (1.2.1) the electric response of macroscopic media is traced back to forced dipole oscillations of bounded electrons. Next, *Poynting's theorem* and its interpretation as continuity equation describing energy conservation is derived and briefly discussed. This chapter is finalized with the derivation of vector wave equation in frequency domain, the *vector Helmholtz equation*, and the physical *boundary conditions* the electromagnetic field at the interfaces between different media has to obey. For more details the reader is referred to textbooks covering classic electromagnetic theory [1, 2, 3].

1.1 Maxwell's Equations in Macroscopic Media

Since this thesis deals with macroscopic media, the electromagnetic fields of interest are spatial averages over the microscopic fields at atomic level associated with discrete charges. These averaged fields are considered as piecewise continuous functions of space and are governed by the *macroscopic Maxwell's equations*. In differential form and SI units they are given by [1]

$$\nabla \times \mathbf{E}(\mathbf{r},t) = -\frac{\partial \mathbf{B}(\mathbf{r},t)}{\partial t}, \tag{1.1}$$

$$\nabla \times \mathbf{H}(\mathbf{r},t) = \frac{\partial \mathbf{D}(\mathbf{r},t)}{\partial t} + \mathbf{j}(\mathbf{r},t), \tag{1.2}$$

$$\nabla \cdot \mathbf{D}(\mathbf{r},t) = \rho(\mathbf{r},t), \tag{1.3}$$

$$\nabla \cdot \mathbf{B}(\mathbf{r},t) = 0, \tag{1.4}$$

where $\mathbf{E}$ denotes the electric field, $\mathbf{D}$ the electric displacement, $\mathbf{H}$ the magnetic field and $\mathbf{B}$ the magnetic induction. The fields are generated by the current density $\mathbf{j}$ and charge

density ρ associated with free charges which are connected by the continuity equation

$$\nabla \cdot \mathbf{j} + \frac{\partial \rho}{\partial t} = 0 \tag{1.5}$$

implicitly included in Maxwell's equations. In order to reference these equations later on we name them according to their experimental heritage, Faraday's law (1.1), generalized Ampere's law (1.2), and Coulomb's law (1.3). The add on 'generalized' in Ampere's law is due to the first term on the right hand side of (1.2), namely the displacement current, which was introduced by Maxwell based on theoretical considerations. The last equation (1.4) merely states the experimental fact that there are no magnetic charges. Neglecting the magnetic response (magnetization) of the medium, the electric displacement $\mathbf{D}$ and the magnetic field $\mathbf{H}$ are given by [1]

$$\mathbf{D} = \epsilon_0 \mathbf{E} + \mathbf{P}, \tag{1.6}$$

$$\mathbf{H} = \frac{\mathbf{B}}{\mu_0}, \tag{1.7}$$

where $\mathbf{P}$ denotes the electric polarization (average electric dipole moment per unit volume), ϵ_0 the permittivity, and μ_0 the permeability of free space.

1.1.1 Time-Harmonic Fields

The time dependence of the electromagnetic field $(\mathbf{E}, \mathbf{H})$ governed by Maxwell's equations (1.1)-(1.4) can be separated from the space dependent part by imposing a sinusoidal time variation $e^{-i\omega t}$. The real monochromatic electric field can then be written as

$$\mathbf{E}(\mathbf{r}, t) = \Re\left\{\mathbf{E}(\mathbf{r}) e^{-i\omega t}\right\} = \frac{1}{2}\left(\mathbf{E}(\mathbf{r}) e^{-i\omega t} + \mathbf{E}^{\star}(\mathbf{r}) e^{i\omega t}\right), \tag{1.8}$$

where $\Re\{.\}$ denotes the real part of the quantity in brackets and $\mathbf{E}^{\star}$ the complex conjugate of $\mathbf{E}$. Similarly expressions (1.8) hold for all the other fields in Maxwell's equations. Substituting (1.6) and (1.7) for $\mathbf{D}$ and $\mathbf{B}$ in (1.1)-(1.4) one yields Maxwell's equations

in frequency domain governing the complex amplitudes

$$\nabla \times \mathbf{E}(\mathbf{r}) = i\omega\mu_0 \mathbf{H}(\mathbf{r}), \tag{1.9}$$

$$\nabla \times \mathbf{H}(\mathbf{r}) = -i\omega \left[\epsilon_0 \mathbf{E}(\mathbf{r}) + \mathbf{P}(\mathbf{r})\right] + \mathbf{j}(\mathbf{r}), \tag{1.10}$$

$$\nabla \cdot \mathbf{E}(\mathbf{r}) = \frac{\rho(\mathbf{r}) - \nabla \cdot \mathbf{P}(\mathbf{r})}{\epsilon_0}, \tag{1.11}$$

$$\nabla \cdot \mathbf{H}(\mathbf{r}) = 0. \tag{1.12}$$

Obviously, the complex field amplitudes depend on the angular frequency ω, i.e. $\mathbf{E}(\mathbf{r}) = \mathbf{E}(\mathbf{r}, \omega)$, however, this dependence is usually not explicitly written in this work. The transition from a time-domain differential equation governing $f(\mathbf{r}, t)$ to the corresponding one for the complex amplitudes $f(\mathbf{r}, \omega)$ can be performed by substituting $f(\mathbf{r}, t)$ with $f(\mathbf{r}, \omega)$ and $\partial_t f(\mathbf{r}, t)$ with $-i\omega f(\mathbf{r}, \omega)$.

1.1.2 Spectral Representation of Time-Dependent Fields

The spectrum $\hat{\mathbf{E}}(\mathbf{r}, \omega)$ of an arbitrary time-dependent field $\mathbf{E}(\mathbf{r}, t)$ is defined by the Fourier transform

$$\hat{\mathbf{E}}(\mathbf{r}, \omega) = \int_{-\infty}^{\infty} \mathbf{E}(\mathbf{r}, t) e^{i\omega t} dt. \tag{1.13}$$

Since $\mathbf{E}(\mathbf{r}, t)$ is a real valued field the spectrum fulfills

$$\hat{\mathbf{E}}^{\star}(\mathbf{r}, \omega) = \hat{\mathbf{E}}(\mathbf{r}, -\omega). \tag{1.14}$$

Substituting (1.6) and (1.7) for $\mathbf{D}$ and $\mathbf{B}$ and applying the Fourier transform (1.13) to Maxwell's equations in time domain (1.1)-(1.4) one yields Maxwell's equations for the spectral components. The resulting set of equations is of the form (1.9)-(1.12), with complex amplitudes replaced by the spectra. Once the solution for $\hat{\mathbf{E}}(\mathbf{r}, \omega)$ has been determined, the time-dependent field is calculated by inverse Fourier transform as

$$\mathbf{E}(\mathbf{r}, t) = \frac{1}{2\pi} \int_{-\infty}^{\infty} \hat{\mathbf{E}}(\mathbf{r}, \omega) e^{-i\omega t} d\omega. \tag{1.15}$$

1.2 Constitutive Relations

The macroscopic Maxwell equations (1.1)-(1.4) together with (1.6) and (1.7) are not sufficient by themselves. They must be supplemented with constitutive relations which relate the response of the medium, in our case described solely by the macroscopic polarization $\mathbf{P}$, to the electromagnetic field. For weak fields the polarization $\mathbf{P}$ depends

linearly on the electric field $\mathbf{E}$ [1]. The most general form of such a linear dependence can be written as

$$\mathbf{P}(\mathbf{r},t) = \int d^3r' \int_{-\infty}^{\infty} dt'\, \epsilon_0 \overleftrightarrow{\boldsymbol{\chi}}(\mathbf{r}-\mathbf{r}', t-t')\mathbf{E}(\mathbf{r}', t'), \tag{1.16}$$

where the response function $\overleftrightarrow{\boldsymbol{\chi}}$ denotes the electric susceptibility tensor. Tensor quantities in this thesis will be marked by a left-right arrow above a bold character. For an isotropic medium the susceptibility tensor $\overleftrightarrow{\boldsymbol{\chi}}$ reduces to the unit tensor times the scalar electric susceptibility χ. Assuming further a local response, that is the polarization at position $\mathbf{r}$ depends solely on the field at this position, equation (1.16) reduces to

$$\mathbf{P}(\mathbf{r},t) = \int_{-\infty}^{\infty} dt'\, \epsilon_0 \chi(\mathbf{r}, t-t')\mathbf{E}(\mathbf{r}, t') \tag{1.17}$$

which can be transformed into a relation in frequency domain

$$\mathbf{P}(\mathbf{r},\omega) = \epsilon_0 \chi(\mathbf{r},\omega)\mathbf{E}(\mathbf{r},\omega) \tag{1.18}$$

using the inverse Fourier transform (1.15). Due to the form of the constitutive equation (1.17), media with a frequency dependent susceptibility χ are called time dispersive.

Causality enforces that the susceptibility $\chi(\mathbf{r}, t-t')$ has to be zero for $t' > t$ because the electric field applied in the future can not influence the present polarization. If one views the integrand $\chi(\mathbf{r},\omega)e^{-i\omega t}$ with $t' = 0$ of the inverse Fourier transform (1.15) as an analytic function of ω defined on the complex plane, the Fourier integral can be calculated by means of the residue theorem [4]. For $t < 0$ the contour has to be (i) closed in the upper half space for which $\Im(\omega) > 0$ because otherwise the contour integral does not exist, and (ii) should not enclose any pole of the integrand for the integral to vanish as required by causality. Thus, necessary requirements for every reasonable physical model are (i) $\chi(\mathbf{r}, -\omega) = \chi^\star(\mathbf{r},\omega)$ so that $\chi(\mathbf{r}, t) \in \mathbb{R}$ and (ii) that $\chi(\mathbf{r},\omega)$ has poles only in the lower half space.

Substituting (1.18) in (1.6) we can define the relative dielectric permittivity $\epsilon_r(\mathbf{r},\omega)$ by

$$\begin{aligned}\mathbf{D}(\mathbf{r},\omega) &= \epsilon_0\epsilon_r(\mathbf{r},\omega)\mathbf{E}(\mathbf{r},\omega) \\ &= \epsilon_0\left[1+\chi(\mathbf{r},\omega)\right]\mathbf{E}(\mathbf{r},\omega).\end{aligned} \tag{1.19}$$

1.2.1 The Dipole Oscillator Model

By treating atoms or molecules, the constituents of a macroscopic media, as classical dipole oscillators forced by the electric field one can derive the frequency dependence of the relative dielectric constant $\epsilon_r(\omega)$ or equivalently the susceptibility $\chi(\omega)$ [5].

If one considers an electron bounded to the nucleus by attractive Coulomb force a light wave interacting with the system enforces oscillations of the electron around its equilibrium position. Damping also takes place due to energy loss by collision processes. Ignoring the motion of the much heavier nucleus the displacement $\mathbf{x}$ of the electron with mass m_e and charge e is governed by an equation of motion of the form

$$m_e \frac{d^2\mathbf{x}}{dt^2} + m_e\gamma\frac{d\mathbf{x}}{dt} + m_e\omega_0^2\mathbf{x} = -e\mathbf{E}, \tag{1.20}$$

with γ denoting the damping rate, ω_0 the resonance frequency and $\mathbf{E}$ the electric field of the light wave. Assuming a monochromatic light wave of angular frequency ω, that is $\mathbf{E} = \mathbf{E}_0 e^{-i\omega t}$, the amplitude $\mathbf{x}_0$ of the displacement $\mathbf{x} = \mathbf{x}_0 e^{-i\omega t}$ is given by

$$\mathbf{x}_0 = -\frac{e}{m_e}\frac{1}{\omega_0^2 - \omega^2 - i\gamma\omega}\mathbf{E}_0. \tag{1.21}$$

The displacement of the electron from its equilibrium position produces a time varying dipole moment $\mathbf{p} = -e\mathbf{x}$. Taking into account that a medium consists of N atoms per unit volume the macroscopic polarization $\mathbf{P}$ (dipole moment per unit volume) is given in frequency domain by

$$\begin{aligned}\mathbf{P} &= \frac{Ne^2}{m_e}\frac{1}{\omega_0^2 - \omega^2 - i\gamma\omega}\mathbf{E} \\ &= \epsilon_0\chi(\omega)\mathbf{E}.\end{aligned} \tag{1.22}$$

In general there exists different bound electron oscillators (different parameters), forced oscillators of other types like vibration of charged ions, or even free electron oscillators if $\omega_0 = 0$. Inspecting (1.22) one can see that the magnitude of $\mathbf{P}$ is small unless the frequency is close to the resonance frequency ω_0. If we assume that the medium of interest has n different forced oscillators with parameters $\{\omega_0^n, \gamma_n\}$ with resonance frequencies in the spectral range of interest, and additionally some non-resonant ones which can be comprehended in a non-resonant background term the electric displacement $\mathbf{D}$ can be

written as

$$\begin{aligned}\mathbf{D} &= \epsilon_0\mathbf{E} + \mathbf{P}_{\text{background}} + \frac{Ne^2}{m_e}\sum_n \frac{1}{\left(\omega_0^n\right)^2 - \omega^2 - i\gamma_n\omega}\mathbf{E} \\ &= \epsilon_0\epsilon_r\mathbf{E}. \end{aligned} \tag{1.23}$$

Then the relative dielectric constant is given by

$$\epsilon_r(\omega) = \epsilon_\infty + \frac{Ne^2}{\epsilon_0 m_e}\sum_n \frac{1}{\left(\omega_0^n\right)^2 - \omega^2 - i\gamma_n\omega} \tag{1.24}$$

where $\epsilon_\infty = 1 + \chi_{\text{background}}$.

1.3 Conservation of Energy: Poynting's Theorem

For a single charge q the rate of doing work by external electromagnetic fields $\mathbf{E}$ and $\mathbf{B}$ is $q\mathbf{v}\cdot\mathbf{E}$, where $\mathbf{v}$ is the velocity of the charge. The magnetic field does no work, since the magnetic force is perpendicular to the velocity. If there exists a continuous distribution of charge and current density, the total rate of doing work by the fields in a volume V is $\int_V \mathbf{j}\cdot\mathbf{E}\,d^3r$. If the scalar product of $\mathbf{E}$ with the generalized Ampere's law (1.2) is subtracted from the scalar product of $\mathbf{H}$ with Faraday's law (1.1) the following equation is obtained:

$$\begin{aligned}\nabla\cdot(\mathbf{E}\times\mathbf{H}) &= \mathbf{H}\cdot(\nabla\times\mathbf{E}) - \mathbf{E}\cdot(\nabla\times\mathbf{H}) \\ &= -\mathbf{H}\cdot\frac{\partial\mathbf{B}}{\partial t} - \mathbf{E}\cdot\frac{\partial\mathbf{D}}{\partial t} - \mathbf{j}\cdot\mathbf{E}. \end{aligned} \tag{1.25}$$

Integrating both sides over the volume V and applying Gauss's theorem which is given for a regular vector field $\mathbf{a}$ by [4]

$$\int_V d^3r\,\nabla\cdot\mathbf{a} = \oint_{\partial V} d^2r\,\mathbf{a}\cdot\hat{\mathbf{n}} \tag{1.26}$$

where $\hat{\mathbf{n}}$ denotes the unit surface normal to the bounding surface ∂V of volume V pointing outwards, equation (1.25) becomes in integral form

$$\int_{\partial V}(\mathbf{E}\times\mathbf{H})\cdot\hat{\mathbf{n}}\,d^2r = -\int_V \mathbf{j}\cdot\mathbf{E}\,d^3r - \int_V \mathbf{H}\cdot\frac{\partial\mathbf{B}}{\partial t} + \mathbf{E}\cdot\frac{\partial\mathbf{D}}{\partial t}\,d^3r. \tag{1.27}$$

By using equations (1.6) and (1.7) one can substitute

$$\mathbf{E}\cdot\frac{\partial\mathbf{D}}{\partial t}=\frac{1}{2}\frac{\partial}{\partial t}\left(\mathbf{E}\cdot\mathbf{D}\right)-\frac{1}{2}\left(\frac{\partial\mathbf{E}}{\partial t}\cdot\mathbf{P}-\mathbf{E}\cdot\frac{\partial\mathbf{P}}{\partial t}\right) \tag{1.28}$$

and

$$\mathbf{H}\cdot\frac{\partial\mathbf{B}}{\partial t}=\frac{\mu_0}{2}\frac{\partial}{\partial t}\mathbf{H}^2 \tag{1.29}$$

in (1.27) yielding *Poynting's theorem* in the form

$$\begin{aligned}\int_{\partial V}\left(\mathbf{E}\times\mathbf{H}\right)\cdot\hat{\mathbf{n}}\,d^2r+\frac{1}{2}\frac{\partial}{\partial t}\int_V\left(\mathbf{E}\cdot\mathbf{D}+\mu_0\left|\mathbf{H}\right|^2\right)\,d^3r&\\ =-\int_V\mathbf{j}\cdot\mathbf{E}\,d^3r-\frac{1}{2}\int_V\left(\mathbf{E}\cdot\frac{\partial\mathbf{P}}{\partial t}-\mathbf{P}\cdot\frac{\partial\mathbf{E}}{\partial t}\right)\,d^3r&\end{aligned} \tag{1.30}$$

If the medium within the volume V is linear and nondispersive the second integral on the right hand side of (1.30) vanishes. By defining the *Poynting vector*

$$\mathbf{S}=\mathbf{E}\times\mathbf{H} \tag{1.31}$$

and the energy flux density

$$u=\frac{1}{2}\left(\mathbf{E}\cdot\mathbf{D}+\mu_0\left|\mathbf{H}\right|^2\right) \tag{1.32}$$

Poynting's theorem (1.30) for linear nondispersive media can be cast into the form of a differential continuity equation or conservation law

$$\nabla\cdot\mathbf{S}+\frac{\partial u}{\partial t}=-\mathbf{j}\cdot\mathbf{E}. \tag{1.33}$$

which states that the time rate of change of electromagnetic energy within a certain volume plus the energy flowing out through the boundary surface of the volume per unit time is equal to the negative of the total work done by the fields on the sources within the volume. This is the statement of conservation of energy.

Poynting's Theorem for Harmonic Fields

Assuming a harmonic time dependence $e^{-i\omega t}$ the time domain fields $\mathbf{E}(\mathbf{r},t)$ and $\mathbf{j}(\mathbf{r},t)$ can be expressed according to equation (1.8) in terms of their corrresponding complex

amplitudes $\mathbf{E}(\mathbf{r})$, $\mathbf{j}(\mathbf{r})$ which leads to the scalar product

$$\mathbf{j}(\mathbf{r},t)\cdot\mathbf{E}(\mathbf{r},t)=\frac{1}{2}\Re\left\{\mathbf{j}^{\star}(\mathbf{r})\cdot\mathbf{E}(\mathbf{r})+\mathbf{j}(\mathbf{r})\cdot\mathbf{E}(\mathbf{r})e^{-2i\omega t}\right\}. \tag{1.34}$$

The time average of these product is thus given by

$$\langle\mathbf{j}(\mathbf{r},t)\cdot\mathbf{E}(\mathbf{r},t)\rangle=\frac{1}{2}\Re\left\{\mathbf{j}^{\star}(\mathbf{r})\cdot\mathbf{E}(\mathbf{r})\right\}. \tag{1.35}$$

Therefore in (1.30) the volume integral $\frac{1}{2}\int_V \mathbf{j}^{\star}\cdot\mathbf{E}\,d^3r$ instead of $\int_V \mathbf{j}\cdot\mathbf{E}\,d^3r$ should be used where its real part gives the time-averaged rate of work done by the fields in the volume V. Following the steps which leads to equation (1.27), but using frequency domain Maxwell's equations (1.9) and (1.10) instead of the time domain ones, yields

$$\frac{1}{2}\int_{\partial V}(\mathbf{E}\times\mathbf{H}^{\star})\cdot\hat{\mathbf{n}}\,d^2r=-\frac{1}{2}\int_V\mathbf{j}^{\star}\cdot\mathbf{E}\,d^3r-\frac{1}{2}i\omega\int_V\left(\epsilon_0\epsilon_r\left|\mathbf{E}\right|^2-\mu_0\left|\mathbf{H}\right|^2\right)\,d^3r. \tag{1.36}$$

Taking the real part of (1.36) and introducing the time averaged *Poynting vector*

$$\langle\mathbf{S}\rangle=\frac{1}{2}\Re\left\{\mathbf{E}\times\mathbf{H}^{\star}\right\} \tag{1.37}$$

one obtains Poynting's theorem for harmonic fields

$$\int_{\partial V}\langle\mathbf{S}\rangle\cdot\hat{\mathbf{n}}\,d^2r=-\frac{1}{2}\int_V\Re\left\{\mathbf{j}^{\star}\cdot\mathbf{E}\right\}\,d^3r+\frac{1}{2}\omega\epsilon_0\int_V\Im\left\{\epsilon_r\right\}\left|\mathbf{E}\right|^2\,d^3r \tag{1.38}$$

where the second term on the right hand side vanishes for lossless dielectrics.

1.4 Vector Helmholtz Equation

Taking the curl of Faraday's law (1.9) and using Ampere's law (1.10) to substitute the curl on the right hand side of the resulting equation one obtains the inhomogeneous *vector Helmholtz equation*

$$\nabla\times\nabla\times\mathbf{E}(\mathbf{r})-k^2\mathbf{E}(\mathbf{r})=i\omega\mu_0\left[\mathbf{j}(\mathbf{r})-i\omega\mathbf{P}(\mathbf{r})\right], \tag{1.39}$$

with the free space wave number $k^2=\omega^2\epsilon_0\mu_0$. By substituting (1.18) for $\mathbf{P}$ this can be expressed entirely in terms of $\mathbf{E}$ and the source current density $\mathbf{j}$ as

$$\nabla\times\nabla\times\mathbf{E}(\mathbf{r})-k^2\epsilon_r(\mathbf{r},\omega)\mathbf{E}(\mathbf{r})=i\omega\mu_0\mathbf{j}(\mathbf{r}). \tag{1.40}$$

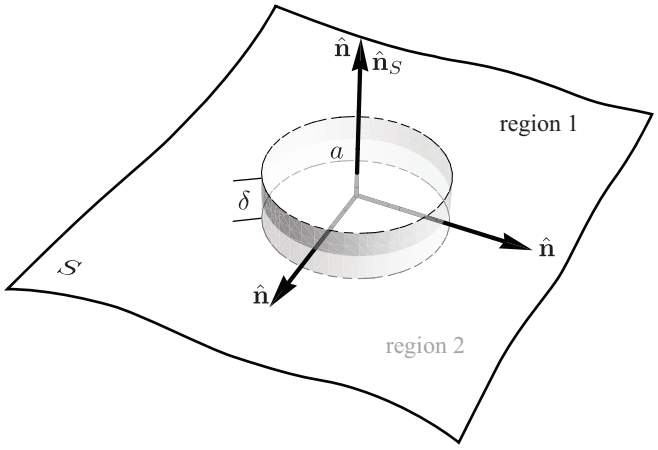

Figure 1.1: The pillbox volume with radius a and thickness δ used to derive the boundary conditions (1.51)-(1.54) for the electromagnetic field between two different media in region 1 and region 2.

Likewise one can derive the vector Helmholtz equation for the magnetic field $\mathbf{H}$ by taking the curl of Ampere's law (1.10) and using (1.9) which yields

$$\begin{aligned} \nabla \times \nabla \times \mathbf{H}(\mathbf{r}) - k^2 \mathbf{H}(\mathbf{r}) &= \nabla \times [\mathbf{j}(\mathbf{r}) - i\omega \mathbf{P}(\mathbf{r})] \\ &= \nabla \times [\mathbf{j}(\mathbf{r}) - i\omega \epsilon_0 \chi(\mathbf{r}, \omega) \mathbf{E}(\mathbf{r})] \,. \end{aligned} \tag{1.41}$$

If the medium is homogeneous, that is $\partial_{\mathbf{r}} \chi = 0$, this simplifies to

$$\nabla \times \nabla \times \mathbf{H}(\mathbf{r}) - k^2 \epsilon_r(\omega) \mathbf{H}(\mathbf{r}) = \nabla \times \mathbf{j}(\mathbf{r}) \tag{1.42}$$

In a source-free and homogeneous region equations (1.40) and (1.42) can be reduced to the homogeneous vector Helmholtz equations

$$\nabla^2 \mathbf{E}(\mathbf{r}) + k^2 \epsilon_r(\omega) \mathbf{E}(\mathbf{r}) = 0 \tag{1.43}$$

$$\nabla^2 \mathbf{H}(\mathbf{r}) + k^2 \epsilon_r(\omega) \mathbf{H}(\mathbf{r}) = 0. \tag{1.44}$$

by using the vector identity

$$\nabla \times \nabla \times \mathbf{a} = \nabla (\nabla \cdot \mathbf{a}) - \nabla^2 \mathbf{a} \tag{1.45}$$

and the divergence-free nature of $\mathbf{E}$ and $\mathbf{H}$ fields (Maxwell's equations (1.11) and (1.12)).

1.5 Boundary Conditions

Maxwell's equations (1.1)-(1.4) have been written in differential form. They must be supplemented with boundary and initial conditions. The boundary conditions can be derived from the integral form of Maxwell's equations. By integrating Maxwell's equations in differential form (1.1)-(1.4) over an arbitrary volume V using Gauss's theorem (1.26) and the identity

$$\int d^3r\, \nabla \times \mathbf{a} = \oint_{\partial V} d^2r\, \hat{\mathbf{n}} \times \mathbf{a} \tag{1.46}$$

which can be derived from (1.26) by substituting $\mathbf{a} \to \mathbf{c} \times \mathbf{a}$ where $\mathbf{c}$ is a constant vector, one obtains Maxwell's equations in integral form

$$\oint_{\partial V} d^2r\, \hat{\mathbf{n}} \times \mathbf{E} = -\int_V d^3r\, \frac{\partial}{\partial t}\mathbf{B} \tag{1.47}$$

$$\oint_{\partial V} d^2r\, \hat{\mathbf{n}} \times \mathbf{H} = \int_V d^3r\, \frac{\partial}{\partial t}\mathbf{D} + \int_V d^3r\, \mathbf{j} \tag{1.48}$$

$$\oint_{\partial V} d^2r\, \hat{\mathbf{n}} \cdot \mathbf{B} = 0 \tag{1.49}$$

$$\oint_{\partial V} d^2r\, \hat{\mathbf{n}} \cdot \mathbf{D} = \int_V d^3r\, \rho. \tag{1.50}$$

Now consider a static interface separating regions 1 and 2 and a small pillbox volume across the boundary interface as it is shown in figure (1.1). Then the partial derivatives with respect to time in (1.47) and (1.48) can be pulled out of the integral and transformed into total derivatives. Now let the volume of the pillbox approach zero in such a way that the thickness of the ribbon side, δ, goes to zero before the top and bottom areas a shrink to a point. The field vectors $\mathbf{E}$, $\mathbf{B}$, $\mathbf{D}$ and $\mathbf{H}$ are assumed to be finite but may be discontinuous across the boundary. Therefore the volume integration over the field vectors in (1.47) and (1.48) approach zero because they are proportional to δ. In the case of a perfect electric conductor where current flow takes place only on the surface, charge and current densities are infinite and their integral over the pillbox volume gives finite results no matter how small the volume is made. However, throughout this thesis we are dealing with dielectrics with zero or finite conductivity so all right hand sides of (1.47)-(1.50) approach zero for a shrinking volume. In the surface integrals on the left the fluxes through the ribbon sides vanish in the limit $\delta \to 0$. Therefore the following

boundary conditions are obtained

$$\hat{\mathbf{n}} \times [\mathbf{E}_1 - \mathbf{E}_2] = 0 \tag{1.51}$$

$$\hat{\mathbf{n}} \times [\mathbf{H}_1 - \mathbf{H}_2] = 0 \tag{1.52}$$

$$\hat{\mathbf{n}} \cdot [\mathbf{B}_1 - \mathbf{B}_2] = 0 \tag{1.53}$$

$$\hat{\mathbf{n}} \cdot [\mathbf{D}_1 - \mathbf{D}_2] = 0. \tag{1.54}$$

Essentially the boundary conditions state that the tangential components of $\mathbf{E}$ and $\mathbf{H}$ and the normal components of $\mathbf{B}$ and $\mathbf{D}$ are continuous across the boundary.

2 The Electromagnetic Field produced by Currents: Formal Solution

This chapter is concerned with the formal solution of the vector Helmholtz equation (1.40) which describes the electric field generated by a given current density $\mathbf{j}$.

By introducing potentials, namely the *scalar potential* ϕ and the *vector potential* $\mathbf{A}$, and the *Lorenz gauge condition* relating them (section 2.1), the solution of the vector Helmholtz equation can be written in terms of $\mathbf{A}$ where each component of $\mathbf{A}$ separately solves a simple *scalar Helmholtz equation*. In the subsequent section the *scalar Green's function* of the scalar Helmholtz operator is (i) derived and (ii) used to write down the general solution of the scalar Helmholtz equation. Finally the *dyadic Green's function* is defined and used to express the solution to the original vector Helmholtz equation. This is in general only possible if one treats the singularity of the Green's function appropriately. A *regularization* procedure well suited for this task is presented. An extensive discussion of the presented material can be found in textbooks such as [6] or [7].

2.1 Vector and Scalar Potentials, Lorenz Gauge

In order to solve Maxwell's equations in the presence of charges and currents one can introduce potentials, obtaining a smaller number of second-order equations, while satisfying the two homogeneous Maxwell equations (1.9) and (1.12) identically.

Since the magnetic induction $\mathbf{B}$ has to be divergence free one can express it through the curl of a *vector potential* $\mathbf{A}$

$$\mathbf{B} = \nabla \times \mathbf{A}. \tag{2.1}$$

Therefore Faraday's law (1.9) becomes

$$\nabla \times [\mathbf{E} - i\omega\mathbf{A}] = 0 \tag{2.2}$$

which can be automatically fulfilled if we replace the curl free term in brackets with the gradient of a scalar function, namely, the *scalar potential* ϕ. Then the electric field $\mathbf{E}$ expressed in terms of the introduced potentials $\{\phi, \mathbf{A}\}$ is given by

$$\mathbf{E} = -\nabla\phi + i\omega\mathbf{A}. \tag{2.3}$$

By inserting (2.1) and (2.3) into Ampere's law (1.10) and substituting $\mathbf{D} = \epsilon_0\epsilon_r\mathbf{E}$ which holds for every isotropic region one obtains

$$\nabla \times \nabla \times \mathbf{A} = \mu_0\mathbf{j} - i\omega\mu_0\epsilon_0\epsilon_r(-\nabla\phi + i\omega\mathbf{A}) \tag{2.4}$$

which can be transformed into

$$\nabla^2\mathbf{A} + k^2\epsilon_r\mathbf{A} = -\mu_0\mathbf{j} - \nabla\left(i\omega\mu_0\epsilon_0\epsilon_r\phi - \nabla\cdot\mathbf{A}\right) \tag{2.5}$$

using the vector identity (1.45). The transformation $\mathbf{A} \to \mathbf{A} + \nabla f$ with an arbitrary scalar function f does not alter $\mathbf{B}$ and if one transform additionally $\phi \to \phi + i\omega f$ the electric field does not changed either. This gauge freedom can be used to choose a set of potentials $\{\phi, \mathbf{A}\}$ satisfying the *Lorenz gauge condition*

$$\nabla\cdot\mathbf{A} - i\omega\mu_0\epsilon_0\epsilon_r\phi = 0. \tag{2.6}$$

which leads to the inhomogenous vector Helmholtz equation

$$\nabla^2\mathbf{A} + k^2\epsilon_r\mathbf{A} = -\mu_0\mathbf{j} \tag{2.7}$$

for the vector potential $\mathbf{A}$. If the solution $\mathbf{A}$ of (2.7) is already obtained, the Lorenz gauge condition (2.6) can be used to replace ϕ in (2.3) yielding the electric field generated by the current density $\mathbf{j}$

$$\mathbf{E} = i\omega\mathbf{A} + \frac{i}{\omega\mu_0\epsilon_0}\nabla\left(\frac{\nabla\cdot\mathbf{A}}{\epsilon_r}\right) \tag{2.8}$$

Thus equations (2.7) , (2.8) and (2.1) form a set of equations equivalent in all respects to Maxwell's equations.

2.2 Solution of the Scalar Helmholtz Equation

Each individual component of equation (2.7) has the basic structure

$$\mathcal{L}_H \psi = -f(\mathbf{r}), \tag{2.9}$$

where $f(\mathbf{r}, \omega)$ is a known source distribution and $\mathcal{L}_H = \nabla^2 + k^2$ the Helmholtz operator. In this chapter it will be shown how one can solve this scalar inhomogeneous Helmholtz equation which is a key point in finding the general solution of Maxwell's equations.

2.2.1 The Scalar Green's Function of Helmholtz's Equation

The *scalar Green's function* $g(\mathbf{r}, \mathbf{r}')$ of the Helmholtz operator $\mathcal{L}_H = \nabla^2 + k^2$ is defined as a solution of (2.9) with a single point source, i.e $f(\mathbf{r}) \to \delta(\mathbf{r} - \mathbf{r}')$. The function $\delta(\mathbf{r})$ acting as a point source is called Dirac delta function and can be defined by [1]

$$\delta\left(\mathbf{r} - \mathbf{r}'\right) = 0 \quad \text{for } \mathbf{r} \neq \mathbf{r}' \tag{2.10}$$

and

$$\int_V \delta\left(\mathbf{r} - \mathbf{r}'\right)\, d^3r' = 1. \tag{2.11}$$

A point-source excitation at $\mathbf{r}' = 0$ in an unbounded medium lead to a spherical symmetric Green's function $g(\mathbf{r}) = g(r)$ which behaves well for all radial distances $r > 0$ from the origin since it satisfies

$$\nabla^2 g(r) + k^2 g(r) = \frac{1}{r}\frac{d^2}{dr^2}\left[r g(r)\right] + k^2 g(r) = 0, \tag{2.12}$$

which can be written as

$$\left(\frac{d^2}{dr^2} + k^2\right) r g(r) = 0. \tag{2.13}$$

The general solution of the above equation is

$$r g(r) = A e^{ikr} + B e^{-ikr} \tag{2.14}$$

and since $r \neq 0$, one obtains

$$g(r) = A\frac{e^{ikr}}{r} + B\frac{e^{-ikr}}{r}. \tag{2.15}$$

The first term represents an outward-traveling and the second term an inward-traveling spherical wave (for $e^{-i\omega t}$ time dependence). There are no sources at infinity and so the inward-traveling wave is nonphysical. Therefore B has to be set to zero. The constant A can be determined by enforcing the proper singular behavior of the Green's function at $r = 0$. Integrating $\mathcal{L}_H \psi = -\delta(\mathbf{r})$ over a small but finite spherical volume V_δ with radius δ around the origin one yields

$$\int_{V_\delta} \nabla^2 \frac{e^{ikr}}{r}\, d^3r + k^2 \int_{V_\delta} \frac{e^{ikr}}{r}\, d^3r = -\frac{1}{A}. \tag{2.16}$$

The second integral on the left side vanishes in the limit $\delta \to 0$ because the integrand is of the order $\mathcal{O}\left(r^{-1}\right)$ while the volume element is $\mathcal{O}\left(r^3\right)$. By looking at the Taylor series expansion of the exponential term around the origin

$$\frac{e^{ikr}}{r} \approx \frac{1}{r} + ik - \frac{k^2}{2} r + \ldots \tag{2.17}$$

one can see that the argument from above is not valid only for the first term in the expansion. Thus the constant A can be calculated by

$$\lim_{\delta \to 0} \int_{V_\delta} \nabla^2 \frac{1}{r} = -\frac{1}{A}. \tag{2.18}$$

Substituting $\frac{1}{r} \to \frac{1}{\sqrt{r^2 + a^2}}$ with a real constant $a > 0$ a calculation in spherical coordinates yields

$$\int_{V_\delta} \nabla^2 \frac{1}{\sqrt{r^2 + a^2}}\, d^3r = -4\pi \frac{\delta^3}{(\delta^2 + a^2)^{\frac{3}{2}}} = -\frac{1}{A} \tag{2.19}$$

Now taking the limit $a \to 0$ at finite δ and afterwards $\delta \to 0$ the fraction on the right side is going to 1. Therefore one can see that $A = 1/4\pi$. Restoring the dependence $\mathbf{r} - \mathbf{r}'$ one obtains finally

$$g(\mathbf{r}, \mathbf{r}') = \frac{e^{ik|\mathbf{r} - \mathbf{r}'|}}{4\pi \left|\mathbf{r} - \mathbf{r}'\right|}. \tag{2.20}$$

as a particular solution of $\mathcal{L}_H g(\mathbf{r}, \mathbf{r}') = -\delta\left(\mathbf{r} - \mathbf{r}'\right)$. If desired one can add homogeneous solutions $g^h(\mathbf{r}, \mathbf{r}')$ of $\mathcal{L}_H g^h(\mathbf{r}, \mathbf{r}') = 0$ to (2.20) to satisfy some desired boundary conditions.

2.2.2 The General Solution and Radiation Boundary Condition

In order to obtain the general solution of (2.9) by using the scalar Green's function (2.20) one starts from Green's second identity [8]

$$\int_V \left[\psi_1 \nabla^2 \psi_2 - \psi_2 \nabla^2 \psi_1\right] \, d^3r = \oint_{\partial V} \left[\psi_1 \nabla \psi_2 - \psi_2 \nabla \psi_1\right] \cdot \hat{\mathbf{n}} \, d^2r, \tag{2.21}$$

where ψ_1 and ψ_2 are required to be continuous differentiable in the closed region $V \cup \partial V$ and having piecewise continuous second derivatives in V. $\hat{\mathbf{n}}$ denotes the unit surface normal pointing out of the volume V. Next one substitutes $\psi_1 = \psi(\mathbf{r}')$ and $\psi_2 = g(\mathbf{r}, \mathbf{r}')$ but has to take into account that $g(\mathbf{r}, \mathbf{r}')$ at the point $\mathbf{r}' = \mathbf{r}$ does not fulfill the mentioned demands for Green's identity. So one has to exclude the point $\mathbf{r}' = \mathbf{r}$ from the integration. This can be achieved by excluding a spherical volume V_δ with radius δ and center $\mathbf{r}$, leading to

$$\begin{aligned}\int_{V-V_\delta} \left[\psi(\mathbf{r}') \nabla'^2 g(\mathbf{r}, \mathbf{r}') - g(\mathbf{r}, \mathbf{r}') \nabla'^2 \psi(\mathbf{r}')\right] \, d^3r' \\ = \oint_{\partial V + \partial V_\delta} \left[\psi(\mathbf{r}') \nabla' g(\mathbf{r}, \mathbf{r}') - g(\mathbf{r}, \mathbf{r}') \nabla' \psi(\mathbf{r}')\right] \cdot \hat{\mathbf{n}} \, d^2r'.\end{aligned} \tag{2.22}$$

Next one can use the inhomogeneous Helmholtz equation (2.9) as well as the definition of the scalar Green's function to obtain

$$\begin{aligned}\int_{V-V_\delta} g(\mathbf{r}, \mathbf{r}') f(\mathbf{r}') \, d^3r' - \oint_{\partial V} \left[\psi(\mathbf{r}') \nabla' g(\mathbf{r}, \mathbf{r}') - g(\mathbf{r}, \mathbf{r}') \nabla' \psi(\mathbf{r}')\right] \cdot \hat{\mathbf{n}} \, d^2r' \\ = \oint_{\partial V_\delta} \left[\psi(\mathbf{r}') \nabla' g(\mathbf{r}, \mathbf{r}') - g(\mathbf{r}, \mathbf{r}') \nabla' \psi(\mathbf{r}')\right] \cdot \hat{\mathbf{n}} \, d^2r'.\end{aligned} \tag{2.23}$$

Substituting the explicit form of the Green's function (2.20) and taking the limit $\delta \to 0$ the right hand side becomes

$$\begin{aligned}ik \frac{\psi(\mathbf{r})}{4\pi} \lim_{\delta \to 0} \frac{e^{ik\delta}}{\delta} \oint_{\partial V_\delta} \hat{\mathbf{R}} \cdot \hat{\mathbf{n}} \, d^2r' - \frac{\psi(\mathbf{r})}{4\pi} \lim_{\delta \to 0} \frac{e^{ik\delta}}{\delta^2} \oint_{\partial V_\delta} \hat{\mathbf{R}} \cdot \hat{\mathbf{n}} \, d^2r' - \\ \frac{1}{4\pi} \lim_{\delta \to 0} \frac{e^{ik\delta}}{\delta} \oint_{\partial V_\delta} \nabla' \psi(\mathbf{r}') \cdot \hat{\mathbf{n}} \, d^2r'\end{aligned} \tag{2.24}$$

where $\hat{\mathbf{R}}$ denotes the unit vector in the direction $\mathbf{R} = \mathbf{r}' - \mathbf{r}$. With the surface element $d^2r' = \delta^2 \sin\theta d\theta d\phi$ one sees that the first and the third terms vanish in the limit $\delta \to 0$ because they are $\mathcal{O}(\delta)$ and in the second term the integration over the solid angle yields

-4π since $\hat{\mathbf{R}} \uparrow\downarrow \hat{\mathbf{n}}$. So the right hand side of (2.23) for $\delta \to 0$ gives $\psi(\mathbf{r})$. By using the explicit form of $g(\mathbf{r}, \mathbf{r}')$ (2.20) in the residual surface integral in (2.23) and taking the limit $\delta \to 0$ one yields

$$\psi(\mathbf{r}) = \lim_{\delta \to 0} \int_{V - V_\delta} g(\mathbf{r}, \mathbf{r}') f(\mathbf{r}')\, d^3 r' + \frac{1}{4\pi} \oint_{\partial V} \frac{e^{ikR}}{R} \left[\nabla' \psi(\mathbf{r}') - \psi(\mathbf{r}') \left(ik\hat{\mathbf{R}} - \frac{\hat{\mathbf{R}}}{R} \right) \right] \cdot \hat{\mathbf{n}}\, d^2 r', \tag{2.25}$$

as a general solution of (2.9) in the sense that no boundary conditions have been specified on ψ or g. Up to now the solution is not yet unique. Applying Green's second identity (2.21) again in a similar way as above but choosing an integration volume V in which there are no sources, that is $f(\mathbf{r}) = 0$ for every $\mathbf{r} \in V$, and which is bounded internally by the surface ∂V_i and externally by the spherical surface ∂V_e yields

$$\psi(\mathbf{r}) = \frac{1}{4\pi} \oint_{\partial V_e + \partial V_i} \frac{e^{ikR}}{R} \left[\nabla' \psi(\mathbf{r}') - \psi(\mathbf{r}') \left(ik\hat{\mathbf{R}} - \frac{\hat{\mathbf{R}}}{R} \right) \right] \cdot \hat{\mathbf{n}}\, d^2 r'. \tag{2.26}$$

Under the assumption that the radius of the spherical surface ∂V_e goes to infinity the integration over ∂V_e

$$\oint_{\partial V_e} \frac{e^{ikR}}{R} \left[\frac{\partial}{\partial R} \psi(R) - ik\psi(R) \right] d^2 r' + \oint_{\partial V_e} e^{ikR} \psi(R)\, d\Omega \tag{2.27}$$

expresses the sum of all waves traveling inwards from ∂V_e. Therefore the surface integral over ∂V_e has to vanish. The second term vanishes because of the demand that ψ has to be regular at infinity, i.e. $\psi \to f(\theta, \phi) \frac{e^{ikR}}{R}$. For the first term to vanish it is sufficient that

$$\lim_{r' \to \infty} R \left[\frac{\partial}{\partial R} \psi(R) - ik\psi(R) \right] = 0. \tag{2.28}$$

Together with this so called *radiation boundary condition* the solution (2.25) is unique. Later on we are interested in solutions in unbounded space and with finite source region. In this case there is just one bounding surface at infinity on which the regular solution has to fulfill the radiation boundary condition (2.28). Then the general solution (2.25) simplifies to

$$\psi(\mathbf{r}) = \lim_{\delta \to 0} \int_{V - V_\delta} g(\mathbf{r}, \mathbf{r}') f(\mathbf{r}')\, d^3 r', \tag{2.29}$$

Because this integral converges, which means that the form of the excluded volume V_δ having a length scale δ does not alter the result in the limit $\delta \to 0$ [6], we write from

now on

$$\psi(\mathbf{r}) = \int_V g(\mathbf{r}, \mathbf{r}') f(\mathbf{r}')\, d^3r' \tag{2.30}$$

but one has to understand it in the sense of (2.29).

2.3 Dyadic Green's function

Each component of equation (2.7) which determines the vector potential $\mathbf{A}$ in Lorenz gauge (2.6) fulfills an inhomogeneous scalar Helmholtz equation (2.9) where the inhomogenity for each component is proportional to the corresponding component of the current density $\mathbf{j}$. In chapter (2.2) the general solution to the inhomogenous Helmholtz equation (2.9) for an arbitrary inhomogenity $f(\mathbf{r})$ was derived. If the source is contained in the finite volume V and placed in infinite free space a particular solution is given by (2.30). Thus, a particular solution for the vector potential $\mathbf{A}$ produced by the current density $\mathbf{j}$ in free space and with finite space extent is given by

$$\mathbf{A}(\mathbf{r}) = \mu_0 \int_V g(\mathbf{r}, \mathbf{r}')\mathbf{j}(\mathbf{r}')\, d^3r'. \tag{2.31}$$

Which leads, according to (2.8), to a partial solution for the electric field

$$\begin{aligned}\mathbf{E}(\mathbf{r}) &= i\omega\mathbf{A}(\mathbf{r}) + \frac{i}{\omega\epsilon_0\mu_0\epsilon_r}\nabla\left[\nabla\cdot\mathbf{A}(\mathbf{r})\right] \\ &= i\omega\mu_0\left(\overleftrightarrow{\mathbf{I}} + \frac{1}{k^2}\nabla\otimes\nabla\right)\int_V g(\mathbf{r}, \mathbf{r}')\mathbf{j}(\mathbf{r}')\, d^3r'.\end{aligned} \tag{2.32}$$

Here $\otimes$ denotes the tensor product defined by $[\mathbf{a}\otimes\mathbf{b}]_{ij} = a_i b_j$. If the view point $\mathbf{r}$ is at a source free position, that is $\mathbf{j}(\mathbf{r}) = 0$ and the current source $\mathbf{j}$ is at least piecewise continuous in V, the integral in (2.32) has constant borders and is well defined so the differential operator and the integration can be interchanged yielding a particular solution of the form

$$\mathbf{E}(\mathbf{r}) = i\omega\mu_0 \int_V \overleftrightarrow{\mathbf{G}}(\mathbf{r}, \mathbf{r}')\mathbf{j}(\mathbf{r}')\, d^3r', \quad \text{for } \mathbf{j}(\mathbf{r}) = 0, \tag{2.33}$$

with the dyadic Green's function

$$\overleftrightarrow{\mathbf{G}}(\mathbf{r}, \mathbf{r}') = \left(\overleftrightarrow{\mathbf{I}} + \frac{1}{k^2}\nabla\otimes\nabla\right) g(\mathbf{r}, \mathbf{r}') \tag{2.34}$$

which can be calculated explicitly from the scalar Green's function (2.20)

$$\overleftrightarrow{\mathbf{G}}(\mathbf{r}, \mathbf{r}') = \frac{e^{ikR}}{4\pi R}\left\{\left(1 + \frac{ikR - 1}{k^2R^2}\right)\overleftrightarrow{\mathbf{I}} + \frac{3 - 3ikR - k^2R^2}{k^2R^2}\frac{\mathbf{R}\otimes\mathbf{R}}{R^2}\right\}. \tag{2.35}$$

From equation (2.32) one can conclude that $\overleftrightarrow{\mathbf{G}}(\mathbf{r},\mathbf{r}')\hat{\mathbf{x}}$, the first column of $\overleftrightarrow{\mathbf{G}}(\mathbf{r},\mathbf{r}')$, is the electric field at position $\mathbf{r}$ due to a point dipole with $\hat{\mathbf{x}}$-direction at position $\mathbf{r}'$ and a current density $\mathbf{j} = (i\omega\mu_0)^{-1}\hat{\mathbf{x}}\delta(\mathbf{r}-\mathbf{r}')$, just as the second and third column are for point dipoles with $\hat{\mathbf{y}}$ and $\hat{\mathbf{z}}$ orientation respectively. Thus the dyadic Green's function is a solution of the following Helmholtz equation

$$\nabla \times \nabla \times \overleftrightarrow{\mathbf{G}}(\mathbf{r},\mathbf{r}') - k^2 \overleftrightarrow{\mathbf{G}}(\mathbf{r},\mathbf{r}') = \overleftrightarrow{\mathbf{I}}\,\delta(\mathbf{r}-\mathbf{r}') \tag{2.36}$$

For $\mathbf{j}(\mathbf{r}) \neq 0$ the interchange of the differential operator and integration which was done in the step from (2.32) to (2.33) is no longer valid because the differentiation leads to singularities $\partial_i\partial_j g(\mathbf{r},\mathbf{r}') \propto |\mathbf{r}-\mathbf{r}'|^{-3}$ which are generally not integrable. But it is possible to split second derivatives of $\mathbf{A}$ in (2.32) into three terms in such a way that each term is a convergent integral without a differential operator in front [9] (a proof is given in appendix A)

$$I_{ij} = \frac{\partial^2}{\partial x_i \partial x_j}\int_V g(\mathbf{r},\mathbf{r}')j(\mathbf{r}')\,d^3r' = A_{ij} + B_{ij} + C_{ij}. \tag{2.37}$$

The separate terms are given by

$$A_{ij} = \int_{V-V^\star} j(\mathbf{r}')\frac{\partial^2}{\partial x_i'\partial x_j'} g(\mathbf{r},\mathbf{r}')\,d^3r', \tag{2.38}$$

$$B_{ij} = j(\mathbf{r})\oint_{\partial V^\star} \frac{\partial}{\partial x_i'} g_0(\mathbf{r},\mathbf{r}')\,(\mathbf{x}_j\cdot\hat{\mathbf{n}})\;d^2r', \tag{2.39}$$

$$C_{ij} = \int_{V^\star}\left(j(\mathbf{r}')\frac{\partial^2}{\partial x_i'\partial x_j'} g(\mathbf{r},\mathbf{r}') - j(\mathbf{r})\frac{\partial^2}{\partial x_i'\partial x_j'} g_0(\mathbf{r},\mathbf{r}')\right)\,d^3r'. \tag{2.40}$$

Here, g_0 denotes the static Green's function

$$g_0(\mathbf{r},\mathbf{r}') = \lim_{k\to 0} g(\mathbf{r},\mathbf{r}') = \frac{1}{4\pi}\frac{1}{|\mathbf{r}-\mathbf{r}'|} \tag{2.41}$$

and $V^\star$ an arbitrary shaped principal volume containing the singular point $\mathbf{r}$.

By substituting (2.37) in (2.32) one obtains finally the regularized partial solution to the vector Helmholtz equation

$$\begin{aligned}\mathbf{E}(\mathbf{r}) = i\omega\mu_0\Bigg\{&\int_{V-V^\star}\overleftrightarrow{\mathbf{G}}(\mathbf{r},\mathbf{r}')\mathbf{j}(\mathbf{r}')d^3r' + \\ &\int_{V^\star}\left[\overleftrightarrow{\mathbf{G}}(\mathbf{r},\mathbf{r}')\mathbf{j}(\mathbf{r}') - \frac{1}{k^2}\left(\nabla\cdot\left[\nabla g_0(\mathbf{r},\mathbf{r}')\right]\right)\mathbf{j}(\mathbf{r})\right]\,d^3r' - \frac{1}{k^2}\overleftrightarrow{\mathbf{L}}\mathbf{j}(\mathbf{r})\Bigg\}.\end{aligned} \tag{2.42}$$

Here $\overleftrightarrow{\mathbf{L}}$ denotes the *source dyadic*

$$\overleftrightarrow{\mathbf{L}} = \frac{1}{4\pi} \oint_{\partial V^\star} \frac{\mathbf{R} \otimes \hat{\mathbf{n}}}{R^3} d^2 r' \tag{2.43}$$

which accounts for the depolarization of the excluded volume $V^\star$ and turns out to depend entirely on the geometry of the principal volume not on its size or position [10].

3 Scattering of Light

Up to now we have derived the formal solution to the vector Helmholtz equation under the assumption that the current density distribution $\mathbf{j}$ is known. However, if one discusses the problem of light scattering on a material body the current density distribution is not given but rather induced by the electric field.

In section (3.1) the expression relating the induced current density and the total electric field are derived leading to the *volume integral equation* whose self-consistent solution is the electric field. For deeper discussions of the material presented in this section the interested reader is referred to textbooks such as [3, 7].

Section (3.2) outlines the derivation of the formal solution to plane wave scattering on infinite long cylinders which can also be found in textbooks, for example in [11]. This chapter is finalized with section (3.3) where the total scattering cross section is defined.

3.1 Volume Equivalence Theorem and The Volume Integral Equation

The electric field $\mathbf{E}_0$ in free space generated by a source current density $\mathbf{j}$ is given by a solution of the inhomogeneous vector Helmholtz equation (1.40)

$$\nabla \times \nabla \times \mathbf{E}_0 - k^2 \mathbf{E}_0 = i\omega\mu_0 \mathbf{j}. \tag{3.1}$$

In the presence of a dielectric medium represented by a space dependent relative permittivity $\epsilon_r(\mathbf{r})$ the same source $\mathbf{j}$ generates the electric field $\mathbf{E}$ governed by

$$\nabla \times \nabla \times \mathbf{E} - k^2 \epsilon_r(\mathbf{r}) \mathbf{E} = i\omega\mu_0 \mathbf{j}. \tag{3.2}$$

Subtracting (3.2) from (3.1) one obtains

$$\nabla \times \nabla \times (\mathbf{E} - \mathbf{E}_0) - k^2 \left(\epsilon_r(\mathbf{r})\mathbf{E} - \mathbf{E}_0\right) = 0 \tag{3.3}$$

Now it is reasonable to define the scattered electric field $\mathbf{E}_s$ to be the difference

$$\mathbf{E}_s = \mathbf{E} - \mathbf{E}_0 \tag{3.4}$$

which vanishes if there is no medium present. Substituting this definition in equation (3.3) it can be rewritten in terms of the scattered field as

$$\begin{aligned} \nabla \times \nabla \times \mathbf{E}_s - k^2 \mathbf{E}_s &= k^2 \left(\epsilon_r(\mathbf{r}) - 1\right) \mathbf{E} \\ &= i\omega\mu_0 \mathbf{j}_{eq}. \end{aligned} \tag{3.5}$$

Equation (3.5) states that the electric field $\mathbf{E}_s$ scattered by a scatterer is generated by the equivalent current density

$$\mathbf{j}_{eq} \;=\; -i\omega\epsilon_0 \left(\epsilon_r(\mathbf{r}) - 1\right) \mathbf{E} \tag{3.6}$$

which exists only in the region where $\epsilon_r \neq 1$, that is inside the scatterer. By using the equivalent volume current $\mathbf{j}_{eq}$ as a source in equation (2.42) and taking into account (3.4) one obtains the volume integral equation

$$\begin{aligned} \mathbf{E}(\mathbf{r}) = \mathbf{E}_0(\mathbf{r}) &+ k^2 \int_{V-V^\star} \Delta\epsilon(\mathbf{r}') \overleftrightarrow{\mathbf{G}}(\mathbf{r}, \mathbf{r}') \mathbf{E}(\mathbf{r}') d^3 r' \\ &+ \int_{V^\star} \left[k^2 \Delta\epsilon(\mathbf{r}') \overleftrightarrow{\mathbf{G}}(\mathbf{r}, \mathbf{r}') \mathbf{E}(\mathbf{r}') - \Delta\epsilon(\mathbf{r}) \left(\nabla \cdot \left[\nabla g_0(\mathbf{r}, \mathbf{r}') \right] \right) \mathbf{E}(\mathbf{r}) \right] d^3 r' \\ &- \Delta\epsilon(\mathbf{r}) \overleftrightarrow{\mathbf{L}} \mathbf{E}(\mathbf{r}) \end{aligned} \tag{3.7}$$

where $\Delta\epsilon = \epsilon_r - 1$ denotes the permittivity contrast between the medium and the background. The self-consistent solution $\mathbf{E}(\mathbf{r})$ of (3.7) is thus the total electric field due to scattering of the incident field $\mathbf{E}_0$ on the scatterer described by $\epsilon_r(\mathbf{r})$.

3.2 Scattering on an Infinitely Long Cylinder

A physically realizable time-harmonic electromagnetic field with complex amplitudes $(\mathbf{E}, \mathbf{H})$ in a linear, isotropic, homogeneous, source free medium must satisfy the homogeneous vector Helmholtz equations as was shown in section 1.4

$$\nabla^2 \mathbf{E} + k^2 \epsilon_r \mathbf{E} = 0 \tag{3.8}$$

$$\nabla^2 \mathbf{H} + k^2 \epsilon_r \mathbf{H} = 0 \tag{3.9}$$

and must be divergence-free. Additionally $\mathbf{E}$ and $\mathbf{H}$ are connected via Maxwell's equations (1.9) and (1.10)

$$\nabla \times \mathbf{E} = i\omega\mu_0\mathbf{H} \tag{3.10}$$

$$\nabla \times \mathbf{H} = -i\omega\epsilon_0\epsilon_r\mathbf{E} \tag{3.11}$$

If one applies the Helmholtz operator $\nabla^2 + k^2\epsilon_r$ on the divergence-free vector function

$$\mathbf{M} = \nabla \times (\mathbf{c}\psi) = -\mathbf{c} \times \nabla\psi \tag{3.12}$$

with ψ being a scalar function and $\mathbf{c}$ an arbitrary constant vector one obtains

$$\nabla^2\mathbf{M} + k^2\epsilon_r\mathbf{M} = \nabla \times \left[\mathbf{c}\left(\nabla^2\psi + k^2\epsilon_r\psi\right)\right] \tag{3.13}$$

by applying the vector identity (1.45) twice. Therefore, $\mathbf{M}$ satisfies the homogeneous vector Helmholtz equation if ψ is a solution to the scalar wave equation

$$\nabla^2\psi + k^2\epsilon_r\psi = 0. \tag{3.14}$$

Another divergence-free vector function $\mathbf{N}$ proportional to $\nabla \times \mathbf{M}$ can be defined as

$$\mathbf{N} = \frac{\nabla \times \mathbf{M}}{k}. \tag{3.15}$$

It is straightforward to show that $\mathbf{N}$ is a solution of a homogeneous vector Helmholtz equation as long as $\mathbf{M}$ is its solution too. Furthermore, the curl of $\mathbf{N}$ is proportional to $\mathbf{M}$

$$\nabla \times \mathbf{N} = k\epsilon_r\mathbf{M}. \tag{3.16}$$

Thus the *vector harmonics* $\mathbf{M}$ and $\mathbf{N}$ have all the required properties of an electromagnetic field; they are divergence-free, satisfy the vector wave equation and the curl of one of the vector harmonics is proportional to the other one. Therefore the problem of finding solutions to the field equations reduces to the problem of finding solutions ψ of the scalar wave equation (3.14) which reads in cylindrical coordinates (ρ, ϕ, z)

$$\frac{1}{\rho}\frac{\partial}{\partial\rho}\left(\rho\frac{\partial\psi}{\partial\rho}\right) + \frac{1}{\rho^2}\frac{\partial^2\psi}{\partial\phi^2} + \frac{\partial^2\psi}{\partial z^2} + k^2\epsilon_r(\mathbf{r})\psi = 0. \tag{3.17}$$

Considering an infinite cylinder with radius a a solution of (3.17) can be derived in closed analytic form. The space dependent permittivity in this case is given by

$$\epsilon_r(\mathbf{r}) = \epsilon_r(\rho) = \begin{cases} \epsilon_r & \text{for } \rho \leq a \\ 1 & \text{for } \rho > a \end{cases}. \tag{3.18}$$

To simplify the discussion the cylinder region with $\rho \leq a$ and the background region with $\rho > a$ are referred to as region I and region II, respectively. Substituting the separation ansatz

$$\psi(\rho, \phi, z) = f(\rho)g(\phi)h(z) \tag{3.19}$$

in (3.17) and converting the partial derivatives to ordinary ones one obtains

$$\frac{1}{f}\frac{d^2 f}{d\rho^2} + \frac{1}{f}\frac{1}{\rho}\frac{df}{d\rho} + \frac{1}{g}\frac{1}{\rho^2}\frac{d^2 g}{d\phi^2} + k^2\epsilon_r = -\frac{1}{h}\frac{d^2 h}{dz^2} \tag{3.20}$$

Only the term on the right hand side depends on z. To fulfill (3.20) for every z the right hand side must be a constant. Choosing the constant to be k_z^2, h has to solve

$$\frac{d^2 h}{dz^2} = -k_z^2 h. \tag{3.21}$$

Substituting this back into (3.20) one obtains

$$\frac{\rho^2}{f}\frac{d^2 f}{d\rho^2} + \frac{\rho}{f}\frac{df}{dr} + \frac{1}{g}\frac{d^2 g}{d\phi^2} + \left(k^2\epsilon_r - k_z^2\right)\rho^2 = 0 \tag{3.22}$$

Now the ϕ-dependence is contained only in the third term on the left hand side of (3.22) and one can use the argument from above to postulate

$$\frac{d^2 g}{d\phi^2} = -n^2 g. \tag{3.23}$$

with $n \in \mathbb{Z}$ because $g(\phi)$ has to be periodic. With this substitution one finally obtains

$$\rho^2\frac{d^2 f}{d\rho^2} + \rho\frac{df}{d\rho} + \left[(k_\rho\rho)^2 - n^2\right] f = 0 \tag{3.24}$$

with

$$k_\rho^2 = k^2\epsilon_r - k_z^2. \tag{3.25}$$

Equation (3.24) is recognized as the Bessel differential equation whose linearly independent solutions are the Bessel functions of first and second kind, J_n and Y_n, of integral

order n [11]. Possible solutions of equations (3.21) and (3.23) are exponential functions. Therefore, the solution of (3.17) can be written as

$$\psi_n(\rho, \phi, z) = Z_n(k_\rho \rho) e^{in\phi} e^{ik_z z} \tag{3.26}$$

where $Z_n(k_\rho \rho)$ is a solution of the Bessel equation (3.24). The solution in region I must be regular at $\rho = 0$, which means that $Z_n^{(\mathrm{I})}(k_\rho \rho)$ has to be proportional to $J_n(k_\rho \rho)$. In region II the solution must be an outward traveling wave regular in the limit $\rho \to \infty$. A solution of Bessel's differential equation which fulfills these requirements is given by the Hankel function of the first kind $H_n^{(1)}(k_\rho \rho) = J_n(k_\rho \rho) + iY_n(k_\rho \rho)$. Therefore $Z_n^{(\mathrm{II})}(k_\rho \rho)$ has to be proportional to $H_n^{(1)}(k_\rho \rho)$ [11].

Form the solutions of the scalar Helmholtz equation ψ_n, full wave solutions can be generated using equations (3.12) and (3.15) with $\mathbf{c} = \hat{\mathbf{z}}$. Thus the electromagnetic field in region I can be expanded as

$$\mathbf{E}^{(\mathrm{I})} = \sum_{n=-\infty}^{\infty} E_n \left(a_n \mathbf{M}_n^{(\mathrm{I})} + b_n \mathbf{N}_n^{(\mathrm{I})} \right) \tag{3.27}$$

$$\mathbf{H}^{(\mathrm{I})} = \frac{k}{i\omega\mu_0} \sum_{n=-\infty}^{\infty} E_n \left(a_n \mathbf{N}_n^{(\mathrm{I})} + \epsilon_r b_n \mathbf{M}_n^{(\mathrm{I})} \right) \tag{3.28}$$

and the scattered field in region II as

$$\mathbf{E}_s = \sum_{n=-\infty}^{\infty} E_n \left(c_n \mathbf{M}_n^{(\mathrm{II})} + d_n \mathbf{N}_n^{(\mathrm{II})} \right) \tag{3.29}$$

$$\mathbf{H}_s = \frac{k}{i\omega\mu_0} \sum_{n=-\infty}^{\infty} E_n \left(c_n \mathbf{N}_n^{(\mathrm{II})} + d_n \mathbf{M}_n^{(\mathrm{II})} \right) \tag{3.30}$$

with unknown constants $\{E_n, a_n, b_n, c_n, d_n\}$. The vector harmonics $\left\{ \mathbf{M}_n^{(\mathrm{I})}, \mathbf{N}_n^{(\mathrm{I})} \right\}$ and $\left\{ \mathbf{M}_n^{(\mathrm{II})}, \mathbf{N}_n^{(\mathrm{II})} \right\}$ in regions I and II are generated by $\psi_m^{(\mathrm{I})} \propto J_n(k_\rho \rho)$ and $\psi_m^{(\mathrm{II})} \propto H_n^{(1)}(k_\rho \rho)$ respectively. The total field $\left(\mathbf{E}^{(\mathrm{II})}, \mathbf{H}^{(\mathrm{II})} \right)$ in region II is given by the sum of the scattered field $(\mathbf{E}_s, \mathbf{H}_s)$ and the incident field $(\mathbf{E}_i, \mathbf{H}_i)$. Having an explicit expression of the incident field $(\mathbf{E}_i, \mathbf{H}_i)$ expanded in vector harmonics, physical boundary conditions (1.51) and (1.52) enforced on the cylinder's interface $\rho = a$ enables the determination of the unknown constants $\{E_n, a_n, b_n, c_n, d_n\}$ and the scattering problem is completely solved.

An incident plane wave $\mathbf{E}_i = \mathbf{E}_0 e^{ik\hat{\mathbf{k}} \cdot \mathbf{r}}$ propagating in the direction $\hat{\mathbf{k}} = -\sin\xi \hat{\mathbf{x}} - \cos\xi \hat{\mathbf{z}}$, where ξ is the angle between the incident wave and the positive z-axis (incident angle), can be decomposed into two orthogonal polarizations where the one with the

electric field polarized parallel to the xz-plane (incident plane) is given as an expansion in vector harmonics by [11]

$$\mathbf{E}_i^{(\parallel)} = \sum_{n=-\infty}^{\infty} E_n^{\parallel} \mathbf{N}_n^{(i)} \tag{3.31}$$

$$\mathbf{H}_i^{(\parallel)} = \frac{k}{i\omega\mu_0} \sum_{n=-\infty}^{\infty} E_n^{\parallel} \mathbf{M}_n^{(i)} \tag{3.32}$$

and the one with electric field polarized orthogonal to the xz-plane by

$$\mathbf{E}_i^{(\perp)} = -i \sum_{n=-\infty}^{\infty} E_n^{\perp} \mathbf{M}_n^{(i)} \tag{3.33}$$

$$\mathbf{H}_i^{(\perp)} = -\frac{k}{\omega\mu_0} \sum_{n=-\infty}^{\infty} E_n^{\perp} \mathbf{N}_n^{(i)} \tag{3.34}$$

where the vector harmonics in both cases are generated by $\psi_n^{(i)} = J_n(k\rho \sin\xi) e^{in\phi} e^{-kz\cos\xi}$ and

$$E_n^{\parallel,\perp} = E_0^{\parallel,\perp} \frac{(-i)^n}{k \sin\xi}. \tag{3.35}$$

In order to satisfy the continuity of the tangential field components (boundary conditions (1.51) and (1.52)) for all values of z on the cylinder's interface, k_z in the generating functions $\psi_m^{(\mathrm{I})}$ and $\psi_m^{(\mathrm{II})}$ has to be equal to the one of the incident field, that is $k_z = -k\cos\xi$. Now the system of equations to determine the constants $\{E_n, a_n, b_n, c_n, d_n\}$ is complete and can in principle be solved.

3.3 The Total Scattering Cross Section

The total scattering cross section σ_s is defined as total time averaged radiated scattered power divided by the norm of the time averaged incident Poynting vector, that is

$$\sigma_s = \frac{\oint_S d^2r\, \hat{\mathbf{n}} \cdot \langle \mathbf{S}_{scat} \rangle}{|\langle \mathbf{S}_{inc} \rangle|}, \tag{3.36}$$

where the integration has to be performed over the closed surface S. $\hat{\mathbf{n}}$ denotes the unit normal pointing out of the surface. If one chooses the surface S to be a sphere far away from the scattering region, one can be sure that the outward traveling scattering wave is transverse. The electric and magnetic field in a transverse electromagnetic wave in

vacuum are related to each other according to

$$\mathbf{H} = \hat{\mathbf{k}} \times \frac{\mathbf{E}}{Z_0} \tag{3.37}$$

where $Z_0 = \sqrt{\mu_0/\epsilon_0}$ denotes the vacuum impedance and $\hat{\mathbf{k}}$ the unit vector in propagation direction. If the incident light is a monochromatic plane wave it is transverse too and the time averaged Pointing vector is given by $\langle \mathbf{S} \rangle = \frac{1}{2} \Re \{ \mathbf{E} \times \mathbf{H}^\star \}$ (see equation 1.37) so that

$$\sigma_s \quad = \quad \frac{\Re \left\{ \oint_S d^2 r \, \hat{\mathbf{n}} \cdot \left[\mathbf{E}_s \times \left(\hat{\mathbf{k}} \times \mathbf{E}_s^\star \right) \right] \right\}}{\left| \Re \left\{ \mathbf{E}_i \times \left(\hat{\mathbf{k}}_i \times \mathbf{E}_i^\star \right) \right\} \right|}. \tag{3.38}$$

Using the vector identity $\mathbf{a} \times (\mathbf{b} \times \mathbf{c}) = \mathbf{b} (\mathbf{a} \cdot \mathbf{c}) - \mathbf{c} (\mathbf{a} \cdot \mathbf{b})$ and the facts that $\mathbf{E} \perp \mathbf{k}$ as well as $\hat{\mathbf{k}} = \hat{\mathbf{n}}$ for a spherical surface at infinity equation (3.38) reduces to

$$\sigma_s = \frac{\oint_S d^2 r \, |\mathbf{E}_s|^2}{|\mathbf{E}_i|^2}. \tag{3.39}$$

4 Principles of Photonic Crystals

The goal of this chapter is to provide the physical ideas and mathematical tools used in the discussion of electromagnetic wave propagation in periodic dielectric media, *photonic crystals*. After rewriting the vector Helmholtz equation in a way that one can identify an Hermitian differential operator (section 4.1) which enables the solution to be expanded in eigenfunctions (so-called eigenmodes or eigenwaves), the influence of periodicity in ϵ_r on the eigenmodes is discussed. Specifically, *Bloch 's theorem* and Bloch's form of eigenwaves are presented in section (4.4). Based on Bloch's theorem the existence of a *band structure* and its symmetries are proven and the *Brillouin zone* is defined. Finally the *retarded Green's function* enabling the formal solution of the vector Helmholtz equation is derived in section (4.5). The chapter should not be considered as a comprehensive introduction to the theory of electromagnetic wave propagation in photonic crystals but rather as a minimal introduction sufficient for the appreciation of the results presented in this thesis. For more details the reader is referred to existing textbooks on the topic such as [12, 13].

4.1 The Wave Equation

The inhomogenous vector Helmholtz equation (1.40) governing the electric field generated by the current density $\mathbf{j}$ can be transformed by dividing through ϵ_r into

$$\frac{1}{\epsilon_r(\mathbf{r})}\nabla\times\nabla\times\mathbf{E}=\frac{\omega^2}{c^2}\mathbf{E}+\frac{i\omega\mu_0}{\epsilon_r(\mathbf{r})}\mathbf{j}. \tag{4.1}$$

By defining a new field $\mathbf{Q}(\mathbf{r})$ via

$$\mathbf{Q}(\mathbf{r})=\sqrt{\epsilon_r(\mathbf{r})}\mathbf{E}(\mathbf{r}) \tag{4.2}$$

equation (4.1) can be written in terms of $\mathbf{Q}$ as

$$\left(\mathcal{H}-\frac{\omega^2}{c^2}\right)\mathbf{Q}=\frac{i\omega\mu_0}{\sqrt{\epsilon_r(\mathbf{r})}}\mathbf{j}, \tag{4.3}$$

with the operator $\mathcal{H}$ defined by

$$\mathcal{H}\mathbf{Q} = \frac{1}{\sqrt{\epsilon_r(\mathbf{r})}}\left(\nabla \times \left(\nabla \times \frac{1}{\sqrt{\epsilon_r(\mathbf{r})}}\mathbf{Q}\right)\right). \tag{4.4}$$

The motivation for this reformulation in terms of $\mathbf{Q}$ is that the differential operator $\mathcal{H}$ is Hermitian for real ϵ_r [12] whereas the original vector Helmholtz operator is not. An operator $\mathcal{L}$ is called Hermitian if $\langle \mathcal{L}\mathbf{F}, \mathbf{G}\rangle = \langle \mathbf{F}, \mathcal{L}\mathbf{G}\rangle$ holds for arbitrary vector fields $\mathbf{F}(\mathbf{r})$ and $\mathbf{G}(\mathbf{r})$. Here the inner product $\langle ., .\rangle$ of the two complex vectorial functions $\mathbf{F}$ and $\mathbf{G}$ is defined by

$$\langle \mathbf{F}, \mathbf{G}\rangle = \int d^3r\, \mathbf{F}(\mathbf{r}) \cdot \mathbf{G}^\star(\mathbf{r}), \tag{4.5}$$

where $\mathbf{G}^\star$ denotes the complex conjugate of $\mathbf{G}$. Using the vector identity

$$\nabla \cdot (\mathbf{a} \times \mathbf{b}) = (\nabla \times \mathbf{a}) \cdot \mathbf{b} - \mathbf{a} \cdot (\nabla \times \mathbf{b}), \tag{4.6}$$

Gauss's theorem (A.3), and the definition of the inner product one derives

$$\begin{aligned}\langle \mathcal{H}\mathbf{Q}_i, \mathbf{Q}_j\rangle &= \int_V d^3r \left[\nabla \times \left(\nabla \times \frac{\mathbf{Q}_i^\star}{\sqrt{\epsilon_r}}\right)\right] \cdot \frac{\mathbf{Q}_j}{\sqrt{\epsilon_r}} \\ &= \oint_{\partial V} d^2r \left[\left(\nabla \times \frac{\mathbf{Q}_i^\star}{\sqrt{\epsilon_r}}\right) \times \frac{\mathbf{Q}_j}{\sqrt{\epsilon_r}}\right] \cdot \hat{\mathbf{n}} + \int_V d^3r \left(\nabla \times \frac{\mathbf{Q}_i^\star}{\sqrt{\epsilon_r}}\right) \cdot \left(\nabla \times \frac{\mathbf{Q}_j}{\sqrt{\epsilon_r}}\right).\end{aligned} \tag{4.7}$$

Here the $\mathbf{Q}_i$'s with subscript $i \in \{0, 1, 2, ..., \infty\}$ denotes the eigenfunctions of $\mathcal{H}$ defined by the eigenvalue equation

$$\mathcal{H}\mathbf{Q}_i(\mathbf{r}) = \frac{\omega_i^2}{c^2}\mathbf{Q}_i(\mathbf{r}). \tag{4.8}$$

Imposing periodic boundary conditions on ∂V (see section 4.4), the surface integral vanishes. Applying identity (4.6) a second time one obtains

$$\begin{aligned}\langle \mathcal{H}\mathbf{Q}_i, \mathbf{Q}_j\rangle &= \int_V d^3r\, \frac{\mathbf{Q}_i^\star}{\sqrt{\epsilon_r}} \cdot \left[\nabla \times \left(\nabla \times \frac{\mathbf{Q}_j}{\sqrt{\epsilon_r}}\right)\right] \\ &= \langle \mathbf{Q}_i, \mathcal{H}\mathbf{Q}_j\rangle\end{aligned} \tag{4.9}$$

which implies that $\mathcal{H}$ is an *Hermitian operator*. It is easy to show that (i) the eigenvalues of an Hermitian operator are real and that (ii) its eigenfunctions constitute an orthogonal complete set [4]. This has two consequences (i) ω_i^2 is a real quantity for every $i \in \{0, 1, 2, ..., \infty\}$ and (ii) that the set of eigenfunctions $\mathbf{Q}_i$ can be used to expand the

solution $\mathbf{Q}$ of equation (4.3). Inspecting again (4.7) with $j = i$ which yields

$$\begin{aligned}\langle \mathcal{H}\mathbf{Q}_i, \mathbf{Q}_i \rangle &= \frac{\omega_i^2}{c^2} \langle \mathbf{Q}_i, \mathbf{Q}_i \rangle \\ &= \int_V d^3r \, \frac{1}{\epsilon_r} \left| \nabla \times \frac{\mathbf{Q}_i}{\sqrt{\epsilon_r}} \right|^2 \end{aligned} \tag{4.10}$$

one can see that $\omega_i^2 \geq 0$. Therefore the eigenfrequencies ω_i are real. Because eigenfunctions with eigenfrequencies ω_i and $-\omega_i$ are identical one can restrict the eigenfrequencies to be non-negative. As long as $\omega_i \neq 0$ it holds

$$\begin{aligned}\nabla \cdot \left(\sqrt{\epsilon_r(\mathbf{r})} \mathbf{Q}_i \right) &= \frac{c^2}{\omega_i^2} \nabla \cdot \left(\nabla \times \left(\nabla \times \frac{1}{\sqrt{\epsilon_r(\mathbf{r})}} \mathbf{Q}_i \right) \right) \\ &\equiv 0. \end{aligned} \tag{4.11}$$

That's why the corresponding eigenmodes are called *quasi-transverse* and will be labeled by (T). Additionally there exist eigenmodes with eigenfrequencies $\omega_i = 0$. They are solutions to

$$\nabla \times \left(\frac{1}{\sqrt{\epsilon_r(\mathbf{r})}} \mathbf{Q}_i \right) = 0 \tag{4.12}$$

and because (4.11) is not fulfilled by these modes they are called *quasi-longitudinal* and they will be labeled by (L). It is important to mention that only the set $\left\{ \mathbf{Q}_i^{(T)}, \mathbf{Q}_i^{(L)} \right\}$ is complete and so this set has to be used as the basis for an expansion.

4.2 Translational Symmetry

Being an optical analogy of crystalline solids, a periodic medium (*photonic crystal*) is a space lattice built of basic blocks, "atoms", with macroscopic dimensions. The lattice is characterized by *translational symmetry*. This means that there exists a basis $\{\mathbf{a}_1, \mathbf{a}_2, \mathbf{a}_3\}$ such that the structure remains invariant under translation with any vector build by an integer linear combination of these basis vectors. If one chooses a basis $\{\hat{\mathbf{a}}_1, \hat{\mathbf{a}}_2, \hat{\mathbf{a}}_3\}$ in such a way, that, if the origin of the coordinate system coincides with a lattice site, the position vector of any other site is given by

$$\mathbf{R} = l_1 \hat{\mathbf{a}}_1 + l_2 \hat{\mathbf{a}}_2 + l_3 \hat{\mathbf{a}}_3 \tag{4.13}$$

where l_α, $\alpha = 1, 2, 3$ are integers, the parallelepiped spanned by the basis is called *unit cell* and the basis vectors $\{\mathbf{a}_1, \mathbf{a}_2, \mathbf{a}_3\}$ primitive unit vectors.

4.3 Periodic Functions and Reciprocal Lattices

A dielectric non-magnetic photonic crystal is described solely by its dielectric function, which, reflecting the translation symmetry of the lattice, must be periodic

$$\epsilon_r(\mathbf{r}+\mathbf{R}) = \epsilon_r(\mathbf{r}) \tag{4.14}$$

for all points $\mathbf{r}$ in space and for all lattice translations $\mathbf{R}$ (4.13). Because of its periodicity we can expand the dielectric function in a Fourier series

$$\epsilon_r(\mathbf{r}) = \sum_{\mathbf{G}} \epsilon_r(\mathbf{G}) e^{i\mathbf{G}\cdot\mathbf{r}}. \tag{4.15}$$

where the $\mathbf{G}$'s are wave-vectors with units $[m^{-1}]$. The periodicity condition (4.14) restricts the wave vectors $\mathbf{G}$ in the Fourier series. The allowed ones have to fulfill the condition

$$\exp(i\mathbf{G}\cdot\mathbf{R}) = 1 \;\Leftrightarrow\; \mathbf{G}\cdot\mathbf{R} = 2\pi n \tag{4.16}$$

for all lattice vectors $\mathbf{R}$ and integers n. $\mathbf{G}$'s which fulfill this condition are called *reciprocal lattice vectors*. One defines a basis $\{\hat{\mathbf{b}}_1, \hat{\mathbf{b}}_2, \hat{\mathbf{b}}_3\}$ in the space of reciprocal lattice vectors, the so called *reciprocal space* by

$$\hat{\mathbf{a}}_\alpha \cdot \hat{\mathbf{b}}_\beta = 2\pi\delta_{\alpha\beta}\,, \quad \alpha,\beta = 1,2,3 \tag{4.17}$$

where the $\hat{\mathbf{a}}$'s are primitive unit vectors of the real lattice and δ_{ij} the Kronecker delta function defined by $\delta_{ii} = 1$ and $\delta_{ij} = 0$ for $i \neq j$. Condition (4.16) is fulfilled if $\mathbf{G}$ is given by an integer linear combination of $\{\hat{\mathbf{b}}_1, \hat{\mathbf{b}}_2, \hat{\mathbf{b}}_3\}$. Therefore the reciprocal space is a periodic lattice too.

In summary, when the Fourier series of a lattice-periodic function $\epsilon_r(\mathbf{r})$ is taken, we only need to include terms with wave vectors that are reciprocal lattice vectors.

4.4 Translation Symmetry and Bloch's Theorem

If the dielectric function is lattice-periodic (4.14), the differential operator $\mathcal{H}$ (4.4) is also lattice-periodic, that means

$$\mathcal{H}(\mathbf{r}+\mathbf{R}) = \mathcal{H}(\mathbf{r}) \tag{4.18}$$

for all points $\mathbf{r}$ in space and for all lattice translations $\mathbf{R}$ (4.13). For every $\mathbf{R}$ we can introduce the *translation operator* $T_{\mathbf{R}}$ such that

$$T_{\mathbf{R}} f(\mathbf{r}) = f(\mathbf{r} + \mathbf{R}) \tag{4.19}$$

where $f(\mathbf{r})$ is an arbitrary function. Then an application of $T_{\mathbf{R}}$ to the eigenvalue equation (4.8) gives

$$\begin{aligned} T_{\mathbf{R}} \mathcal{H}(\mathbf{r}) \mathbf{Q}_i(\mathbf{r}) &= \mathcal{H}(\mathbf{r} + \mathbf{R}) \mathbf{Q}_i(\mathbf{r} + \mathbf{R}) \\ &= \mathcal{H}(\mathbf{r}) \mathbf{Q}_i(\mathbf{r} + \mathbf{R}) \\ &= \mathcal{H}(\mathbf{r}) T_{\mathbf{R}} \mathbf{Q}_i(\mathbf{r}). \end{aligned} \tag{4.20}$$

This simply means that $T_{\mathbf{R}}$ commutes with $\mathcal{H}$. Thus the operators $\mathcal{H}$ and $T_{\mathbf{R}}$ have a common system of eigenfunctions (e.g. [14]):

$$\begin{aligned} \mathcal{H} \mathbf{Q}_i(\mathbf{r}) &= \frac{\omega_i^2}{c^2} \mathbf{Q}_i(\mathbf{r}) \\ T_{\mathbf{R}} \mathbf{Q}_i(\mathbf{r}) &= c(\mathbf{R}) \mathbf{Q}_i(\mathbf{r}) \end{aligned} \tag{4.21}$$

Applying two successive translations to the eigenfunction $\mathbf{Q}_i(\mathbf{r})$ we get

$$\begin{array}{ccccc} T_{\mathbf{R}} T_{\mathbf{R}'} \mathbf{Q}_i(\mathbf{r}) & = & c(\mathbf{R}) T_{\mathbf{R}'} \mathbf{Q}_i(\mathbf{r}) & = & c(\mathbf{R}) c(\mathbf{R}') \mathbf{Q}_i(\mathbf{r}) \\ \| & & & & \\ T_{\mathbf{R}+\mathbf{R}'} \mathbf{Q}_i(\mathbf{r}) & = & c(\mathbf{R} + \mathbf{R}') \mathbf{Q}_i(\mathbf{r}) & & \end{array} \tag{4.22}$$

It can be seen that the eigenvalues of the translation operator have to obey

$$c(\mathbf{R} + \mathbf{R}') = c(\mathbf{R}) c(\mathbf{R}') \tag{4.23}$$

which is fulfilled if one chooses

$$c(\mathbf{R}) = e^{i\mathbf{k}\cdot\mathbf{R}}. \tag{4.24}$$

Up to now $\mathbf{k}$ can be any wave vector, i.e. any linear combination of the reciprocal basis vectors $\left\{\hat{\mathbf{b}}_1, \hat{\mathbf{b}}_2, \hat{\mathbf{b}}_3\right\}$ but for the eigenfunctions $\mathbf{Q}_i(\mathbf{r})$ to fulfill periodic boundary condition in each space direction

$$\begin{aligned} \mathbf{Q}_i(\mathbf{r} + N_\alpha \hat{\mathbf{a}}_\alpha) &= \mathbf{Q}_i(\mathbf{r}) \\ &= e^{iN_\alpha \mathbf{k}\cdot\hat{\mathbf{a}}_\alpha} \mathbf{Q}_i(\mathbf{r}) \end{aligned} \tag{4.25}$$

with $\alpha \in \{1,2,3\}$, a set of integers N_α, and the lattice basis vectors $\hat{\mathbf{a}}_\alpha$, $\mathbf{k}$ must be a reciprocal lattice vector

$$\mathbf{k} = \sum_{\alpha=1}^{3} m_\alpha \hat{\mathbf{b}}_\alpha \tag{4.26}$$

with integer m_α. Therefore

$$T_{\mathbf{R}} Q_i(\mathbf{r}) = e^{i\mathbf{k}\cdot\mathbf{R}} Q_i(\mathbf{r}) \tag{4.27}$$

with $\mathbf{k}$ being a reciprocal lattice vector, must hold for every eigenfunction $\mathbf{Q}_i(\mathbf{r})$ of a translational invariant operator. Equation (4.27) is known as *Bloch's theorem*.

4.4.1 Bloch Eigenwaves

There is another common way to formulate *Bloch's theorem*: The eigenfunction $\mathbf{Q}_i(\mathbf{r})$ of a translational invariant operator, can be chosen to have the form of a plane wave times a vector function $\mathbf{q}_\mathbf{k}(\mathbf{r})$ having the periodicity of the lattice, i.e.

$$\mathbf{Q}_i(\mathbf{r}) = \mathbf{q}_\mathbf{k}(\mathbf{r}) e^{i\mathbf{k}\cdot\mathbf{r}} \tag{4.28}$$

with

$$\mathbf{q}_\mathbf{k}(\mathbf{r}+\mathbf{R}) = \mathbf{q}_\mathbf{k}(\mathbf{r}) \tag{4.29}$$

for all points $\mathbf{r}$ in space and all lattice translations $\mathbf{R}$. This can be seen by substituting (4.28) in (4.27)

$$T_{\mathbf{R}} \mathbf{Q}_i(\mathbf{r}) = \mathbf{q}_\mathbf{k}(\mathbf{r}+\mathbf{R}) e^{i\mathbf{k}\cdot(\mathbf{r}+\mathbf{R})} = e^{i\mathbf{k}\cdot\mathbf{R}} \mathbf{q}_\mathbf{k}(\mathbf{r}) e^{i\mathbf{k}\cdot\mathbf{r}}, \tag{4.30}$$

which holds if $\mathbf{q}_\mathbf{k}(\mathbf{r})$ is a lattice periodic function. Eigenfunctions of the eigenvalue problem (4.8) in the form (4.28) are called Bloch eigenwaves, or simply, *Bloch waves*. They are the eigenmodes of a periodic medium and form a complete set of orthogonal functions which can be used to expand any solution of the eigenvalue problem (4.8) .

4.4.2 Existence of Photonic Band Structure

Imposing eigenfunctions in the Bloch form

$$\mathbf{Q}_{\mathbf{k}n}(\mathbf{r}) = \mathbf{q}_{\mathbf{k}n}(\mathbf{r}) e^{i\mathbf{k}\cdot\mathbf{r}}, \tag{4.31}$$

the lattice periodic function $\mathbf{q}_{\mathbf{k}n}(\mathbf{r})$ is determined by the eigenvalue problem

$$\frac{1}{\sqrt{\epsilon_r(\mathbf{r})}}\Big[(\nabla + i\mathbf{k}) \times \Big[(\nabla + i\mathbf{k}) \times \frac{1}{\sqrt{\epsilon(\mathbf{r})}}\mathbf{q}_{\mathbf{k}n}(\mathbf{r})\Big]\Big] = \frac{\omega_{\mathbf{k}n}^2}{c^2}\mathbf{q}_{\mathbf{k}n}(\mathbf{r}) \tag{4.32}$$

which justifies the use of the parameter $\mathbf{k}$ as a label for the eigenfunctions. There could be many solutions for a given $\mathbf{k}$ which are labeled in increasing order of their corresponding discrete eigenvalues by the index $n \in \{1, 2, \ldots, \infty\}$, the so called *band index* [12]. Because of the lattice periodicity of $\mathbf{q}_{\mathbf{k}n}$ we can regard (4.32) as an Hermitian eigenvalue problem restricted to a single unit cell of the crystal. Each of the discrete eigenvalues is expected to vary continuously as the wave vector varies. In this way, a family of continuous functions, the *dispersion relation*, $\omega = \omega_n(\mathbf{k})$ is defined. The information contained in the dispersion relation is called the *photonic band structure* of the photonic crystal.

4.4.3 Brillouin Zone

One important feature of Bloch waves is that different values of the wave vector $\mathbf{k}$ do not necessarily lead to different eigenwaves. In fact, for an eigenwave with the wave vector $\mathbf{k} = \mathbf{k}' + \mathbf{G}$, where $\mathbf{G}$ is a reciprocal lattice vector, Bloch's theorem (4.27) reads

$$\begin{aligned}\mathbf{Q}_{\mathbf{k}n}(\mathbf{r} + \mathbf{R}) &= e^{i(\mathbf{k}'+\mathbf{G})\cdot\mathbf{R}}\mathbf{Q}_{\mathbf{k}n}(\mathbf{r}) \\ &= e^{i\mathbf{k}'\cdot\mathbf{R}}e^{i\mathbf{G}\cdot\mathbf{R}}\mathbf{Q}_{\mathbf{k}n}(\mathbf{r}) \\ &= e^{i\mathbf{k}'\cdot\mathbf{R}}\mathbf{Q}_{\mathbf{k}n}(\mathbf{r}).\end{aligned} \tag{4.33}$$

The last equality is due to the definition of the reciprocal lattice vector $\mathbf{G}$ (4.16). In other words, relation (4.33) states that the eigenmode $\mathbf{Q}_{\mathbf{k}n}(\mathbf{r})$ satisfies Bloch's theorem (4.27) for a wave vector $\mathbf{k}'$. So the original label $\mathbf{k}$ is not unique. Therefore, every eigenmode has a whole group of possible wave vectors, differing from one another by the vectors of the reciprocal lattice.

It is common to choose the value of $\mathbf{G}$ in $\mathbf{k} = \mathbf{k}' + \mathbf{G}$ to make $|\mathbf{k}'|$ as small as possible, i.e. to be nearest to the origin of the reciprocal lattice. The zone given by this condition is called the *first Brillouin zone*. It is evident that one can reduce any wave vector $\mathbf{k}$ in the reciprocal space to a point in the first Brillouin zone, so any eigenwave can be characterized by its *reduced wave vector*.

4.4.4 Time-Reversal Symmetry

There is another useful property of photonic bands namely time reversal symmetry. The time reversal symmetry states that any photonic band structure has inversion symmetry even though the crystal structure does not necessarily have it.

Comparing the wave equation (4.32) with its complex conjugate

$$\frac{1}{\sqrt{\epsilon_r(\mathbf{r})}}\Big[(\nabla - i\mathbf{k}) \times \Big[(\nabla - i\mathbf{k}) \times \frac{1}{\sqrt{\epsilon_r(\mathbf{r})}}\mathbf{q}^*_{\mathbf{k}n}(\mathbf{r})\Big]\Big] = \frac{\omega^2_{\mathbf{k}n}}{c^2}\mathbf{q}^*_{\mathbf{k}n}(\mathbf{r}) \tag{4.34}$$

taking into account that eigenfrequencies are real (section 4.1), one can see that the Bloch wave $\mathbf{q}^*_{\mathbf{k}n}(\mathbf{r})$ satisfies the same wave equation as $\mathbf{q}_{\mathbf{k}n}(\mathbf{r})$ (4.32) with exactly the same eigenfrequency, but with the wave vector $-\mathbf{k}$. It follows that

$$\omega_n(\mathbf{k}) = \omega_n(-\mathbf{k}) \tag{4.35}$$

$$\mathbf{q}_{-\mathbf{k}n}(\mathbf{r}) = \mathbf{q}^*_{\mathbf{k}n}(\mathbf{r}). \tag{4.36}$$

So the band structure of the crystal has inversion symmetry even if the crystal itself has not. Taking the complex conjugate of $\mathbf{q}_{\mathbf{k}n}$ is equivalent to reversing the sign of time in the Maxwell equations. So, the properties (4.35) and (4.36) are consequences of the time-reversal symmetry of Maxwell's equations.

4.5 Retarded Green's Function, Solutions of the Wave Equation

To calculate the electric field generated by currents one has to solve the inhomogenous vector Helmholtz equation (1.40) which can be written in the alternative form (4.3)

$$\left(\mathcal{H} - \frac{\omega^2}{c^2}\right)\mathbf{Q} = \tilde{\mathbf{j}} \tag{4.37}$$

with a source

$$\tilde{\mathbf{j}} = \frac{i\omega\mu_0}{\sqrt{\epsilon_r(\mathbf{r})}}\mathbf{j}. \tag{4.38}$$

The eigenmodes $\mathbf{Q}_{\mathbf{k}n}$ of the operator $\mathcal{H}$ form a complete set due to the Hermitian nature of $\mathcal{H}$ (see section 4.1) therefore the solution to (4.37) can be written as a superposition of eigenmodes

$$\mathbf{Q} = \sum_{\mathbf{k},n} c_{\mathbf{k}n}\mathbf{Q}_{\mathbf{k}n} \tag{4.39}$$

with coefficients $c_{\mathbf{k}n}$. Using the eigenvalue equation (4.3) and the form (4.39) of $\mathbf{Q}$, equation (4.37) reads

$$\sum_{\mathbf{k},n} c_{\mathbf{k}n} \left(\frac{\omega_{\mathbf{k}n}^2}{c^2} - \frac{\omega^2}{c^2} \right) \mathbf{Q}_{\mathbf{k}n} = \tilde{\mathbf{j}}. \tag{4.40}$$

If one normalizes the eigenmodes so that

$$\int_V d^3r \, \mathbf{Q}^\star_{\mathbf{k}'n'}(\mathbf{r}) \cdot \mathbf{Q}_{\mathbf{k}n}(\mathbf{r}) = V \delta_{\mathbf{k}'\mathbf{k}} \delta_{n'n} \tag{4.41}$$

where V denotes the volume of the photonic crystal, one derives

$$c_{\mathbf{k}n} = \frac{c^2}{V\left(\omega_{\mathbf{k}n}^2 - \omega^2\right)} \int_V d^3r \, \mathbf{Q}^\star_{\mathbf{k}n}(\mathbf{r}) \cdot \tilde{\mathbf{j}}(\mathbf{r}) \tag{4.42}$$

by multiplying (4.40) with $\mathbf{Q}^\star_{\mathbf{k}'n'}$ and integrating over the volume V. Substituting (4.42) back into (4.39) and using the vector identity $(\mathbf{a}\cdot\mathbf{b})\mathbf{c} = (\mathbf{a} \otimes \mathbf{c})\,\mathbf{b}$ one obtains the solution of equation (4.37) in the form

$$\mathbf{Q}(\mathbf{r}) = \int_V d^3r' \overleftrightarrow{\mathbf{G}}(\mathbf{r}, \mathbf{r}') \tilde{\mathbf{j}}(\mathbf{r}'). \tag{4.43}$$

with the dyadic Green's function $\overleftrightarrow{\mathbf{G}}(\mathbf{r}, \mathbf{r}')$ given by

$$\overleftrightarrow{\mathbf{G}}(\mathbf{r}, \mathbf{r}') = -\frac{c^2}{V} \lim_{\delta \to 0^+} \sum_{\mathbf{k},n} \frac{\mathbf{Q}_{\mathbf{k}n}(\mathbf{r}) \otimes \mathbf{Q}^\star_{\mathbf{k}n}(\mathbf{r}')}{(\omega - \omega_{\mathbf{k}n} + i\delta)\,(\omega + \omega_{\mathbf{k}n} + i\delta)}. \tag{4.44}$$

The infinitesimal positive constant δ is introduced to assure causality in time space as will be shown shortly. The inverse Fourier transform (1.15) applied to the solution in frequency domain (4.43) yields the solution in time domain

$$\mathbf{Q}(\mathbf{r}, t) = \int_V d^3r' \int_{-\infty}^{\infty} dt' \, \overleftrightarrow{\mathcal{G}}(\mathbf{r}, \mathbf{r}', t - t') \mathbf{j}(\mathbf{r}', t') \tag{4.45}$$

with the dyadic Green's function in time domain $\overleftrightarrow{\mathcal{G}}(\mathbf{r},\mathbf{r}',\tau)$ given by the inverse Fourier transform of $\overleftrightarrow{\mathbf{G}}(\mathbf{r},\mathbf{r}')$

$$\begin{aligned}\overleftrightarrow{\mathcal{G}}(\mathbf{r},\mathbf{r}',\tau) &= \frac{1}{2\pi}\int_{-\infty}^{\infty} d\omega\, \overleftrightarrow{\mathbf{G}}(\mathbf{r},\mathbf{r}',\omega)e^{-i\omega\tau} \\ &= -\frac{c^2}{2\pi V}\sum_{\mathbf{k}n} \mathbf{Q}_{\mathbf{k}n}(\mathbf{r})\otimes\mathbf{Q}^{\star}_{\mathbf{k}n}(\mathbf{r}') \\ &\quad \cdot \lim_{\delta\to 0^+}\int_{-\infty}^{\infty}\frac{e^{-i\omega\tau}d\omega}{(\omega-\omega_{\mathbf{k}n}+i\delta)\,(\omega+\omega_{\mathbf{k}n}+i\delta)}. \end{aligned} \tag{4.46}$$

In order to assure causality it is required that

$$\mathcal{G}(\mathbf{r},\mathbf{r}',t-t') = 0 \quad t' > t. \tag{4.47}$$

Using the residue theorem with contours as depicted in figure (4.1) one obtains the causal result of the integral in (4.46)

$$\lim_{\delta\to 0}\int_{-\infty}^{\infty}\frac{e^{-i\omega\tau}d\omega}{(\omega-\omega_{\mathbf{k}n}+i\delta)\,(\omega+\omega_{\mathbf{k}n}+i\delta)} = \begin{cases} -\frac{2\pi\sin(\omega_{\mathbf{k}n}\tau)}{\omega_{\mathbf{k}n}} & \text{for } \tau \geq 0 \\ 0 & \text{for } \tau < 0 \end{cases}. \tag{4.48}$$

Therefore the *retarded dyadic Green's function* in time space results in

$$\mathcal{G}(\mathbf{r},\mathbf{r}',t-t') = \frac{c^2}{V}\sum_{\mathbf{k}n}\frac{\sin\left(\omega_{\mathbf{k}n}\,(t-t')\right)}{\omega_{\mathbf{k}n}}\mathbf{Q}_{\mathbf{k}n}(\mathbf{r})\otimes\mathbf{Q}^{\star}_{\mathbf{k}n}(\mathbf{r}'). \tag{4.49}$$

In this work we assume that the whole $\mathbb{R}^3$ is filled by the photonic crystal. In this case the sum over $\mathbf{k}$ goes over into an integration over $\mathbf{k}$. This transition can be deduced in the following way. If one considers a square volume $V = L^3$, taking into account the Bloch form of the modes (4.28) and imposing periodic boundary condition on V for the plane wave part $\exp(i\mathbf{k}\cdot\mathbf{r}) = \prod_{\alpha=1}^{3}\exp(ik_\alpha r_\alpha)$ of the modes, it has to fulfill

$$\exp(ik_\alpha r_\alpha) = \exp\left(ik_\alpha(r_\alpha + L)\right) \tag{4.50}$$

which restricts the wave vector k to be of the form

$$k_\alpha = \frac{2\pi n_\alpha}{L} \tag{4.51}$$

with $n_\alpha \in \mathbb{Z}$. Thus a $\mathbf{k}$-space-volume of $\left(\frac{2\pi}{L}\right) = \frac{(2\pi)^3}{V}$ belongs to every triple (n_1, n_2, n_3)

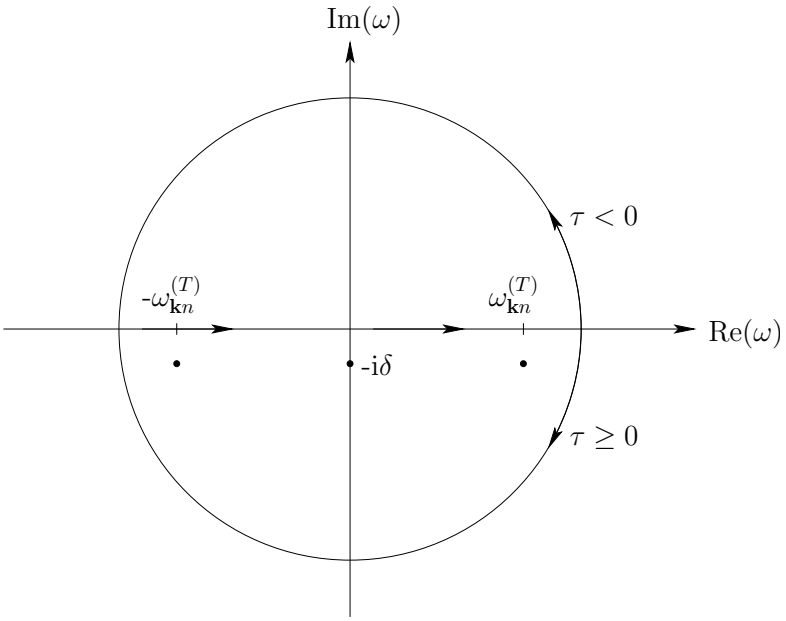

Figure 4.1: Contour used to perform integration (4.48)

so that one can make the substitution

$$\sum_{\mathbf{k}} \ldots \overset{V\to\mathbb{R}^3}{\longrightarrow} \frac{V}{(2\pi)^3} \int_{BZ} d^3k \ldots \tag{4.52}$$

where the subscript BZ indicates that one has to integrate over the first Brillouin zone (see section 4.4.3). Applying this substitution in equation (4.43) and splitting the complete set of eigenmodes into quasi-transverse (T) and quasi-longitudinal (L) modes (see section 4.1) one derives the electric field in frequency space due to a current density $\mathbf{j}(\mathbf{r},\omega)$

$$\mathbf{E}(\mathbf{r}) = -i\frac{\omega}{(2\pi)^3 \epsilon_0} \lim_{\delta\to 0^+} \sum_n \int_{BZ} d^3k \int d^3r' \left(\frac{\mathbf{E}^{(T)}_{\mathbf{k}n}(\mathbf{r}) \otimes \mathbf{E}^{(T)\star}_{\mathbf{k}n}(\mathbf{r}')}{(\omega - \omega_{\mathbf{k}n} + i\delta)(\omega + \omega_{\mathbf{k}n} + i\delta)} + \frac{\mathbf{E}^{(L)}_{\mathbf{k}n}(\mathbf{r}) \otimes \mathbf{E}^{(L)\star}_{\mathbf{k}n}(\mathbf{r}')}{(\omega + i\delta)^2} \right) \mathbf{j}(\mathbf{r}',\omega) \tag{4.53}$$

where the definition of $\mathbf{Q}$ (4.2) was used to express the solution in electric field modes $\mathbf{E}^{(T)}_{\mathbf{k}n}$ and $\mathbf{E}^{(L)}_{\mathbf{k}n}$ which are solutions of

$$\nabla \times \nabla \times \mathbf{E}^{(T)}_{\mathbf{k}n} = \frac{\omega^2_{\mathbf{k}n}}{c^2} \epsilon_r(\mathbf{r}) \mathbf{E}^{(T)}_{\mathbf{k}n} \tag{4.54}$$

and

$$\nabla \times \mathbf{E}_{\mathbf{k}n}^{(L)} = 0 \tag{4.55}$$

respectively. The orthonormalization condition (4.41) in terms of $\mathbf{E}_{\mathbf{k}n}$ and in infinite space reads

$$\int d^3r\, \epsilon(\mathbf{r}) \mathbf{E}_{\mathbf{k}n}^{(\alpha)} \cdot \mathbf{E}_{\mathbf{k}'n'}^{(\beta)\star} = (2\pi)^3\, \delta_{\alpha\beta}\delta_{nn'}\delta(\mathbf{k}-\mathbf{k}') \tag{4.56}$$

where $\alpha,\, \beta \in \{T, L\}$.

The solution of the wave equation in time domain

$$\nabla \times \nabla \times \mathbf{E}(\mathbf{r},t) + \frac{\epsilon_r(\mathbf{r})}{c^2}\frac{\partial^2}{\partial t^2}\mathbf{E}(\mathbf{r},t) = -\mu_0 \partial_t \mathbf{j} \tag{4.57}$$

can be written by using the dyadic Green's function (4.49) in time space as

$$\begin{aligned}\mathbf{E}(\mathbf{r},t) = \frac{1}{(2\pi)^3\,\epsilon_0}\sum_n \int_{BZ} d^3k \int d^3r' \int_{-\infty}^{t} dt' \\ \left(\frac{\sin\left(\omega_{\mathbf{k}n}\,(t-t')\right)}{\omega_{\mathbf{k}n}}\mathbf{E}_{\mathbf{k}n}^{(T)}(\mathbf{r}) \otimes \mathbf{E}_{\mathbf{k}n}^{(T)\star}(\mathbf{r}') + (t-t')\mathbf{E}_{\mathbf{k}n}^{(L)}(\mathbf{r}) \otimes \mathbf{E}_{\mathbf{k}n}^{(L)\star}(\mathbf{r}')\right)\frac{\partial}{\partial t'}\mathbf{j}(\mathbf{r}',t')\end{aligned} \tag{4.58}$$

where the pre factor $(t-t')$ of the longitudinal modes comes into play because

$$\lim_{\omega_{\mathbf{k}n}\to 0} \frac{\sin\left(\omega_{\mathbf{k}n}\,(t-t')\right)}{\omega_{\mathbf{k}n}} = t - t'. \tag{4.59}$$

If one assumes further that the current source is switched on adiabatically, that means $\mathbf{j}(\mathbf{r}, -\infty) = 0$, the t'-integration can be carry out by parts which results in

$$\begin{aligned}\mathbf{E}(\mathbf{r},t) = \frac{1}{(2\pi)^3\,\epsilon_0}\sum_n \int_{BZ} d^3k \int d^3r' \int_{-\infty}^{t} dt' \\ \left(\cos\left(\omega_{\mathbf{k}n}\left(t-t'\right)\right)\mathbf{E}_{\mathbf{k}n}^{(T)}(\mathbf{r}) \otimes \mathbf{E}_{\mathbf{k}n}^{(T)\star}(\mathbf{r}') + \mathbf{E}_{\mathbf{k}n}^{(L)}(\mathbf{r}) \otimes \mathbf{E}_{\mathbf{k}n}^{(L)\star}(\mathbf{r}')\right)\mathbf{j}(\mathbf{r}',t').\end{aligned} \tag{4.60}$$

Equations (4.53) and (4.60) are the main results of this chapter and they form the basis for our subsequent work.

4.6 Two-dimensional Photonic Crystals

A two-dimensional photonic crystal is periodic in a plane and continuously in the perpendicular direction. The eigenmodes $\mathbf{Q}_{\mathbf{k}n}$ as well as $\mathbf{E}_{\mathbf{k}n}$ in such a crystal depend only on the vector $\mathbf{r}_{\parallel}$ laying in the periodicity plane. Choosing the coordinate system in such

a way that $\mathbf{r}_\parallel = x\hat{\mathbf{x}} + y\hat{\mathbf{y}}$ and $\mathbf{r}_\perp = z\hat{\mathbf{z}}$, the derivatives with respect to z have to be zero and so the eigenvalue equation (4.37) splits into

$$\mathcal{H}^{(2)}\mathbf{Q}^{(2)}_{\mathbf{k}_\parallel n}(\mathbf{r}_\parallel) = \frac{\omega^2_{\mathbf{k}_\parallel n}}{c^2}\mathbf{Q}^{(2)}_{\mathbf{k}_\parallel n}(\mathbf{r}_\parallel) \tag{4.61}$$

and

$$\mathcal{H}^{(1)}Q_{z,\mathbf{k}_\parallel n}(\mathbf{r}_\parallel) = \frac{\omega^2_{\mathbf{k}_\parallel n}}{c^2}Q_{z,\mathbf{k}_\parallel n}(\mathbf{r}_\parallel) \tag{4.62}$$

with

$$\mathcal{H}^{(2)} = \frac{1}{\sqrt{\varepsilon(\mathbf{r}_\parallel)}}\begin{pmatrix} -\partial_y^2 & \partial_x\partial_y \\ \partial_x\partial_y & -\partial_x^2 \end{pmatrix}\frac{1}{\sqrt{\varepsilon(\mathbf{r}_\parallel)}} \tag{4.63}$$

and

$$\mathcal{H}^{(1)} = -\frac{1}{\sqrt{\varepsilon(\mathbf{r}_\parallel)}}\left(\partial_x^2 + \partial_y^2\right)\frac{1}{\sqrt{\varepsilon(\mathbf{r}_\parallel)}}. \tag{4.64}$$

The operator $\mathcal{H}^{(1)}$ and $\mathcal{H}^{(2)}$ are both Hermitian [12]. Therefore each of their corresponding eigenfunctions $\{Q_{z,\mathbf{k}_\parallel n}(\mathbf{r}_\parallel)\}$ and $\{\mathbf{Q}^{(2)}_{\mathbf{k}_\parallel n}(\mathbf{r}_\parallel)\}$ separately form an orthogonal complete set. If the current density does not depend on z, one only needs the set $\{\mathbf{Q}^{(2)}_{\mathbf{k}_\parallel n}(\mathbf{r}_\parallel)\}$, which separates into quasi-transverse (T) and quasi-longitudinal (L) modes (see section 4.1), in the expansion of the dyadic Green's function. Normalizing these eigenfunctions according to

$$\int_{V^{(2)}} d^2r_\parallel\, \mathbf{Q}^{(2)(\alpha)*}_{\mathbf{k}_\parallel n}(\mathbf{r}_\parallel)\cdot\mathbf{Q}^{(2)(\beta)}_{\mathbf{k}'_\parallel n'}(\mathbf{r}_\parallel) = V^{(2)}\delta_{\alpha\beta}\delta_{\mathbf{k}_\parallel\mathbf{k}'_\parallel}\delta_{nn'} \tag{4.65}$$

where $V^{(2)}$ is the 2D volume (plane) on which periodic boundary conditions are imposed and $\alpha, \beta \in \{T, L\}$ for transverse and longitudinal modes respectively, equation (4.43) still describes the solution of (4.37) but with the transitions $V \to V^{(2)}$ and $\mathbf{Q}_{\mathbf{k}n} \to \mathbf{Q}^{(2)}_{\mathbf{k}_\parallel n}$ in the Green's function (4.44). Thus the dyadic Green's function in this case is only 2 dimensional. The transition from finite to infinite 2D photonic crystal causes $V^{(2)} \to \mathbb{R}^2$ and $\sum_{\mathbf{k}_\parallel}\ldots \to \frac{V^{(2)}}{(2\pi)^2}\int_{BZ} d^2k_\parallel\ldots$ so that the normalization condition in terms of $\mathbf{E}^{(2)}_{\mathbf{k}_\parallel n}(\mathbf{r}_\parallel)$ becomes

$$\int d^2r_\parallel\, \epsilon(\mathbf{r}_\parallel)\mathbf{E}^{(2)(\alpha)*}_{\mathbf{k}_\parallel n}(\mathbf{r}_\parallel)\cdot\mathbf{E}^{(2)(\beta)}_{\mathbf{k}'_\parallel n'}(\mathbf{r}_\parallel) = (2\pi)^2\,\delta_{\alpha\beta}\delta(\mathbf{k}_\parallel - \mathbf{k}'_\parallel)\delta_{nn'} \tag{4.66}$$

and the electric field solutions

$$\mathbf{E}(\mathbf{r}_\parallel) = -i\frac{\omega}{(2\pi)^2 \epsilon_0} \lim_{\delta\to 0^+} \sum_n \int_{BZ} d^2k_\parallel \int d^2r'_\parallel \left(\frac{\mathbf{E}^{(2)(T)}_{\mathbf{k}_\parallel n}(\mathbf{r}_\parallel) \otimes \mathbf{E}^{(2)(T)\star}_{\mathbf{k}_\parallel n}(\mathbf{r}'_\parallel)}{\left(\omega - \omega_{\mathbf{k}_\parallel n} + i\delta\right)\left(\omega + \omega_{\mathbf{k}_\parallel n} + i\delta\right)} + \frac{\mathbf{E}^{(2)(L)}_{\mathbf{k}_\parallel n}(\mathbf{r}_\parallel) \otimes \mathbf{E}^{(2)(L)\star}_{\mathbf{k}_\parallel n}(\mathbf{r}'_\parallel)}{(\omega + i\delta)^2} \right) \mathbf{j}(\mathbf{r}'_\parallel, \omega) \quad (4.67)$$

and

$$\mathbf{E}(\mathbf{r}_\parallel, t) = \frac{1}{(2\pi)^2 \epsilon_0} \sum_n \int_{BZ} d^2k_\parallel \int d^2r'_\parallel \int_{-\infty}^{t} dt' \left(\cos\left(\omega_{\mathbf{k}_\parallel n}\left(t - t'\right)\right) \mathbf{E}^{(2)(T)}_{\mathbf{k}_\parallel n}(\mathbf{r}_\parallel) \otimes \mathbf{E}^{(2)(T)\star}_{\mathbf{k}_\parallel n}(\mathbf{r}'_\parallel) + \mathbf{E}^{(2)(L)}_{\mathbf{k}_\parallel n}(\mathbf{r}_\parallel) \otimes \mathbf{E}^{(2)(L)\star}_{\mathbf{k}_\parallel n}(\mathbf{r}'_\parallel) \right) \mathbf{j}(\mathbf{r}'_\parallel, t') \quad (4.68)$$

in frequency and time domain respectively.

References

[1] J. D. Jackson. *Classical Electrodynamics Third Edition.* Wiley, 1998.

[2] J. A. Kong. *Electromagnetic Wave Theory.* Wiley, 1987.

[3] C. A. Balanis. *Advanced engineering electromagnetics.* Wiley, 1989.

[4] K. F. Riley, M. P. Hobson, and S. J. Bence. *Mathematical Methods for Physics and Engineering: A Comprehensive Guide.* Cambridge University Press, 2006.

[5] M. Fox. *Optical Properties of Solids.* Oxford University Press, 2010.

[6] G. W. Hanson and A. B. Yakovlev. *Operator theory for electromagnetics: an introduction*, volume 1. Springer, 2002.

[7] J. Bladel. *Electromagnetic fields.* Wiley-IEEE, 2007.

[8] J. A. Stratton. *Electromagnetic Theory.* Wiley-IEEE Press, 2007.

[9] S. W. Lee, J. Boersma, C. L. Law, and G. Deschamps. Singularity in Green's function and its numerical evaluation. *Antennas and Propagation, IEEE Transactions on*, 28(3):311–317, 1980.

[10] A.D. Yaghjian. Electric dyadic Green's functions in the source region. *Proceedings of the IEEE*, 68(2):248–263, 1980.

[11] C. F. Bohren and D. R. Huffman. *Absorption and Scattering of Light by Small Particles (Wiley science paperback series).* Wiley-VCH, 1998.

[12] K. Sakoda. *Optical properties of photonic crystals.* Springer, 2005.

[13] J. D. Joannopoulos, S. G. Johnson, J. N. Winn, and R. D. Meade. *Photonic Crystals: Molding the Flow of Light.* Princeton University Press, 2008.

[14] C. Kittel. *Introduction To Solid State Physics, 7Th Ed.* Wiley India Pvt. Ltd., 2009.

Part II

Optical Antennas

5 Light Scattering on Nanowire Antennas[1]

5.1 Introduction

Since decades antennas are used in everyday devices in the radio and microwave spectral range as a bridge between propagating radiation and localized fields. In this spectral range semi-analytical models exist [1], offering insight into interaction processes and guiding engineers in antenna design. In the same time, for practical antenna design and optimization well established numerical tools are typically used [2]. Shifting antenna resonances towards optical spectral range brings new challenges both from the fabrication and the theoretical perspectives. At optical frequencies metal can no longer be treated as perfect electric conductor and dimensions of the antenna might be as small as several tens of nanometers [3]. Recent progresses in nanotechnology have enabled the fabrication of optical antennas (nano-antennas) [3, 4] and opened many exciting possibilities towards nano-antenna applications. For example, it has been recently demonstrated that nano-antennas can enhance [5] and direct the emission of single molecules [6] and that they can play a key role in sensing application [7]. Great potential in improving the efficiency of solar-cells should also be mentioned [8].

Design and optimization of optical antennas are mainly done using general numerical Maxwell solvers [9], which demand huge computational resources. Therefore accurate analytical and semi-analytical models predicting characteristics and performance of nano-antenna are of great importance. There are just very few exact analytical solutions available. Light scattering on spheres [10], infinite long cylinders [10] and spheroids [11] can be derived in closed analytical form. Furthermore, one can solve the scattering problem in the static limit, where one neglects all retardation effects. In this limit one derives the Rayleigh approximation [10] valid only for particles very small compared

[1] This chapter is based on: C. Kremers, D. N. Chigrin, *Light Scattering on Nanowire Antennas: A Semi-Analytical Approach*, to appear in Photonics Nanostruct. Fundam. and Appl., March 2011

with the wavelength. Additionally an improvement of Rayleigh's approximation was derived in [12]. In figure 5.1 the total scattering cross section (section 3.3) calculated with the original Rayleigh approximation as well as with Karam's improvement [12] for normally incident light scattered on a typical gold nano antenna with radius of 10nm and a length of 100nm is shown and compared with a rigorous numerical result obtained with the discrete dipole approximation (DDA) method [13]. One can see that the resonance frequency of both approximate methods are shifted some 100THz to lower frequencies compared with the numerical result. So these methods do not provided results accurate enough for practical purposes. A semi analytical solution of the light scattering problem involving a finite length nanowire with high conductivity based on introducing an appropriate surface impedance can be used to improve these results [14].

The main goal of this chapter is to derive further improvements of the above mentioned semi analytical approach [14], which provides better accuracy especially in the case of nano-antennas with small aspect ratio. In section (5.2) the problem of light scattering on a thin perfectly conducting wire is reviewed. Pocklington's integral equation is introduced and extended to the case of a nanowire of finite conductivity. We demonstrate how one can use the knowledge of the exact solution of the problem of plane wave scattering on an infinite cylinder in order to improve the accuracy of the surface impedance method [14]. In Sections (5.3) and (5.4) new numerical method to solve the resulting one-dimensional (1D) integral equations are introduced. The method involves a method of moments (MoM) like discretization scheme and does not require any specific boundary conditions to be imposed at the nanowire ends. In section (5.5) numerical calculations of scattering cross-sections for plane wave scattering on gold nanowires with varying geometries is presented and compared with numerically rigorous discrete dipole approximation (DDA) calculations [13].

5.2 Integral Equations of Pocklington's Type

In infinite free space the electric field $\mathbf{E}(\mathbf{r})$ generated by a time harmonic current density distribution $\mathbf{j}(\mathbf{r})$ (time dependence $e^{-i\omega t}$) enclosed in the finite volume V is given by equation (2.32)

$$\mathbf{E}(\mathbf{r}) = \mathbf{E}^{inc}(\mathbf{r}) + i\omega\mu_0 \left(\overleftrightarrow{\mathbf{I}} + \frac{1}{k^2} \nabla \otimes \nabla \right) \int_V g(\mathbf{r}, \mathbf{r}') \mathbf{j}(\mathbf{r}') \, d^3 r' \tag{5.1}$$

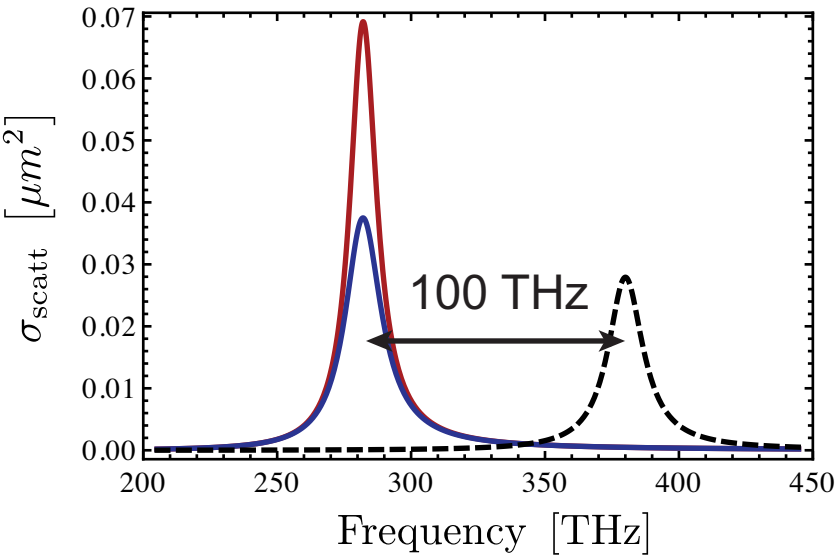

Figure 5.1: Comparison of the scattering cross section for light scattering on a gold cylinder (radius 10nm, length 100nm, normal incidence) calculated with the approximate Rayleigh method (red), a improved retarded method [12] (blue) and with the numerical rigorous DDA method (dashed).

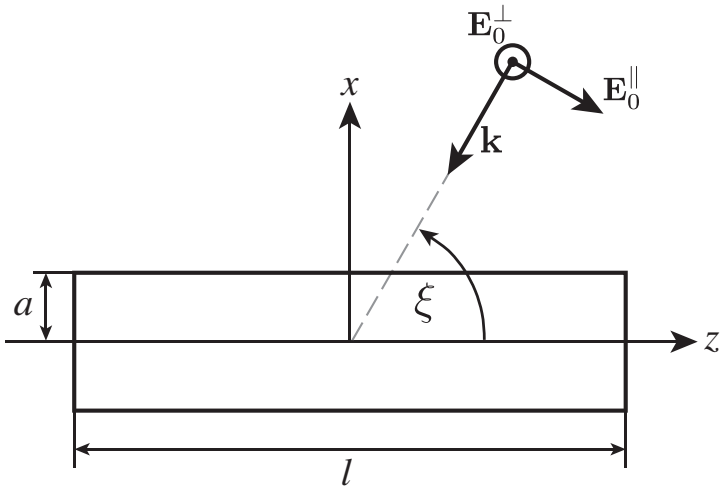

Figure 5.2: Definition of the geometrical parameters, radius a and length l, of the scattering cylinder as well as the chosen body centered coordinate system. Additionally the incident angle ξ and the polarization basis vector $\mathbf{E}_0^{\parallel}$ are depicted in the incident plane.

where $\overleftrightarrow{\mathbf{I}}$ denotes the three-dimensional unit tensor, $\otimes$ is the tensor product defined by $(\mathbf{a} \otimes \mathbf{b})_{ij} = a_i b_j$,

$$g(\mathbf{r}, \mathbf{r}') = \frac{e^{ik|\mathbf{r}-\mathbf{r}'|}}{4\pi\,|\mathbf{r}-\mathbf{r}'|} \tag{5.2}$$

is the scalar Green's function and $k = \frac{\omega}{c}$ the free space wave number. $\mathbf{E}^{inc}$ is an electric field due to sources not contained in V. In scattering problems the driving current density is not controlled from the outside, but instead induced by $\mathbf{E}^{inc}$ which plays the role of an incident field in this case.

In what follows we consider light scattering on a cylinder (wire) with length l and radius a (figure 5.2). The geometry of the problem including a body centered coordinate system with z-axis parallel to the cylinder axis is depicted in figure 5.2. The wave vector $\mathbf{k}$ enclosing the incident angle ξ with the positive z-axis lies in the xz-plane (incident plane). To excite longitudinal resonances only the projection of the incident plane wave electric field on the incident plane $\mathbf{E}_0^{\parallel} = E_0^{\parallel}\,(\sin\xi\hat{\mathbf{z}} - \cos\xi\hat{\mathbf{x}})$ have to be taken into account. The perpendicular polarization component can be safely ignored. Under the assumption that the cylinder diameter is much smaller than the free space wavelength, i.e. $ka \ll 1$, the incident electric field interacting with the cylinder can be viewed as a function depending only on z

$$\mathbf{E}^{inc}(z) \;\approx\; \mathbf{E}_0^{\parallel} e^{-ikz\cos\xi}. \tag{5.3}$$

First we briefly review the derivation of Pocklington's equation for scattering on a thin perfectly conducting wire [1]. In this case in cylindrical coordinates $\{\rho, \phi, z\}$ the induced current density $\mathbf{j}(\mathbf{r})$ has only a z-component, shows no ϕ-dependence and exists solely on the antenna interface. Then the induced current $I(z)$ is related to the current density $\mathbf{j}(\mathbf{r})$ as

$$\mathbf{j}(\mathbf{r}) = \hat{\mathbf{z}} I(z) \frac{\delta(\rho - a)}{2\pi a} \tag{5.4}$$

so that

$$I(z) = \int_0^{2\pi} d\phi \int_0^a \rho d\rho\, j(\mathbf{r}). \tag{5.5}$$

Using (5.4) in (5.1) and performing the ρ'-integration one yields for the z-component of the electric field on the cylinder surface the following integro-differential equation

$$E_z(a, z) = E_z^{inc}(z) + i\frac{\omega\mu_0}{2\pi}\left(1 + \frac{1}{k^2}\frac{\partial^2}{\partial z^2}\right)\int_{-\frac{l}{2}}^{\frac{l}{2}} dz' \int_0^{2\pi} d\phi'\, g_a(\phi', z - z') I(z'). \tag{5.6}$$

where $g_a(\phi', z - z') = g(\mathbf{r}, \mathbf{r}')$ with $\mathbf{r} = (a, 0, z)$ and $\mathbf{r}' = (a, \phi', z')$ in cylindrical coordi-

nates. While the antenna is perfectly conducting, the z-component of the total field at the antenna surface has to vanish, $E_z(a,z) = 0$. Applying this boundary condition to equation (5.6) one can derive Pocklington's integro-differential equation in the form

$$E_z^{inc}(z) = -i\frac{\omega\mu_0}{2\pi}\left(1 + \frac{1}{k^2}\frac{\partial^2}{\partial z^2}\right)\int_{-\frac{l}{2}}^{\frac{l}{2}} dz' \int_0^{2\pi} d\phi'\, g_a(\phi', z - z')I(z'), \tag{5.7}$$

which can be solved subject to the constraint that the current $I(z)$ vanishes at the antenna ends, that is $I(l/2) = I(-l/2) = 0$ [1]. In the derivation of (5.7) the fact, that the antenna is perfectly conducting, is taken into account twice, first by assuming a special form of the induced current (5.4) and second by enforcing the boundary condition $E_z(a,z) = 0$.

A typical nano-antenna at optical frequency range possesses high, but finite conductivity. In this case the surface current approximation (5.4) is still applicable, while the boundary condition $E_z(a,z) = 0$ is generally not. In order to use a Pocklington's like equation at this frequency range, one needs a relationship between the field $E_z(a,z)$ and the current $I(z)$ at the antenna interface.

Assuming a long nanowire, i.e. $l \gg a$, it is reasonable to expect that the internal electric field is separable similar to the solution of the equivalent problem involving an infinite cylinder. In section (3.2) the closed form solution of this problem was presented. Considering an electrically thin wire, that is $ka \ll 1$, one can show that the z-component of order $n = 0$ by far dominates the expansion (3.27) of the resulting internal electric field $\mathbf{E}^{(\mathrm{I})}$. Solving the set of equations determining the constants $\{E_n,\, a_n,\, b_n,\, c_n,\, d_n\}$ as outlined in section 3.2 one can calculate the ratios

$$\frac{\left(\mathbf{E}_n^{(\mathrm{I})} + \mathbf{E}_{-n}^{(\mathrm{I})}\right)\cdot\hat{\mathbf{e}}_i}{\mathbf{E}_0^{(\mathrm{I})}\cdot\hat{\mathbf{e}}_z} \tag{5.8}$$

between the components ($i \in \{x, y, z\}$) of the low order modes, that is

$$\mathbf{E}_n^{(\mathrm{I})} = E_n\left(a_n\mathbf{M}_n^{(\mathrm{I})} + b_n\mathbf{N}_n^{(\mathrm{I})}\right) \tag{5.9}$$

with small integer n, and the fundamental z-component of zeroth order ($n = 0$). An expansion in $k\rho$ up to linear order of these ratios are shown in table (5.1). The items proportional to $k\rho$ can be surely neglected for small wire diameters. So the only components which can possibly show significant influence on the internal field besides $\mathbf{E}_0^{(\mathrm{I})}\cdot\hat{\mathbf{e}}_z$ are the x- and y-components for $n = 1$ but as long as $|\epsilon_r| \gg 0$ and ξ is not to small, these

	$n=0$	$n=1$	$n=2$
$i=x$	$\frac{i\cos\xi}{2}k\rho$	$2\frac{-\cos\phi\cos\xi+\frac{E_0^\perp}{E_0^\parallel}\sin\phi}{\sin\xi(\epsilon_r+1)}$	$i\frac{\cos\xi\cos(2\phi)-\frac{E_0^\perp}{E_0^\parallel}\sin(2\phi)}{(\epsilon_r+1)}k\rho$
$i=y$	$-\frac{iE_0^\perp}{2E_0^\parallel}k\rho$	$2\frac{\sin\phi\cos\xi+\frac{E_0^\perp}{E_0^\parallel}\cos\phi}{\sin\xi(\epsilon_r+1)}$	$-i\frac{\cos\xi\sin(2\phi)+\frac{E_0^\perp}{E_0^\parallel}\cos(2\phi)}{(\epsilon_r+1)}k\rho$
$i=z$	1	$i\frac{[\cos(2\xi)-\epsilon_r]\cos\phi+\frac{E_0^\perp}{E_0^\parallel}(\epsilon_r-1)\sin\phi\cos\xi}{\sin\xi(\epsilon_r+1)}k\rho$	0

Table 5.1: Ratios $\left[\left(\mathbf{E}_n^{(\mathrm{I})}+\mathbf{E}_{-n}^{(\mathrm{I})}\right)\cdot\hat{\mathbf{e}}_i\right]/\left(\mathbf{E}_0^{(\mathrm{I})}\cdot\hat{\mathbf{e}}_z\right)$ expanded in $k\rho$.

components can be neglected too. Therefore, assuming that these relations are fulfilled, it is reasonable to expect an electric field inside the finite wire of the approximate form

$$\mathbf{E}(\mathbf{r})\approx\hat{\mathbf{z}}f(z)J_0\left(k_\rho\rho\right) \tag{5.10}$$

where $J_0\left(k_\rho\rho\right)$ denotes the Bessel function of the first kind, $k_\rho=k\sqrt{\epsilon_r-\cos^2\xi}$ with relative permittivity ϵ_r of the wire and $f(z)$ an unknown z-dependent function giving the amplitude of the internal field along the wire. A connection between the induced current density and the internal electric field is given by means of the volume equivalence theorem (see section 3.1, equation (3.6)) by

$$\mathbf{j}(\mathbf{r})=-i\omega\epsilon_0\Delta\epsilon_r\mathbf{E}(\mathbf{r}) \tag{5.11}$$

with $\Delta\epsilon_r=\epsilon_r-1$. Combining (5.10) and (5.11) the total current through the wire can be calculated

$$\begin{aligned}I(z)&=\int_0^{2\pi}d\phi\int_0^a\rho d\rho\, j_z(\rho,z)\\&=-i\omega\epsilon_0\Delta\epsilon_r 2\pi a\frac{J_1\left(k_\rho a\right)}{k_\rho}f(z).\end{aligned} \tag{5.12}$$

Further comparing results of the integration in (5.12) with (5.10) one can derive the following relation between the electric field and the total current at the wire interface

$$E_z(a,z)=Z_S I(z) \tag{5.13}$$

with the surface impedance

$$Z_S=i\frac{J_0(k_\rho a)k_\rho}{2\pi a\omega\epsilon_0\Delta\epsilon_r J_1(k_\rho a)}. \tag{5.14}$$

Using relation (5.13) the following Pocklington like integro-differential equation for the induced total current I, the surface impedance (SI) integro-differential equation [14], can be obtained from equation (5.6)

$$Z_S I(z) = E_z^{inc}(z) + i\frac{\omega\mu_0}{2\pi}\left(1 + \frac{1}{k^2}\frac{\partial^2}{\partial z^2}\right)\int_{-\frac{l}{2}}^{\frac{l}{2}} dz' \int_0^{2\pi} d\phi'\, g_a(\phi', z - z')I(z'). \quad (5.15)$$

We propose a further improvement to the approximation (5.15) by releasing the solely surface current ansatz (5.4). In order to do that, we assume that the induced current density on the right hand side of equation (5.1) can be factorize similar to the internal field (5.10). In this way substituting (5.10) in equation (5.1) both on the left hand side as boundary condition as well as by using (5.11) on the right hand side to rewrite the induced current density one obtains a self-consistent integro-differential equation for the unknown amplitude $f(z)$

$$f(z)J_0\left(k_\rho a\right) = E_z^{inc}(z) + k^2\Delta\epsilon_r\left(1 + \frac{1}{k^2}\frac{\partial^2}{\partial z^2}\right)\int_V d^3r'\, g(a, z; \mathbf{r}')f(z')J_0\left(k_\rho\rho'\right) \quad (5.16)$$

where $g(a, z; \mathbf{r}') = g(\mathbf{r}, \mathbf{r}')$ with $\mathbf{r} = (a, 0, z)$ in cylindrical coordinates. This volume current (VC) integro-differential equation takes into account both appropriate boundary conditions at the wire interface and an appropriate volume current distribution inside the wire. In order to solve numerically the integro-differential equations (5.15) and (5.16) one has to impose additional boundary conditions at the nano-antenna edges. A common choice is to impose the total current $I(z)$ to be equal to zero for $z = \pm l/2$ [14]. For a solid wire with finite conductivity this choice is generally not justified, while the total current can be discontinuous at the wire edges [15]. To overcome the requirement of additional boundary condition one has to convert the integro-differential equations into purely integral ones.

5.3 Discrete Form of the Volume Current Integro-Differential Equation

Our goal is to discretize equation (5.16). First we have to bring the differential operator $\left(1 + k^{-2}\partial_z^2\right)$ inside the integral. This procedure results in singularities of the order $|\mathbf{r} - \mathbf{r}'|^3$ which are generally not integrable over a volume. However, using the splitting (2.37) proofed in appendix A we can treat this problem and obtain the regularized VC

equation (5.16)

$$(1+\Delta\epsilon_r L_{33})\, E_z(a,z) = E_z^{inc}(z) + k^2\Delta\epsilon_r \left\{ \int_{V-V^\star} G_{33}(a,z;\mathbf{r}')E_z(\rho',z')d^3r' + \int_{V^\star}\left[G_{33}(a,z;\mathbf{r}')E_z(\rho',z') - \frac{1}{k^2}\frac{\partial^2}{\partial z^2} g_0(a,z;\mathbf{r}')E_z(a,z)\right] d^3r' \right\} \quad (5.17)$$

where $E_z(\rho,z) = f(z)J_0(k_\rho\rho)$. Here $V^\star$ denotes a finite and arbitrary shaped principal volume $V^\star$ containing the singular point $\mathbf{r} = (a,0,z)$, $g_0(\mathbf{r},\mathbf{r}') = \lim_{k\to 0} g(\mathbf{r},\mathbf{r}')$ is the static scalar Green's function, G_{33} is the zz-element of the dyadic Green's function (2.34)

$$G_{33}(\mathbf{r},\mathbf{r}') = \left(1 + \frac{1}{k^2}\frac{\partial^2}{\partial z^2}\right) g(\mathbf{r},\mathbf{r}'), \quad (5.18)$$

and L_{33} the zz-element of the source dyadic (2.43)

$$L_{33} = \frac{1}{4\pi}\oint_{\partial V^\star} d^2r'\, \frac{(z'-z)\,(\hat{\mathbf{n}}\cdot\hat{\mathbf{z}})}{|\mathbf{r}-\mathbf{r}'|^3}. \quad (5.19)$$

The surface integration in (5.19) has to be performed over the surface $\partial V^\star$ enclosing the principal volume $V^\star$, $\hat{\mathbf{n}}$ denotes the outer surface normal.

The main advantage of the regularization scheme (2.37) is (i) that all singularities disappear and (ii) that the principal volume $V^\star$ can be finite and arbitrary shaped. We choose a cylinder with length Δ, radius $\frac{\Delta}{2}$ and center at the singular point $\mathbf{r} = (a,0,z)$ as the principal volume (figure 5.3). We assume Δ to be small, such that both the Bessel function $J_0(k_\rho\rho')$ and the amplitude function $f(z')$ are approximately constant over $V^\star$. Taking that into account, writing the volume integrals in the regularized VC equation (5.17) in cylindrical coordinates (ρ,ϕ,z) and collecting all terms containing $f(z)$ on the left and all terms containing $f(z'\neq z)$ on the right hand side, one obtains a one-dimensional integral equation in the form

$$f(z)\Gamma \;\approx\; E_z^{inc}(z) \;+\; \int_{-\frac{l}{2}}^{z-\frac{\Delta}{2}} dz' f(z')\mathcal{L}(\left|z-z'\right|) \;+\; \int_{z+\frac{\Delta}{2}}^{\frac{l}{2}} dz' f(z')\mathcal{L}(\left|z-z'\right|), \quad (5.20)$$

with

$$\Gamma = J_0(k_\rho a)\left\{1 + \Delta\epsilon_r L_{33} - \eta_{in}\right\} - \eta_{out}, \quad (5.21)$$

where

$$\eta_{in} = 4k^2\Delta\epsilon_r \int_0^{\frac{\Delta}{2}} d\tilde{z} \left(\int_{\phi_{min}}^{\pi} d\tilde{\phi} \int_0^{\frac{\Delta}{2}} \tilde{\rho} d\tilde{\rho} + \int_{\frac{\pi}{2}}^{\phi_{min}} d\tilde{\phi} \int_0^{\rho_{max}(\tilde{\phi})} \tilde{\rho} d\tilde{\rho} \right) \left(G_{33}(\mathbf{0}, \tilde{\mathbf{r}}) - \frac{1}{k^2} \frac{\partial^2}{\partial z^2} g_0(\mathbf{0}, \tilde{\mathbf{r}}) \right) \Bigg\}, \quad (5.22)$$

$$\eta_{out} = 4k^2\Delta\epsilon_r \int_0^{\frac{\Delta}{2}} d\tilde{z} \int_{\phi_{min}}^{\pi} d\tilde{\phi} \int_{\frac{\Delta}{2}}^{\rho_{max}(\tilde{\phi})} \tilde{\rho} d\tilde{\rho} \left\{ J_0 \left[k_\rho \rho'(\tilde{\rho}, \tilde{\phi}) \right] G_{33}(\mathbf{0}, \tilde{\mathbf{r}}) \right\} \quad (5.23)$$

and

$$\mathcal{L}(\left| z - z' \right|) = 2k^2\Delta\epsilon_r \int_0^a \rho' d\rho' J_0 \left(k_\rho \rho' \right) \int_0^{\pi} d\phi' G_{33}(a, z; \rho', z'). \quad (5.24)$$

In (5.22) the integration is performed over the principal volume $V^\star$, while in (5.23) over the corresponding wire slice of thickness Δ centered at $z = z'$ but with excluded principal volume $V^\star$. To calculate these two integrals a new coordinate system with its center at the singular point has been chosen (figure (5.3)). In the new coordinate system with cylindrical coordinates $\left(\tilde{\rho}, \tilde{\phi}, \tilde{z}\right)$ the source dyadic (5.19) can be explicitly written as

$$L_{33} = \frac{(\pi - \phi_{min}) \left(2 - \sqrt{2}\right)}{2\pi} + \frac{\left(\phi_{min} - \frac{\pi}{2}\right)}{\pi} - \frac{\Delta}{\pi} \int_{\frac{\pi}{2}}^{\phi_{min}} d\tilde{\phi} \frac{1}{\sqrt{4\rho_{max}^2(\tilde{\phi}) + \Delta^2}}. \quad (5.25)$$

The radius vector ρ' and the integration ranges in (5.22,5.23,5.25) parametrically depend on the nanowire radius a and the wire slice thickness Δ and are given by

$$\rho'(\tilde{\rho}, \tilde{\phi}) = \left| \begin{pmatrix} a \\ 0 \end{pmatrix} + \begin{pmatrix} \tilde{\rho} \cos \tilde{\phi} \\ \tilde{\rho} \sin \tilde{\phi} \end{pmatrix} \right|, \quad (5.26)$$

$$\begin{aligned} \rho_{max}(\tilde{\phi}) &= -2a \cos \tilde{\phi} \\ \phi_{min} &= \arccos \left[-\frac{\Delta}{4a} \right]. \end{aligned} \quad (5.27)$$

Taking into account that the nanowire diameter is small in comparison to the wavelength one can further simplify the integrals in (5.22) and (5.23) by expanding the Green's

function G_{33} in power of k up to the linear term

$$G_{33}^{NF}(R) \approx \frac{1}{4\pi}\left(\frac{3R_z^2 - R^2}{k^2 R^5} + \frac{R_z^2 + R^2}{2R^3} + i\frac{2}{3}k\right) \tag{5.28}$$

where $\mathbf{R} = \mathbf{r}' - \mathbf{r}$. Using (5.28) one can analytically integrate equation (5.22) over $\tilde{z}$ and $\tilde{\rho}$ and equation (5.23) over $\tilde{z}$. The residual integrations in (5.22), (5.23) and (5.25) have to be performed numerically. The regularization scheme (5.17) ensures, that the numerical integrations are convergent. In this way Γ in (5.20) can be efficiently calculated once for given radius a of the nanowire antenna, Δ and wavelength.

Equation (5.20) can be solved numerically by a method of moments (MoM). In general, a MoM approach consists of i) expressing the unknown function in terms of a linear combination of certain basis functions and ii) projecting the integral equation over a set of test functions [16]. A straightforward choice is to expand

$$f(z') = \sum_{i=1}^{n} f_i B\left(z' - z_i\right) \tag{5.29}$$

with pulse basis functions

$$B(z' - z_i) = \begin{cases} 1 & \text{for } |z' - z_i| \leq \frac{1}{2}\Delta \\ 0 & \text{otherwise} \end{cases} \tag{5.30}$$

and choosing Dirac delta functions $\delta(z' - z_i)$ as test functions. f_i denotes the discrete function values $f(z_i)$ at positions $z_i = -\frac{l-\Delta}{2} + (i-1)\Delta$ for $i \in \{1, \ldots, n\}$ where $z_n = \frac{l-\Delta}{2}$. This approach leads to the discrete approximation of equation (5.20) in the form

$$E_z^{inc}(z_i) \;\approx\; -\sum_{j=1}^{i-1} f_j \int_{z_j - \frac{\Delta}{2}}^{z_j + \frac{\Delta}{2}} dz' \mathcal{L}(\left|z_i - z'\right|) + f_i \Gamma - \sum_{j=i+1}^{n} f_j \int_{z_j - \frac{\Delta}{2}}^{z_j + \frac{\Delta}{2}} dz' \mathcal{L}(\left|z_i - z'\right|), \tag{5.31}$$

which can be rewritten in matrix form

$$\left(\Gamma \overleftrightarrow{\mathbf{I}} - \overleftrightarrow{\mathbf{M}}\right) \mathbf{f} = \mathbf{E}^{inc} \tag{5.32}$$

with the n-dimensional unit tensor $\overleftrightarrow{\mathbf{I}}$, $E_i^{inc} = E_z^{inc}(z_i)$ and the matrix elements

$$M_{ij} = \begin{cases} \int_{z_j-\frac{\Delta}{2}}^{z_j+\frac{\Delta}{2}} dz' \mathcal{L}\left(|z_i - z'|\right) & \text{for } i \neq j \\ 0 & \text{for } i = j \end{cases} \tag{5.33}$$

Equation (5.32) can be inverted numerically to yield the discrete set of values $f(z_i)$. While the Green's function depends on the distance between two slices $|z - z'|$, only the first row M_{1j} for $j \in \{1, \ldots, n\}$ has to be calculated. All other elements can be filled using the rule $M_{ij} = M_{i-1,j-1}$.

Using the Green's function expansion (5.28) in the calculation of the matrix elements M_{1j} for $j < \frac{2a}{\Delta}$ the integration over z' can be done analytically. Only the integration over the nanowire profile has to be done numerically. In the calculation of the matrix elements M_{1j} for $j > \frac{2a}{\Delta}$ the full dyadic Green's function have to be used and so the complete volume integral has to be done numerically. These integrations are done over $\mathbf{r}'$-regions far from the singularity and they demonstrate good convergence. An additional performance improvement can be achieved by expanding the Bessel function J_0 for small arguments as [17]

$$J_0(x) \approx 1 - \frac{x^2}{4} + \frac{x^4}{64} + \mathcal{O}(x^6). \tag{5.34}$$

Having the amplitude function $f(z)$ calculated from (5.32) the z-component of the induced electric field is given by the ansatz (5.10).

However, an internal electric field of the form (5.10) is not divergence free as it should be in a charge free region according to Coulomb's law (1.11). Assuming the internal field to be of the more realistic form

$$\mathbf{E}(\mathbf{r}) = f(z) J_0\left(k_\rho \rho\right) \hat{\mathbf{z}} + E_\rho(\rho, z) \hat{\boldsymbol{\rho}} \tag{5.35}$$

it can be made divergence less if E_ρ solves

$$\frac{1}{\rho} \frac{\partial}{\partial \rho} \left(\rho E_\rho\right) + J_0\left(k_\rho \rho\right) \frac{\partial}{\partial z} f(z) = 0 \tag{5.36}$$

which leads to

$$E_\rho(\rho, z) = -\frac{J_1\left(k_\rho \rho\right)}{k_\rho} \frac{\partial}{\partial z} f(z) + \frac{const.}{\rho}. \tag{5.37}$$

Due to symmetry $E_\rho(0, z) = 0$ must hold so the constant have to be set to zero. This

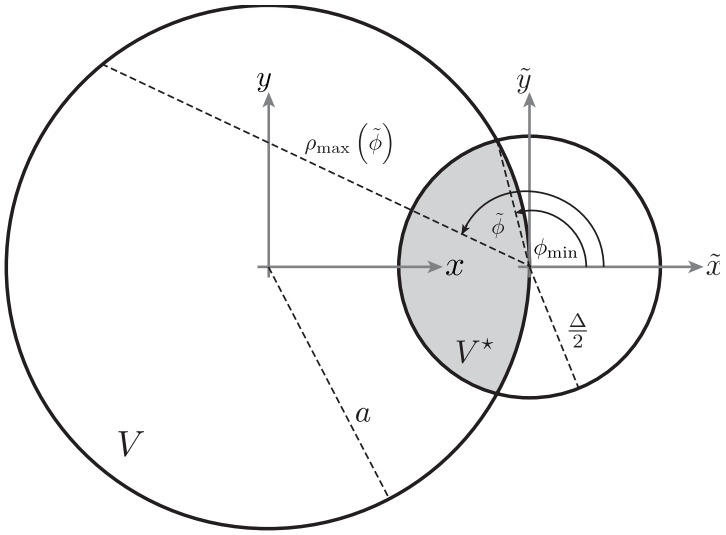

Figure 5.3: Cross-section of the nanowire (big circle) and the principal volume $V^\star$ (small circle) together with the definition of the coordinate systems used to calculate integrals in equation (5.20).

leads finally to the corrected internal electric field

$$\mathbf{E}(\mathbf{r}) = f(z)J_0\left(k_\rho\rho\right)\hat{\mathbf{z}} - \frac{J_1\left(k_\rho\rho\right)}{k_\rho}\frac{\partial}{\partial z}f(z)\hat{\boldsymbol{\rho}}. \tag{5.38}$$

5.4 Discrete Form of the Surface Impedance Integro-Differential Equation

In this section we present two approaches to solve the SI-IE (5.15) (i) by well known Hallen's approach imposing boundary conditions $I\left(-\frac{l}{2}\right) = I\left(\frac{l}{2}\right) = 0$ [16] and (ii) by adapting the regularization already discussed in section 5.3 to the case of surface currents with the advantage that no boundary conditions have to be imposed.

5.4.1 Hallen's Approach

The SI-IE (5.15) can be written in the form

$$Z_S I(z) - E_z^{inc}(z) = \left(1 + \frac{1}{k^2}\frac{\partial^2}{\partial z^2}\right)V(z). \tag{5.39}$$

with $V(z)$ defined as

$$V(z) = i\frac{\omega\mu_0}{2\pi}\int_{-\frac{l}{2}}^{\frac{l}{2}} dz'\, I(z')\mathcal{G}(z-z'). \tag{5.40}$$

The kernel $\mathcal{G}$ in this definition is given by

$$\mathcal{G}(z-z') = \int_0^{2\pi} d\phi'\, g^a(\phi', z-z'). \tag{5.41}$$

The general solution of the inhomogeneous differential equation (5.39) is the sum of the homogenous solution V_h, that is the general solution of $\left(1+k^{-2}\partial_z^2\right) V_h(z) = 0$, and a particular solution of equation (5.39)

$$V(z) = C_1 e^{ikz} + C_2 e^{-ikz} + \int_{-\frac{l}{2}}^{\frac{l}{2}} dz'\, F(z-z') \left[Z_S I(z') - E_z^{inc}(z')\right] \tag{5.42}$$

with constants C_1 and C_2 and $F(z)$ being a solution of

$$\left(1 + \frac{1}{k^2}\frac{\partial^2}{\partial z^2}\right) F(z) = \delta(z). \tag{5.43}$$

A possible choice [16] for $F(z)$ is given by

$$F(z) = i\frac{k}{2} e^{-ik|z|}. \tag{5.44}$$

The definition of $V(z)$ (5.40) has to be equal to the solution (5.42) of the differential equation (5.39) leading to

$$\begin{aligned}\int_{-\frac{l}{2}}^{\frac{l}{2}} dz'\, I(z') \left[i\frac{\omega\mu_0}{2\pi}\mathcal{G}(z-z') - Z_S F(z-z')\right] =& C_1 e^{ikz} + C_2 e^{-ikz} \\ & - \int_{-\frac{l}{2}}^{\frac{l}{2}} dz'\, F(z-z') E_z^{inc}(z').\end{aligned} \tag{5.45}$$

This integral equation can be solved by the method of moments (MoM). In particular we choose a MoM scheme with pulse basis functions (5.30) and Dirac delta functions $\delta(z'-z_m)$ as test functions. This scheme was explained in more detail in section (5.3). This kind of MoM results in the n-dimensional matrix equation

$$\overleftrightarrow{\mathbf{M}}\mathbf{I} = \mathbf{v}\,(C_1, C_2) \tag{5.46}$$

where the elements of the matrix $\overleftrightarrow{\mathbf{M}}$ are given by

$$M_{ij} = \int_{z_j-\frac{\Delta}{2}}^{z_j+\frac{\Delta}{2}} dz' \left\{\left[i\frac{\omega\mu_0}{2\pi}\mathcal{G}(z_i-z') - Z_S F(z_i-z')\right]\right\} \tag{5.47}$$

and the j'th components of $\mathbf{I}$ and $\mathbf{v}$ are the current values and the values of the right hand side of (5.45) at the discrete point z_j of the antenna respectively. By enforcing $I_1 = I_n = 0$ the constants C_1 and C_2 can be determined and subsequent (5.46) can be inverted to yield the discrete current values $I_1, \ldots, I_n$.

5.4.2 Regularization

As long as one excludes the singularity point from the integration range the differential operator in (5.15) can be applied on the integrant so (5.15) can be written as

$$Z_S I(z) = E_z^{inc}(z) + i\frac{\omega\mu_0}{2\pi}\left\{\left(\int_{-\frac{l}{2}}^{z-\frac{\Delta}{2}} dz' + \int_{z+\frac{\Delta}{2}}^{\frac{l}{2}} dz'\right) I(z')\mathcal{L}\left(z-z'\right) + \int_{z-\frac{\Delta}{2}}^{z+\frac{\Delta}{2}} dz'\, I(z')\mathcal{G}(z-z') + \frac{1}{k^2}\frac{\partial^2}{\partial z^2}\int_{z-\frac{\Delta}{2}}^{z+\frac{\Delta}{2}} dz'\, I(z')\mathcal{G}(z-z')\right\} \quad (5.48)$$

with

$$\mathcal{L}(z-z') = \int_0^{2\pi} d\phi'\, G_{33}^a(\phi', z-z'). \quad (5.49)$$

where G_{33}^a denotes the zz-componente of the dyadic Green's function (2.34) at the wire interface

$$G_{33}^a(\phi', z-z') = \left(1 + \frac{1}{k^2}\frac{\partial^2}{\partial z^2}\right) g^a(\phi', z-z') \quad (5.50)$$

and $\mathcal{G}$ is given by (5.41). The last term in (5.48) has to be treated with care because the singularity which arises by changing the order of integration and differentiation is generally not integrable. However, if we substitute

$$\frac{\partial^2}{\partial z^2}\int_{z-\frac{\Delta}{2}}^{z+\frac{\Delta}{2}} dz'\, I(z')\mathcal{G}(z-z') = \frac{\partial^2}{\partial z^2}\int_{V^\star} d^3r'\, \tilde{g}(a, z; \mathbf{r}')I(z') \quad (5.51)$$

with $\int_{V^\star} d^3r' = \int_{z-\frac{\Delta}{2}}^{z+\frac{\Delta}{2}} dz' \int_0^a \rho' d\rho' \int_0^{2\pi} d\phi'$ and

$$\tilde{g}(a, z; \mathbf{r}') = \frac{\delta(\rho' - a)}{\rho'} g(a, z; \mathbf{r}') \quad (5.52)$$

where $g(a,z;\mathbf{r}') = g(\mathbf{r},\mathbf{r}')$ with $\mathbf{r} = (a,0,z)$ and $\mathbf{r}'$ in cylindrical coordinates Lee's regularization (2.37) can be used. This results in

$$\frac{\partial^2}{\partial z^2}\int_{z-\frac{\Delta}{2}}^{z+\frac{\Delta}{2}} dz'\, I(z')\mathcal{G}(z-z') = I(z)\oint_{\partial V^\star} d^2r'\,\frac{\partial}{\partial z'}\tilde{g}_0(z,\mathbf{r}')\,(\hat{\mathbf{z}}\cdot\hat{\mathbf{n}}) + \int_{V^\star}\left\{I(z')\frac{\partial^2}{\partial z'^2}\tilde{g}(z,\mathbf{r}') - I(z)\frac{\partial^2}{\partial z'^2}\tilde{g}_0(z,\mathbf{r}')\right\}$$

with $\tilde{g}_0 = \lim_{k\to 0}\tilde{g}$. Plugging in the explicit form of $\tilde{g}$ (5.52) we can use the symmetries $g(z,z') = g(|z-z'|)$ and $g(\phi') = g(-\phi')$ to reduce the integration range and additionally the Dirac delta function to integrate over ρ'. The result we get is

$$\frac{\partial^2}{\partial z^2}\int_{z-\frac{\Delta}{2}}^{z+\frac{\Delta}{2}} dz'\, I(z')\mathcal{G}(z-z') = -I(z)\frac{\Delta}{2\pi}\int_0^\pi d\phi'\,\frac{1}{\sqrt{\left(\frac{\Delta}{2}\right)^2 + 4a^2\sin^2\left(\frac{\phi'}{2}\right)}^3} + 4\int_0^{\frac{\Delta}{2}} dz'\int_0^\pi d\phi'\left\{I(z')\frac{\partial^2}{\partial z'^2}g^a(\phi',z') - I(z)\frac{\partial^2}{\partial z'^2}g_0^a(\phi',z')\right\}. \quad (5.53)$$

Substituting this regularization back in (5.48) we derive the regularized surface impedance integral equation in the form

$$I(z)\left(Z_S + \frac{i\omega\mu_0}{2\pi}\frac{1}{k^2}L\right) = E_z^{inc}(z) + i\frac{\omega\mu_0}{2\pi}\Bigg\{\left(\int_{-\frac{l}{2}}^{z-\frac{\Delta}{2}} dz' + \int_{z+\frac{\Delta}{2}}^{\frac{l}{2}} dz'\right) I(z')\mathcal{L}\left(z-z'\right) + 4\int_0^{\frac{\Delta}{2}} dz'\int_0^\pi d\phi'\left[I(z')G_{33}^a(\phi',z') - \frac{I(z)}{k^2}\frac{\partial^2}{\partial z'^2}g_0^a(\phi',z')\right]\Bigg\} \quad (5.54)$$

Here, L plays the same role that the source dyadic $\overleftrightarrow{\mathbf{L}}$ (2.43) plays in the volume integration equation (2.42) and is given by

$$L = \frac{\Delta}{2\pi}\int_0^\pi d\phi'\,\frac{1}{\sqrt{\left(\frac{\Delta}{2}\right)^2 + 4a^2\sin^2\left(\frac{\phi'}{2}\right)}^3} \quad (5.55)$$

which can be expressed in terms of the complete elliptic integral of the second kind [17]

$$E(m) = \int_0^{\frac{\pi}{2}} d\theta\,\sqrt{1 - m\sin^2\theta}. \quad (5.56)$$

as

$$L = \frac{2}{\pi\left[\left(\frac{\Delta}{2}\right)^2 + 4a^2\right]} E\left(-\frac{16a^2}{\Delta^2}\right) \tag{5.57}$$

Equation (5.54) can now be discretized in the same manner as (5.20) in section 5.3 using a MoM with pulse function basis and point matching. The resulting n-dimensional matrix equation is given by

$$\left(\Gamma \overleftrightarrow{\mathbf{I}} - \overleftrightarrow{\mathbf{M}}^r\right) \mathbf{I} = \mathbf{E}_z^{inc} \tag{5.58}$$

with matrix elements

$$M_{ij}^r = \begin{cases} i\frac{\omega\mu_0}{2\pi} \int_{z_j-\frac{\Delta}{2}}^{z_j+\frac{\Delta}{2}} dz'\, \mathcal{L}(z_i - z') & \text{for } i \neq j \\ 0 & \text{for } i = j \end{cases} \tag{5.59}$$

and

$$\Gamma = Z_S + i\frac{\omega\mu_0}{2\pi}\left(\frac{L}{k^2} - 4\int_0^{\frac{\Delta}{2}} dz' \int_0^{\pi} d\phi' \left[G_{33}^a(\phi', z') - \frac{1}{k^2}\frac{\partial^2}{\partial z'^2} g_0^a(\phi', z')\right]\right) \tag{5.60}$$

5.5 Numerical results and discussion

In this section the semi-analytical methods developed in sections 5.3 and 5.4 are evaluated and compared with numerically rigorous methods. Plane wave scattering on a gold nanowire is considered in the optical and near-infrared spectral range. The relative permittivity of gold in this spectral range can be modeled by a free electron Drude Sommerfeld model (that is Lorenz's model (1.24) with one pole and $\omega_0 = 0$)

$$\epsilon_r(\omega) \approx \epsilon_\infty - \frac{\omega_p^2}{\omega^2 + i\gamma\omega} \tag{5.61}$$

with parameters $\epsilon_\infty = 9$, $\omega_p = 1.36674 \cdot 10^{16}\, s^{-1}$ and $\gamma = 7.59297 \cdot 10^{13}\, s^{-1}$ [9]. The quantity used for comparison purposes is the total scattering cross section σ_s as given by equation (3.39). The derivation of explicit expressions for the VC-IE and the SI-IE are given in appendix (B) equation (B.12) and equation (B.15) respectively.

Figure 5.4 shows results of convergence checks of the proposed methods. For a typical gold nanowire with length $l = 200nm$ and radius $a = 10nm$ we calculated the spectral positions of the first three maxima of total scattering cross section σ_s under slanting incidents ($\xi = \frac{\pi}{4}$) with varying discretization Δ. The dashed and dotted lines represent

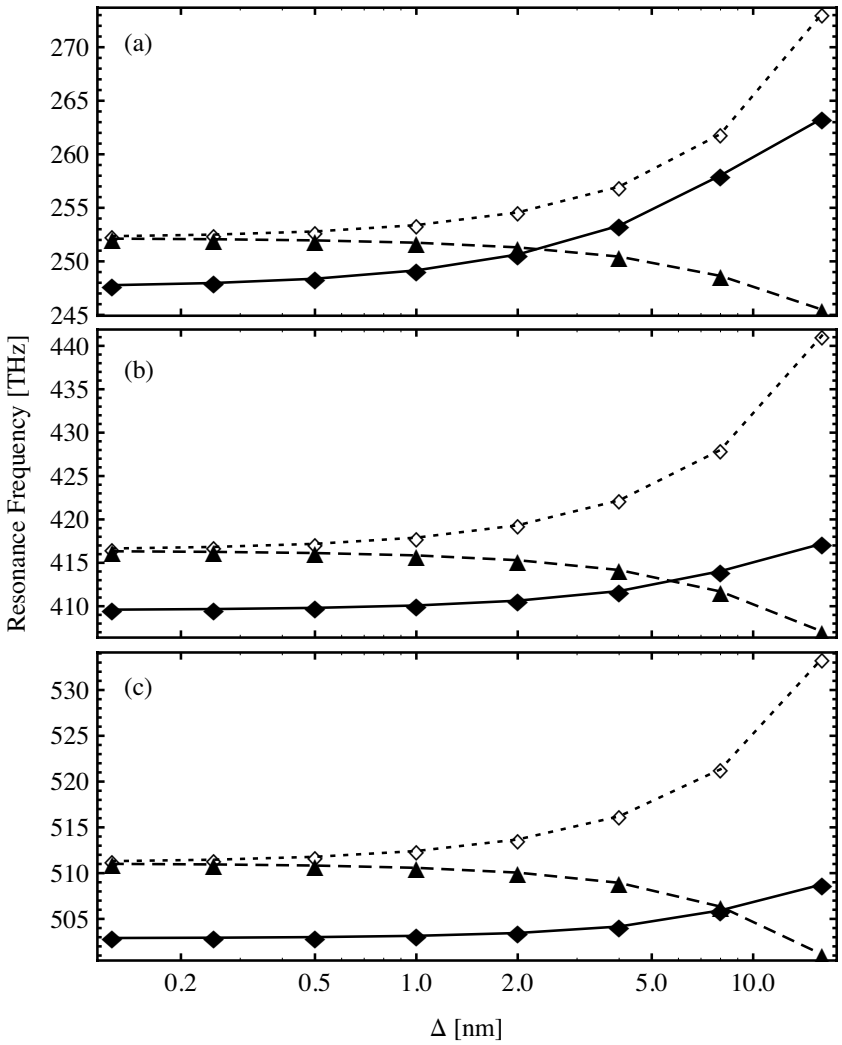

Figure 5.4: Convergence of the first three resonances (from top to bottom panel) of a gold nanowire ($l = 200nm$, $a = 10nm$) under slanting incidence ($\xi = \frac{\pi}{4}$) calculated with VC-IE method (solid line), SI-IE method (dashed) and Hallen's method (dotted).

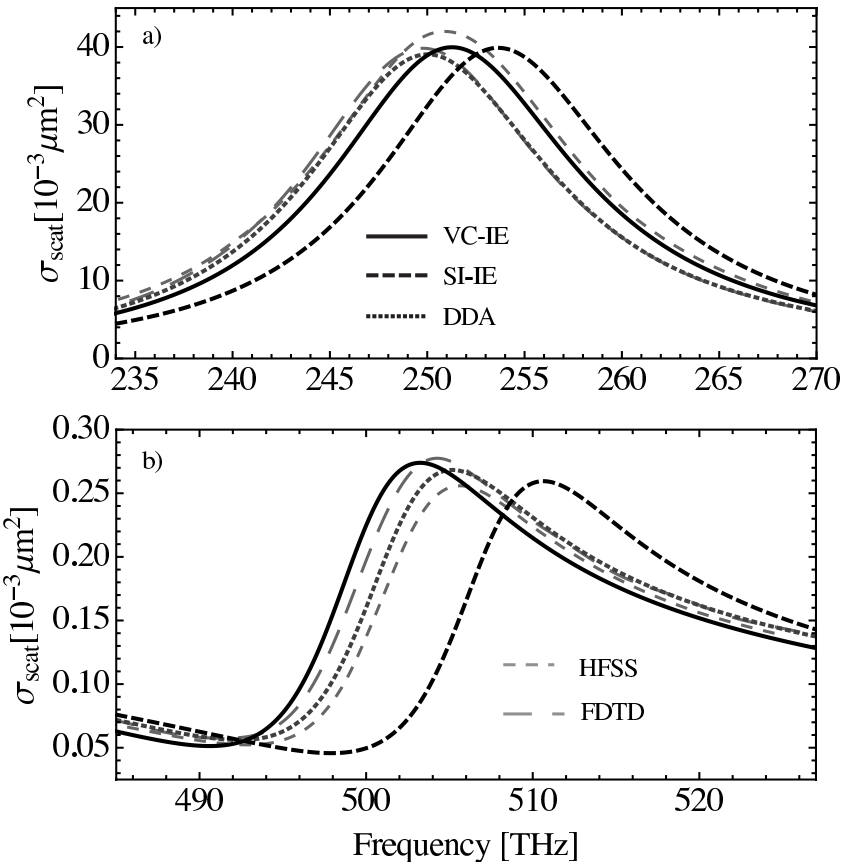

Figure 5.5: Scattering cross-section of a gold nanowire ($l = 200nm$, $a = 10nm$) under slanting incidence ($\xi = \frac{\pi}{4}$) calculated with different rigorous numerical methods as well as the proposed volume current and surface impedance one-dimensional integral equations. In the top panel (a) the first and in the bottom panel (b) the third resonance peak are shown.

the solutions of the SI-IE (5.15) calculated by regularization method (5.58) and Hallen's method (5.46) respectively. The solution of the VC-IE (5.32) is represented by the solid lines. We can conclude (i) that both methods solving the SI-IE converge to the same value but the convergence of our regularization procedure is faster and (ii) that a discretization of $\Delta = 1nm$ in the regularization procedures (5.58) and (5.32) shows a discrepancy between their corresponding convergence values of less than 1 THz. Thus we use $\Delta = 1nm$ and the regularized solution for the SI-IE (5.58) in all the following studies.

In figure 5.5 the first (top panel) and the third (bottom panel) resonance peaks of the cross-section spectra are shown for a gold nanowire with same parameters and incidence as above ($a = 10nm$, $l = 200nm$, $\xi = \frac{\pi}{4}$). Results of both different rigorous numerical methods and our proposed semi-analytical 1D integral equations are compared. For the rigorous numerical calculations we used (i) HFSS, a commercial finite-element frequency-domain Maxwell solver from ANSYS, (ii) an in-house implementation of the finite-difference time-domain method (FDTD) [18] and (iii) ADDA, an open-source software package for calculating scattering parameters using the discrete dipole approximation (DDA) algorithm [13]. The space discretization in the shown DDA and FDTD calculations was set to $1nm$. Discrepancies among the scattering cross-section spectra calculated using different rigorous three-dimensional (3D) Maxwell solvers are comparable with discrepancies of these spectra with the spectrum calculated using VC integral equation method. The accuracy of the SI integral equation method is slightly worse but still very reasonable. Most important are the differences in used computational resources and execution time. The calculation of one frequency point in VC (SI) integral equation method requires approximately 2 (1) seconds on one core of a workstation using Mathematica. In contrast DDA calculations requires around 8 minutes per frequency point on the same workstation. HFSS needs around 6 minutes per frequency point if the mesh is optimized for one frequency only and is reused without optimization for 30 other frequencies. With FDTD one gets the complete spectra in one run in around 250 minutes on one core. In conclusion the newly proposed 1D semi-analytical methods provide a speed-up in execution time close to 200 times compared to general 3D Maxwell solvers. Additionally up to 100 times less RAM is required for the semi-analytical calculations.

In figure 5.6 the position of the scattering cross-section maxima are shown for gold nanowires with different aspect ratios. Radius is $a = 10nm$ and length varies from $l = 50nm$ (shown in the inset) to $l = 300nm$. Normal incidence ($\xi = \frac{\pi}{2}$) is considered. VC integral equation method (full black line), SI integral equation method (dashed line) and DDA (dotted line) are compared. As it is expected the accuracy of both semi-analytical

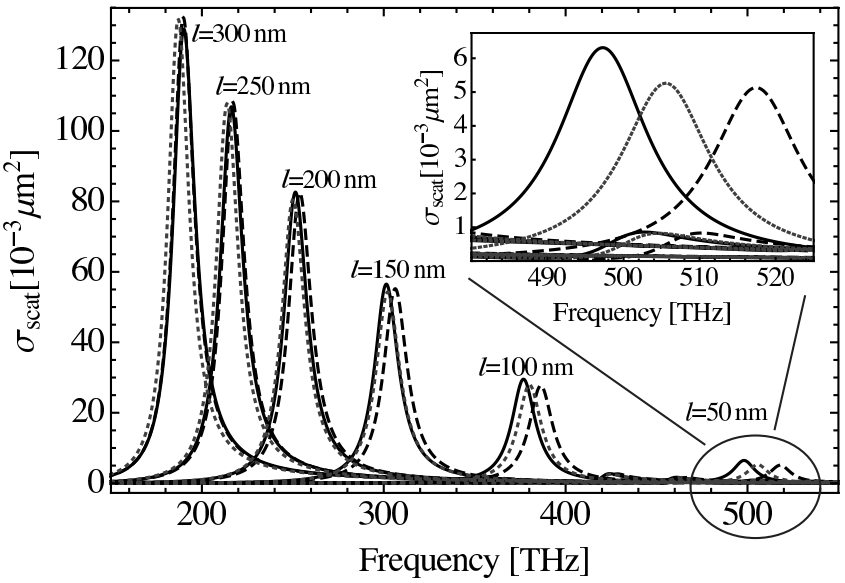

Figure 5.6: Scattering cross-sections of gold nanowire with fixed radius $a = 10nm$ and different lengths. The full and dashed lines show the VC and SI integral equation results, respectively. The dotted line is the numerically rigorous reference calculated using DDA method.

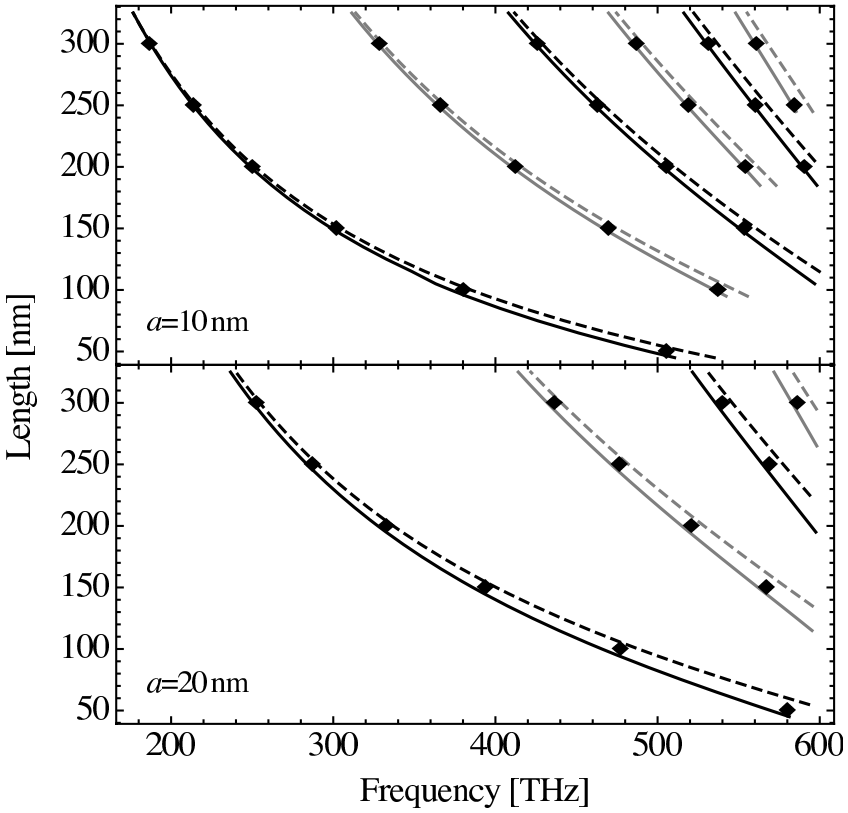

Figure 5.7: Contours plot of the resonance frequencies of the nanowires with different lengths under slanting incidence ($\xi = \frac{\pi}{4}$). Top panel radius is $a = 10nm$, bottom panel $a = 20nm$. The full and dashed lines show the VC and SI integral equation results, respectively. The dots are represents the numerically rigorous DDA calculations.

methods deteriorates with decreasing aspect ratio. However even for considerable low aspect ratio $\frac{5}{4}$ ($l = 50nm$) the first resonance peak predicted using approximate methods represents the rigorous numerical result with a good relative accuracy (2% of the central frequency).

In general VC integral equation method demonstrate better agreement with the DDA calculations in comparison with the SI method (Fig. 5.5 and 5.7). This can be best seen in figure 5.7, where the resonance frequencies of increasing order (from left to right) against the wire length are depicted for nanowires with radius $a = 10nm$ (top panel) and $a = 20nm$ (bottom panel). The VC integral equation method (solid line), SI integral equation method (dashed line) are presented. Dots represent DDA results. The brighter (darker) curves are the resonances of even (odd) orders. All calculations are done under slanting incidence ($\xi = \frac{\pi}{4}$). The better accuracy of the VC integral equation method can be systematical traced back in figure 5.7 especially for wires with smaller aspect ratio.

5.6 Summary

Two alternative methods to solve the scattering problem on optical nanowire antenna, the volume current integral equation (VC-IE) method and the surface impedance integral equation (SI-IE) method are introduced. In order to reduce the general 3D volume integral equation describing the scattering problem to a simple semi-analytical 1D integro-differential equation, both methods utilize solutions of the problem of plane wave scattering on infinite cylinder. A regularization and discretization scheme is proposed in order to transform integro-differential equations into solely integral equation. This transformation enables to solve the original problem without necessity to impose additional boundary conditions at the nanowire edges. Numerical evaluation of the proposed methods and their comparison with different numerically rigorous methods is presented for scattering cross-section calculations. Gold nanowires are analyzed at optical and near-infrared spectral range. The introduced one-dimensional semi-analytical methods demonstrate good agreement and superior numerical performance in comparison with rigorous numerical methods.

References

[1] C. A. Balanis. *Advanced engineering electromagnetics*. Wiley, 1989.

[2] J. Volakis. *Antenna Engineering Handbook, Fourth Edition*. McGraw-Hill Professional, 2007.

[3] P. Bharadwaj, B. Deutsch, and L. Novotny. Optical Antennas. *Advances in Optics and Photonics*, 1(3):438, August 2009.

[4] P. Mühlschlegel, H. J. Eisler, O. J. F. Martin, B. Hecht, and D. W. Pohl. Resonant optical antennas. *Science (New York, N.Y.)*, 308(5728):1607–9, June 2005.

[5] L. Rogobete, F. Kaminski, M. Agio, and V. Sandoghdar. Design of plasmonic nanoantennae for enhancing spontaneous emission. *Optics Letters*, 32(12):1623, June 2007.

[6] T. H. Taminiau, F. D. Stefani, F. B. Segerink, and N. F. van Hulst. Optical antennas direct single-molecule emission. *Nature Photonics*, 2(4):234–237, March 2008.

[7] G. Raschke, S Kowarik, T. Franzl, C. Sönnichsen, T. A. Klar, J. Feldmann, A Nichtl, and K. Kürzinger. Biomolecular Recognition Based on Single Gold Nanoparticle Light Scattering, May 2003.

[8] H. A. Atwater and A. Polman. Plasmonics for improved photovoltaic devices. *Nature materials*, 9(3):205–13, March 2010.

[9] V. Myroshnychenko, J. Rodríguez-Fernández, I. Pastoriza-Santos, A. M. Funston, C. Novo, P. Mulvaney, L. M. Liz-Marzán, and F. J. García De Abajo. Modelling the optical response of gold nanoparticles. *Chemical Society reviews*, 37(9):1792–805, September 2008.

[10] C. F. Bohren and D. R. Huffman. *Absorption and Scattering of Light by Small Particles (Wiley science paperback series)*. Wiley-VCH, 1998.

[11] B. P. Sinha and R. H. MacPhie. Electromagnetic scattering by prolate spheroids for plane waves with arbitrary polarization and angle of incidence. *Radio Science*, 12(2):171–184, April 1977.

[12] M. A. Karam. Electromagnetic wave interactions with dielectric particles. I. Integral equation reformation. *Applied Optics*, 36(21):5238, July 1997.

[13] M. Yurkin and A. Hoekstra. The discrete dipole approximation: An overview and recent developments. *Journal of Quantitative Spectroscopy and Radiative Transfer*, 106(1-3):558–589, July 2007.

[14] G. W. Hanson. On the Applicability of the Surface Impedance Integral Equation for Optical and Near Infrared Copper Dipole Antennas. *IEEE Transactions on Antennas and Propagation*, 54(12):3677–3685, December 2006.

[15] J. Bladel. *Electromagnetic fields*. Wiley-IEEE, 2007.

[16] S. J. Orfanidis. *Electromagnetic Waves and Antennas*. http://www.ece.rutgers.edu/~orfanidi/ewa/, 2010.

[17] I. A. Stegun and M. Abramowitz. *Handbook of Mathematical Functions: with Formulas, Graphs, and Mathematical Tables*. Dover Publications, 1965.

[18] A. Taflove and S. C. Hagnes. *Computational Electrodynamics: The Finite-Difference Time-Domain Method*. Artech House, 2000.

Part III

Cherenkov Radiation in Periodic Dielectric Media

6 Introduction

Back in 1934 Cherenkov reported the observation of the electromagnetic radiation produced by an electron moving in a dielectric medium at a velocity greater than the phase velocity of light in this medium [1]. Such a radiation possesses a unique angular and frequency spectrum and is called *the Cherenkov radiation* [2]. A nontrivial dispersion relation of a medium leads to substantial modifications of the Cherenkov radiation. It has been shown that an electron moving in a homogeneous medium with dispersion should emit at any velocity [3]. Richer spatial distribution of the emitted radiation including intensity oscillations behind the Cherenkov cone is a signature of the radiation in such a medium [4, 5, 6].

To understand the properties of the Cherenkov radiation one can represent the moving electron with space-time dependence of the corresponding current density $\mathbf{j}(\mathbf{r},t) \sim \delta(\mathbf{r}-\mathbf{v}t)$ as a superposition of plane waves $\delta(\mathbf{r}-\mathbf{v}t) = \sum_{\mathbf{k}} \exp(i\mathbf{k}\cdot\mathbf{r} - i\mathbf{k}\cdot\mathbf{v}t)$ with different wave vectors $\mathbf{k}$ and frequency $\mathbf{k}\cdot\mathbf{v}$, where $\mathbf{v}$ is the electron velocity. Only plane waves with frequency and wave vector fitting the medium dispersion $\omega(\mathbf{k})$ can resonantly excite electromagnetic modes in the medium, which gives the Cherenkov resonance condition [7]:

$$\omega(\mathbf{k}) = \mathbf{k}\cdot\mathbf{v}. \tag{6.1}$$

In a homogeneous, non-dispersive medium with refractive index n, the dispersion relation is simply given by $\omega(\mathbf{k}) = (c/n)|\mathbf{k}|$ and the Cherenkov condition (6.1) leads to the well known conical wave front with an aperture $\cos\phi = c/(n|\mathbf{v}|)$ and a condition on the electron velocity $|\mathbf{v}| > c/n$ [7, 2], c being the vacuum speed of light. In an inhomogeneous medium the interplay between interference and propagation can result in an engineered nontrivial dispersion relation $\omega(\mathbf{k})$. For example, periodic dielectric media (photonic crystals) [8, 9] substantially modify both dispersion and diffraction of electromagnetic waves possessing many unusual and novel optical phenomena, including modification of emission dynamics [10, 11, 12], ultra-refraction [13, 14, 15, 16] and photon focusing [17, 18, 19] effects.

Several studies on the modification of the radiation produced by a charged particle moving near or inside photonic crystals are available. The modification of the Smith-

Purcell radiation has been recently studied both theoretically and experimentally near a surface of a two- (2D) and three-dimensional (3D) photonic crystal [20, 21, 22, 23, 24, 25]. The Cherenkov radiation generated by an electron moving inside an air pore of a 2D photonic crystal perpendicular to the periodicity plane has been used to map its photonic band structure in Refs. [26]. In all above mentioned reports, the theoretical analysis of the Cherenkov effect has been done in the plane wave basis. Spatial and spectral modifications of the Cherenkov radiation produced by an electron moving in the periodicity plane of a 2D photonic crystal have been studied in [27] using the finite-difference time-domain (FDTD) method [28].

To date, there do not exist any reports on the general theory of the Cherenkov effect in an arbitrary 3D periodic medium. In this part of the thesis such a theory is developed providing a simple expression for the Cherenkov emission spectrum (energy loss spectrum) (chapter 7) and its spatial distribution (chapter 8) both inside general 3D and 2D photonic crystals.

The problem we face in the two subsequent chapter is defined in the following way. A point charge q (electron) moves uniformly with a velocity $\mathbf{v}$ in a general infinite dielectric periodic 2D or 3D medium described by $\epsilon_r(\mathbf{r}) = \epsilon_r(\mathbf{r} + \mathbf{R})$ with $\mathbf{R}$ being a vector of the direct Bravais lattice (section 4.3). The current density describing the moving charge is given by

$$\mathbf{j}(\mathbf{r}, t) = q\mathbf{v}\delta(\mathbf{r} - \mathbf{v}t). \tag{6.2}$$

With given current density (6.2) the generated electric field can be expanded in terms of eigenmodes as it was shown in section (4.5) and section (4.6) for 3D and 2D photonic crystals respectively. The expressions given there exhibit the starting point for our discussion in this part.

7 Emission Spectrum[1]

The goal of this chapter is to derive an analytical expression for the power emitted per unit length of the charge trajectory. This expression is further reduced to a simple contour integral (3D case) or a one-dimensional sum (2D case) over a small fraction of the reciprocal space. As a result, to calculate the Cherenkov emission spectrum, Bloch eigenmodes and their corresponding group velocities are required only along an integration path (3D case) or at a discrete set of k-points (2D case), considerably reducing computational demands. The integration path and the discrete set of points are defined by the generalized Cherenkov condition. Our theory confirms that the Cherenkov radiation does exist in a periodic medium for an arbitrary electron velocity [27]. It also predicts an enhancement of the radiated power near the frequencies corresponding to the vanishing component of the group velocity, which is orthogonal to the electron trajectory.

The chapter is organized as follows. In Section 7.1 the general solution of Maxwell's equations is summarized for an arbitrary periodic medium. In Section 7.2 an analytical expression for the power radiated per unit length by a moving point charge is derived both for 3D and 2D periodic media. In Section 7.3 we apply our approach to calculate the Cherenkov emission spectra in the particular case of a 2D photonic crystal. Predictions of the analytical theory are substantiated by numerically rigorous finite-difference time-domain (FDTD) [28] calculations.

7.1 Radiated Field

The starting point for our discussion in this chapter is the general solution of Maxwell's equations in Fourier space with the Cherenkov current density (6.2) as a source. Combining equation (4.53) for 3D crystals and equation (4.67) for 2D crystal by introducing the dimensionality $d \in \{2, 3\}$ the electric field in frequency space generated by the Cherenkov

[1]This chapter is based on: C. Kremers, D. N. Chigrin and J. Kroha, "Theory of Cherenkov radiation in periodic dielectric media: Emission spectrum", *Phys. Rev. A*, **79**(1)

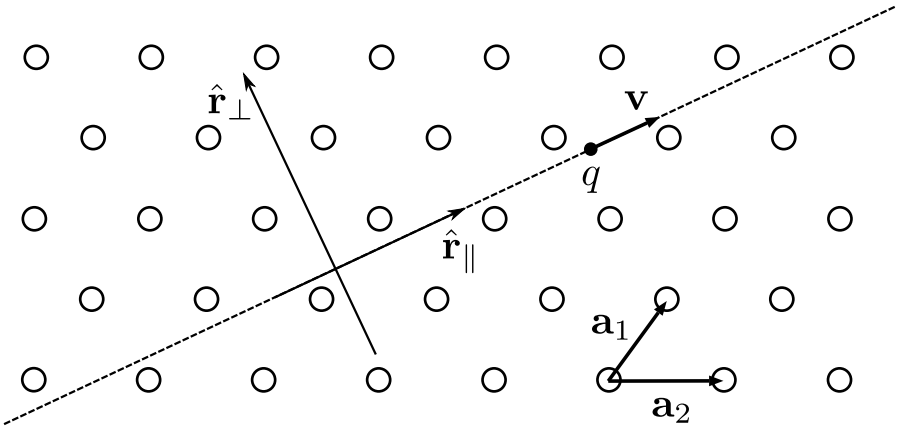

Figure 7.1: A sketch of a periodic medium and a point charge trajectory. Basis vectors $\mathbf{a}_i$ of the lattice are shown. The coordinate system is chosen with one axis along ($\hat{\mathbf{r}}_\parallel$) and the other perpendicular ($\hat{\mathbf{r}}_\perp$) to the charge trajectory.

source $\mathbf{j}(\mathbf{r}', \omega)$ is given by

$$\mathbf{E}(\mathbf{r}) = -i\frac{\omega}{(2\pi)^d \epsilon_0} \lim_{\delta\to 0^+} \sum_n \int_{BZ} d^d k \int d^d r' \left(\frac{\mathbf{E}^{(T)}_{\mathbf{k}n}(\mathbf{r}) \otimes \mathbf{E}^{(T)\star}_{\mathbf{k}n}(\mathbf{r}')}{(\omega - \omega_{\mathbf{k}n} + i\delta)(\omega + \omega_{\mathbf{k}n} + i\delta)} + \frac{\mathbf{E}^{(L)}_{\mathbf{k}n}(\mathbf{r}) \otimes \mathbf{E}^{(L)\star}_{\mathbf{k}n}(\mathbf{r}')}{(\omega + i\delta)^2} \right) \mathbf{j}(\mathbf{r}', \omega). \quad (7.1)$$

Here, $\mathbf{E}^{(T)}_{\mathbf{k}n}(\mathbf{r})$ and $\mathbf{E}^{(L)}_{\mathbf{k}n}(\mathbf{r})$ are quasi-transverse and quasi-longitudinal Bloch eigenmodes (see sections 4.1 and 4.4) characterized by the band index n, the wave vector $\mathbf{k}$ and the eigenfrequencies $\omega^{(T)}_{\mathbf{k}n}$ and $\omega^{(L)}_{\mathbf{k}n} = 0$, respectively. The k-space integration is performed over the first Brillouin zone (BZ) of the periodic medium and the summation is carried out over different photonic bands. The positive infinitesimal δ in (7.1) assures causality in time space (see section 4.5). The limit $\delta \to 0^+$ will be carried out later but we do not write it in the following however keeping it in mind. The spectral current $\mathbf{j}(\mathbf{r}, \omega)$ is the Fourier transform of the Cherenkov current density (6.2)

$$\begin{aligned} \mathbf{j}(\mathbf{r}, \omega) &= q\mathbf{v} \int_{-\infty}^{\infty} dt\, \delta(\mathbf{r} - \mathbf{v}t)\, e^{i\omega t} \\ &= q\mathbf{v}\delta(\mathbf{r}_\perp) \int_{-\infty}^{\infty} dt\, \delta\left(r_\parallel - |\mathbf{v}|\, t\right) e^{i\omega t} \\ &= q\hat{\mathbf{r}}_\parallel \delta(\mathbf{r}_\perp) \exp\left(i\omega \frac{r_\parallel}{|\mathbf{v}|}\right). \end{aligned} \quad (7.2)$$

Here, $\hat{\mathbf{r}}_\parallel$ denotes the unit vector pointing in the direction of $\mathbf{v}$ and $\mathbf{r}_\perp$ denotes a vector lying in the plane perpendicular to $\mathbf{v}$ (figure 7.1). In the last step we used the generalized

scaling property of the Dirac delta function [29]

$$\int_{-\infty}^{\infty} f(x)\delta\left[g(x)\right]\,dx = \sum_i \frac{f(x_i)}{|g'(x_i)|} \tag{7.3}$$

where x_i are the roots of $g(x_i) = 0$.

7.2 Emission Spectrum

The emitted power of the Cherenkov radiation in a dielectric medium is given by the rate at which the moving charge does work on the surrounding electromagnetic field. For an arbitrary current density $\mathbf{J}(\mathbf{r}, t)$ in a 2D or 3D volume V_0, the time-dependent emitted power is therefore given by (1.31)

$$P(t) = -\int_{V_0} d^d r\, \mathbf{J}(\mathbf{r}, t) \cdot \mathbf{E}(\mathbf{r}, t)\,. \tag{7.4}$$

The total energy U radiated by the current $\mathbf{J}(\mathbf{r}, t)$ is obtained by integrating (7.4) over all moments of time

$$U = \int_{-\infty}^{\infty} dt\, P(t)\,. \tag{7.5}$$

The time integral in (7.5) can be further transformed into the integral over frequency (see appendix C)

$$U = \int_{0}^{\infty} d\omega\, P(\omega)\,, \tag{7.6}$$

with a total power radiated per frequency interval $[\omega,\, \omega + d\omega]$ given by

$$P(\omega) = -\frac{1}{\pi}\Re\left[\int_{V_0} d^d r\, \mathbf{J}(\mathbf{r}, \omega) \cdot \mathbf{E}^{\star}(\mathbf{r}, \omega)\right]. \tag{7.7}$$

To obtain the power emitted per unit length of the electron trajectory the integration volume V_0 should be chosen as a cylinder coaxial with the electron trajectory, while the integral itself should be normalized by the cylinder length l. In the 2D case, the volume integral is reduced to the line integral over a rectangle coaxial with the electron trajectory and the result should be normalized to the rectangle length.

We further derive the spectral dependence of the power (dP/dl) (7.7) radiated per unit length by the point charge (6.2) uniformly moving in a periodic medium. Assuming that the presence of the moving charge does not change the band structure of the peri-

odic medium, the electromagnetic field $\mathbf{E}(\mathbf{r},\omega)$ surrounding the moving charge can be expressed in the form of the Bloch eigenmode expansion (7.1). This expansion is valid for any point $\mathbf{r}$ in the medium being different from, but as close as required to, the charge trajectory. Substituting the Fourier transform of the Cherenkov current density (7.2) and the Bloch mode expansion (7.1) in equation (7.7) we obtain the power radiated per unit length

$$\frac{dP}{dl} = -\frac{1}{(2\pi)^d}\frac{\omega}{\pi\epsilon_0}\sum_n \int_{BZ} d^d k \\ \Re\left[-\mathrm{i}\left\{\frac{I^{(T)}}{\left(\omega-\omega_{\mathbf{k}n}^{(T)}+i\delta\right)\left(\omega+\omega_{\mathbf{k}n}^{(T)}+i\delta\right)}+\frac{I^{(L)}}{(\omega+i\delta)^2}\right\}\right] \quad (7.8)$$

with

$$I^{(\alpha)} = q^2 I_1^{(\alpha)} I_2^{(\alpha)} = q^2\left\{\int_{-\infty}^{\infty} dr_\parallel \left(\mathbf{e}_{\mathbf{k}n}^{(\alpha)\star}\left(r_\parallel\right)\cdot\hat{\mathbf{r}}_\parallel\right) e^{-i\left(k_\parallel-\frac{\omega}{|\mathbf{v}|}\right)r_\parallel}\right\}\cdot \\ \left\{\frac{1}{l}\int_{-l/2}^{l/2} dr_\parallel \left(\mathbf{e}_{\mathbf{k}n}^{(\alpha)}\left(r_\parallel\right)\cdot\hat{\mathbf{r}}_\parallel\right) e^{i\left(k_\parallel-\frac{\omega}{|\mathbf{v}|}\right)r_\parallel}\right\}, \quad (7.9)$$

where $\alpha = T, L$. We have readily performed the space integration in the transverse direction $\hat{\mathbf{r}}_\perp$ and used the Bloch theorem $\mathbf{E}_{\mathbf{k}n}^{(\alpha)}(\mathbf{r}) = \mathbf{e}_{\mathbf{k}n}^{(\alpha)}(\mathbf{r})\exp(\mathrm{i}\mathbf{k}\cdot\mathbf{r})$, where $\mathbf{e}_{\mathbf{k}n}^{(\alpha)}(\mathbf{r})$ is a lattice periodic function (section 4.4). To avoid having to deal with the "bremsstrahlung" radiation we limit ourselves to the electron trajectories which do not cut dielectric interfaces in the periodic medium. Such trajectories are necessarily rationally oriented with respect to the periodic lattice. In this case the function $\left(\mathbf{e}_{\mathbf{k}n}^{(\alpha)}\left(r_\parallel\right)\cdot\hat{\mathbf{r}}_\parallel\right)$ in (7.9) as well as its complex conjugate are both one dimensional periodic functions with a period a defined by the particular orientation of the electron trajectory. Then, Eq. (7.9) can be further simplified to (see appendix D)

$$I^{(\alpha)} = 2\pi q^2 \sum_m \left|c_m^{(\alpha)}(\mathbf{k};n)\right|^2 \delta\left(k_\parallel - \frac{\omega}{|\mathbf{v}|} - \frac{2\pi}{a}m\right). \quad (7.10)$$

Here $k_\parallel$ is the component of the wave vector parallel to the electron trajectory. $c_m(\mathbf{k};n)$ is the m-th ($m\in\mathbb{Z}$) Fourier coefficient of the periodic function $\left(\mathbf{e}_{\mathbf{k}n}^{(\alpha)}\left(r_\parallel\right)\cdot\hat{\mathbf{r}}_\parallel\right)$ defined as

$$c_m^{(\alpha)}(\mathbf{k};n) = \frac{1}{a}\int_0^a dr_\parallel \left(\mathbf{e}_{\mathbf{k}n}^{(\alpha)}\left(r_\parallel\right)\cdot\hat{\mathbf{r}}_\parallel\right)\mathrm{e}^{-\mathrm{i}\frac{2\pi}{a}mr_\parallel}. \quad (7.11)$$

Taking into account the expression (7.10) and the relation $\Re\{i(\Re[z]+i\Im[z])\} = -i\Im[z]$, the power radiated by a moving electron per unit length is given by

$$\frac{dP}{dl} = -\frac{1}{(2\pi)^{d-1}}\frac{\omega q^2}{\pi\epsilon_0}\sum_{nm}\int_{BZ} d^d k\,\delta\left(k_{\parallel} - \frac{\omega}{|\mathbf{v}|} - \frac{2\pi}{a}m\right) \left\{\left|c_m^{(T)}(\mathbf{k};n)\right|^2 \Im\left[\frac{1}{\left(\omega-\omega_{\mathbf{k}n}^{(T)}+i\delta\right)\left(\omega+\omega_{\mathbf{k}n}^{(T)}+i\delta\right)}\right] + \left|c_m^{(L)}(\mathbf{k};n)\right|^2 \Im\left[\frac{1}{(\omega+i\delta)^2}\right]\right\}. \quad (7.12)$$

This expression can be further integrated along the direction $k_{\parallel}$ in the k-space yielding

$$\frac{dP}{dl} = -\frac{1}{(2\pi)^{d-1}}\frac{\omega q^2}{\pi\epsilon_0}\sum_{nm}\int_{\mathcal{S}^{d-1}} d^{d-1}k_{\perp} \left\{\left|c_m^{(T)}(\mathbf{k};n)\right|^2 \Im\left[\frac{1}{\left(\omega-\omega_{\mathbf{k}n}^{(T)}+i\delta\right)\left(\omega+\omega_{\mathbf{k}n}^{(T)}+i\delta\right)}\right] + \left|c_m^{(L)}(\mathbf{k};n)\right|^2 \Im\left[\frac{1}{(\omega+i\delta)^2}\right]\right\}. \quad (7.13)$$

In the 3D case, the resulting surface integral is taken over the plane $\mathcal{S}^2 = \mathcal{S}$ and in the 2D case over the line $\mathcal{S}^1 = \mathcal{C}$ (see figure 7.2). Both the integration plane $\mathcal{S}$ and the integration line $\mathcal{C}$ should be orthogonal to the electron trajectory and are defined by the following relation

$$k_{\parallel} = \frac{\omega}{|\mathbf{v}|} + \frac{2\pi}{a}m. \quad (7.14)$$

Here the integer m should be chosen in such a way that the wave vector $k_{\parallel}$ stays in the first BZ. Further, taking finally the limit $\delta \to 0^+$ and using [30]

$$\Im\left[\lim_{\delta\to 0^+}\frac{1}{\omega \pm \omega_{\mathbf{k}n}^{(T)} + i\delta}\right] = -\pi\delta\left(\omega \pm \omega_{\mathbf{k}n}^{(T)}\right), \quad (7.15)$$

the spectral radiated power (7.13) can be expressed in the form

$$\frac{dP}{dl} = \frac{1}{(2\pi)^{d-1}} \frac{\omega q^2}{\pi \epsilon_0} \sum_{nm} \int_{\mathcal{S}^{d-1}} d^{d-1}k_\perp \left\{ \frac{\pi}{2\omega_{\mathbf{k}n}^{(T)}} \left| c_m^{(T)}(\mathbf{k}; n) \right|^2 \left[\delta\left(\omega - \omega_{\mathbf{k}n}^{(T)}\right) - \delta\left(\omega + \omega_{\mathbf{k}n}^{(T)}\right) \right] + \frac{2\pi}{\omega} \left| c_m^{(L)}(\mathbf{k}; n) \right|^2 \delta(\omega) \right\}. \quad (7.16)$$

The eigenfrequencies of the Bloch modes are positive (section 4.1), so the second term in Eq. (7.16) containing the delta function $\delta\left(\omega + \omega_{\mathbf{k}n}^{(T)}\right)$ is zero for all frequencies. The third term in Eq. (7.16) is due to the work the current does on the longitudinal part of the electromagnetic field. In the presence of free charges the longitudinal part of the field corresponds to the static electric field and the work done against it results in non-radiative energy transfer with a nonzero contribution only at zero frequency. In what follows we will disregard this non-radiative contribution and will limit ourselves to the radiation into propagating electromagnetic waves only. Then the spectral radiated power is given by

$$\frac{dP}{dl} = \frac{1}{(2\pi)^{d-2}} \frac{\omega q^2}{4\pi \epsilon_0} \sum_{nm} \int_{\mathcal{S}^{d-1}} d^{d-1}k_\perp \frac{\left| c_m^{(T)}(\mathbf{k}; n) \right|^2 \delta\left(\omega - \omega_{\mathbf{k}n}^{(T)}\right)}{\omega_{\mathbf{k}n}^{(T)}} \quad (7.17)$$

The argument of the Dirac delta function in Eq. (7.17) is a function of the wave vector. This can be used to reduce further the dimensionality of the $(d-1)$ k-space integral. In the 3D case, using the relation [31]

$$\int_{\mathcal{V}} d^d k\, f(\mathbf{k})\, \delta(g(\mathbf{k})) = \int_{\partial\mathcal{V}} d^{d-1}k \frac{f(\mathbf{k})}{|\nabla_{\mathbf{k}} g(\mathbf{k})|}, \quad (7.18)$$

where $\partial\mathcal{V}$ is the $(d-1)$ dimensional surface defined by $g(\mathbf{k}) = 0$, the integral over the plane $\mathcal{S}$ can be converted into the contour integral

$$\left(\frac{dP}{dl}\right)^{3D} = \frac{q^2}{8\pi^2 \epsilon_0} \sum_{nm} \int_{\partial\mathcal{S}} dk \frac{\left| c_m^{(T)}(\mathbf{k}; n) \right|^2}{\left| \nabla_{\mathbf{k}_\perp} \omega_{\mathbf{k}n}^{(T)} \right|}. \quad (7.19)$$

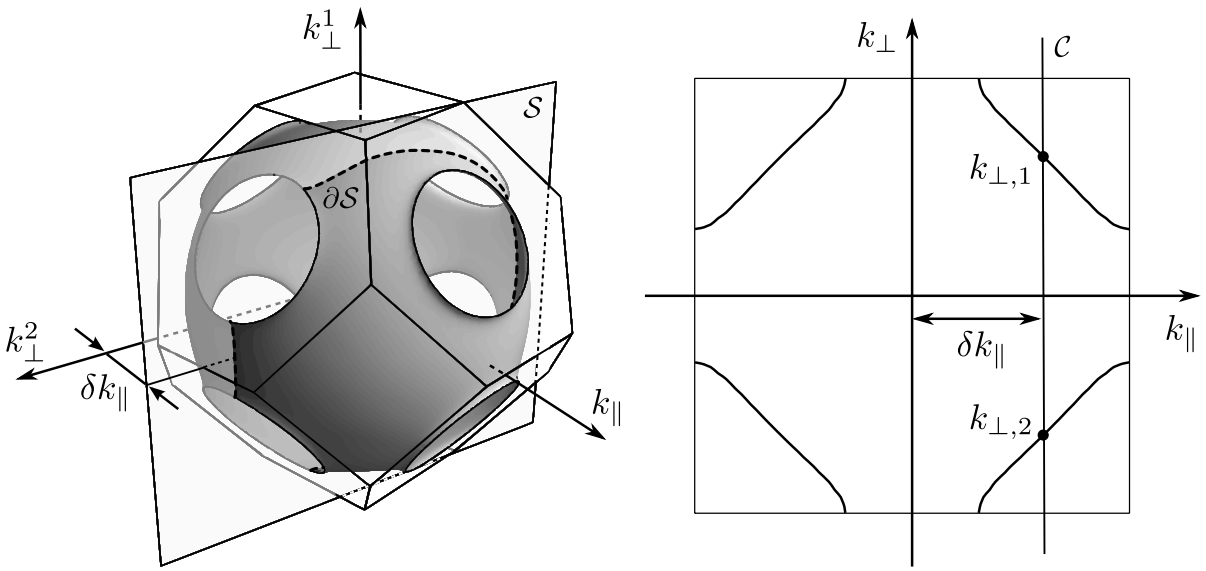

Figure 7.2: (Left) Diagram to define the integration plane $\mathcal{S}$ and the integration contour $\partial\mathcal{S}$ (dashed line) in Eq. (7.13,7.19). The iso-frequency surface enclosed in the first BZ of the FCC lattice is shown for the normalized frequency $\omega_{\mathbf{k}n} = \omega$ inside the first bandgap of a 3D inverted opal. (Right) Diagram to define the integration line $\mathcal{C}$ and the set of points $\left\{k_{\perp,i}\right\}$ (two thick dots) in Eqs. (7.13,7.22). The iso-frequency contour enclosed in the first BZ of a square lattice PhC is shown for the normalized frequency $\omega_{\mathbf{k}n} = \omega$ inside the first bandgap. The plane $\mathcal{S}$ and the line $\mathcal{C}$ are defined by the relation $k_\parallel = \delta k_\parallel = \frac{\omega}{|\mathbf{v}|} + \frac{2\pi}{a}m$. The choice of the coordinate system with one axis, $k_\parallel$, parallel to the electron trajectory is shown.

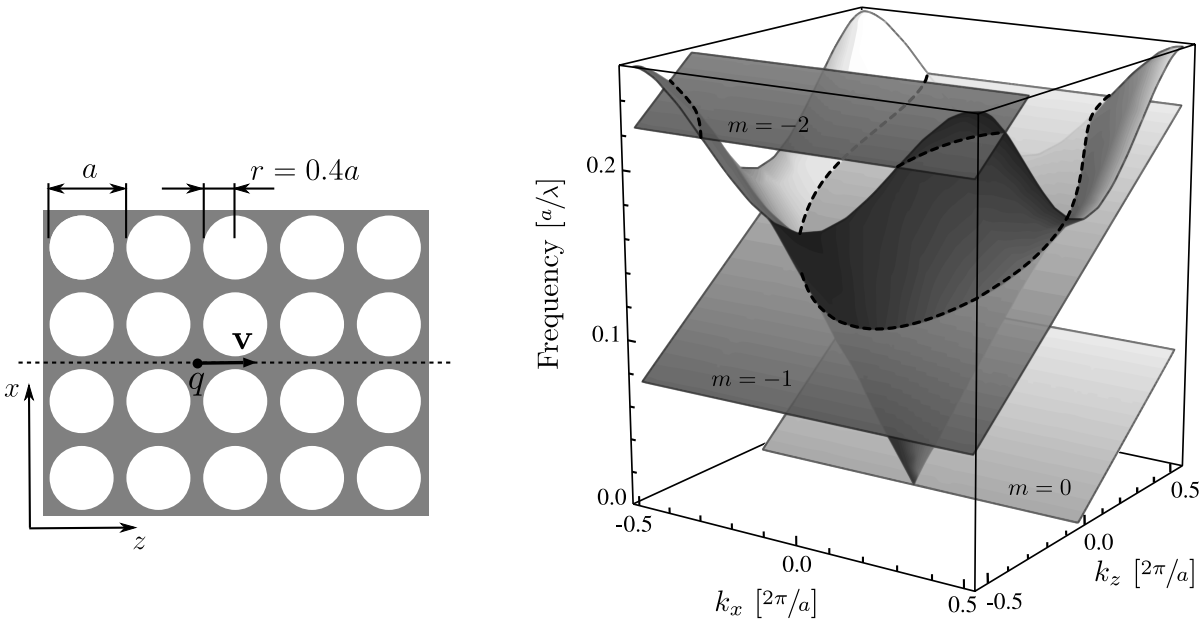

Figure 7.3: Diagram to illustrate the generalized Cherenkov condition (7.23). A 3D representation of the photonic band structure (right) of the 2D PhC (left) is shown for TE polarization. An infinite 2D square lattice of air holes in a dielectric medium is considered. The radius of the holes is $r = 0.4a$, the dielectric constant of the background medium is $\epsilon_r = 12$. Only the first band in the first BZ is presented. The right-hand side of Eq. (7.23) defines the set of planes for different m. Intersection of these planes with the band structure (dashed line) determines the Bloch modes contributing to the Cherenkov radiation. Here it is supposed that a point charge moves along the z-axis in the crystal with the velocity $|\mathbf{v}| = 0.15c$.

The contour $\partial\mathcal{S}$ is defined by the relation (7.14) and

$$\omega_{\mathbf{k}n}^{(T)} = \omega. \tag{7.20}$$

It is an intersection of the iso-frequency surface with the plane $\mathcal{S}$ (Fig. 7.2-left).

In the 2D case, the relation (7.3) can be used, where summation is taken over all solutions of the equation $f(k) = 0$. Substituting (7.3) into (7.17) we obtain

$$\left(\frac{dP}{dl}\right)^{2D} = \frac{\omega q^2}{4\pi\epsilon_0} \sum_{nmi} \int_{\mathcal{C}} dk_\perp \frac{\left|c_m^{(T)}(\mathbf{k};n)\right|^2 \delta\left(k_\perp - k_{\perp,i}\right)}{\omega_{\mathbf{k}n}^{(T)} \left(\left|\partial\omega_{\mathbf{k}n}^{(T)}/\partial k_\perp\right|\right)\Big|_{k_{\perp,i}}}, \tag{7.21}$$

where $\left\{k_{\perp,i}\right\}$ are simultaneous solutions of the equations (7.14) and (7.20) given by the intersections of the iso-frequency contour with the line $\mathcal{C}$ (Fig. 7.2-right). Performing the k-space integration, we finally obtain

$$\left(\frac{dP}{dl}\right)^{2D} = \frac{q^2}{4\pi\epsilon_0} \sum_{nmi} \left(\frac{\left|c_m^{(T)}(\mathbf{k};n)\right|^2}{\left|\partial\omega_{\mathbf{k}n}^{(T)}/\partial k_\perp\right|}\right)\Bigg|_{k_{\perp,i}}, \tag{7.22}$$

where the function in brackets is calculated for the wave vectors corresponding to the set $\left\{k_{\perp,i}\right\}$.

Formulas (7.19) and (7.22) constitute the main result of the present chapter. They give the power radiated by the moving point charge q in the spectral interval $[\omega,\ \omega + d\omega]$ per unit length of the trajectory for a 3D and 2D periodic medium, respectively. The radiated power is proportional to the Fourier coefficients $c_m^{(T)}(\mathbf{k};n)$, which effectively describes the local coupling strength between the current density produced by a moving electron and the electromagnetic field at the electron location. The gradient and derivative of the dispersion relation $\mathbf{v}_\perp^g = \nabla_{\mathbf{k}_\perp}\omega_{\mathbf{k}n}^{(T)}$ and $v_\perp^g = \partial\omega_{\mathbf{k}n}^{(T)}/\partial k_\perp$ yield the component of the group velocity, $\mathbf{v}^g$, of the Bloch eigenmode $(\mathbf{k};n)$, which is orthogonal to the electron trajectory. The Cherenkov radiated power is proportional to the inverse of this component of the group velocity. That means that the radiated power can be *strongly enhanced* not only if the group velocity itself is small for some frequency, but also if the component of the group velocity orthogonal to the electron trajectory becomes small. At the same time *suppression* of the Cherenkov radiation is possible if for some frequency the current density produced by a moving electron is not coupled to the corresponding Bloch mode and the Fourier coefficients $c_m^{(T)}(\mathbf{k};n)$ is small.

Only eigenmodes with their wave vectors on the contour $\partial\mathcal{S}$ (7.19) and from the set

$\left\{k_{\perp,i}\right\}$ (7.22) contribute to the radiated power at a given frequency. It is important to realize that Eqs. (7.14) and (7.20) defining the contour $\partial\mathcal{S}$ and the set $\left\{k_{\perp,i}\right\}$ are equivalent to the Cherenkov resonance condition (6.1). In fact, substituting (7.20) in (7.14) and taking into account that the scalar product in (6.1) results in $\mathbf{v}\cdot\mathbf{k} = |\mathbf{v}|\,k_{\parallel}$ one obtains *the generalized Cherenkov condition* for a periodic medium

$$\omega_{\mathbf{k}n}^{(T)} = |\mathbf{v}|\,k_{\parallel} - |\mathbf{v}|\,\frac{2\pi}{a}m. \tag{7.23}$$

In the 4D (3D) (ω-k)-space the right-hand side of the relation (7.23) defines a hyperplane (plane) whose intersection with the band structure, $\omega_{\mathbf{k}n}^{(T)}$, determines Bloch modes contributing to the Cherenkov radiation (Fig. 7.3-top). Nonzero integers m ensure that such an intersection and consequently the Cherenkov radiation exist in a periodic medium for an *arbitrarily small* electron velocity. In a homogeneous medium is $m = 0$ and the Cherenkov condition reduces to its standard form $\omega_{\mathbf{k}} = |\mathbf{v}|\,k_{\parallel}$.

As a simple check of our theory we show in the following that the final formulas (7.19,7.22) reproduce the limit of a homogeneous medium with the dielectric constant ϵ_r. For a given frequency ω, the wave vector $|\mathbf{k}|$ and the group velocity $\left|\mathbf{v}_{\perp}^{g}\right|$ are given by $|\mathbf{k}| = \left(\omega\sqrt{\epsilon_r}\right)/c$ and $\left|\mathbf{v}_{\perp}^{g}\right| = \left(c\,|\mathbf{k}_{\perp}|\right)/\left(\sqrt{\epsilon_r}\,|\mathbf{k}|\right)$ respectively, with $\mathbf{k}_{\perp} = \mathbf{k} - \mathbf{k}_{\parallel}$ being the component of the wave vector perpendicular to the electron trajectory. The appropriately normalized eigenmodes are plane waves $\mathbf{E} = \left(1/\sqrt{\epsilon_r}\right)\hat{\mathbf{e}}\exp\left(i\mathbf{k}\cdot\mathbf{r}\right)$, where $\hat{\mathbf{e}}$ is a polarization unit vector orthogonal to the wave vector $\mathbf{k}$. Further, according to the Eq. (7.14) the wave vector component $k_{\parallel}$ is equal to $k_{\parallel} = \omega/|\mathbf{v}|$ with $m = 0$ and the coefficient c_0 is given by $c_0 = |\mathbf{k}_{\perp}|\,/\left(\sqrt{\epsilon_r}\,|\mathbf{k}|\right)$. Then in the 3D case, taking into account that the integration contour $\partial\mathcal{S}$ is a circle of radius $|\mathbf{k}_{\perp}|$ and performing integration in polar coordinates with $dk = |\mathbf{k}_{\perp}|\,d\phi$, the radiated power (7.19) is given by

$$\left(\frac{dP}{dl}\right)_h^{3D} = \frac{1}{4\pi\epsilon_0}\frac{q^2}{c\sqrt{\epsilon_r}}\,|\mathbf{k}|\left(1 - \left(\frac{\left|\mathbf{k}_{\parallel}\right|}{|\mathbf{k}|}\right)^2\right), \tag{7.24}$$

which finally yields the usual results of the Frank-Tamm theory [7]

$$\left(\frac{dP}{dl}\right)_h^{3D} = \frac{q^2\omega}{4\pi\epsilon_0 c^2}\left(1 - \frac{c^2}{\epsilon_r\,|\mathbf{v}|^2}\right). \tag{7.25}$$

In the 2D case Eq. (7.22) yields

$$\left(\frac{dP}{dl}\right)_h^{2D} = \frac{1}{2\pi\epsilon_0}\frac{q^2}{c\sqrt{\epsilon}}\sqrt{1 - \frac{c^2}{\epsilon_r\,|\mathbf{v}|^2}}. \tag{7.26}$$

7.3 Numerical Results

In this section the analytical results developed in the previous section are applied to study the Cherenkov radiation in a 2D photonic crystal. An infinite 2D square lattice of air holes in a dielectric medium is considered. The radius of the holes is $r = 0.4a$, while the dielectric constant of the background medium is $\epsilon_r = 12$. A line charge oriented perpendicular to the periodicity plane of the crystal moves along the z-axis with a velocity v, staying always in the space between air holes (Fig. 7.3 bottom). The corresponding current density, Eqs. (6.2) and (7.2), generates an electric field (7.1) polarized in the periodicity plane (transverse electric or TE polarization) because the Bloch modes to which the current density can couple are polarized in this way. The first TE band for the considered PhC is presented in the figure 7.3-top. The band structure was calculated using the plane wave expansion method [32].

To find the power radiated by a charge moving with a given velocity v, all Bloch modes contributing to the radiation should be determined. These modes $(\mathbf{k}; n)$ are given by the solutions of relation (7.23). In what follows we restrict our analysis to the frequency range of the first band of the considered PhC structure. In figure 7.3-top, solutions of the Cherenkov relations (7.23) are graphically illustrated for $m = 0, -1, -2$ (dashed lines) and charge velocity $v = 0.15c$. The spectral range of the intersections determine the frequencies of the nonzero contribution to the Cherenkov radiated power, *the Cherenkov band*. The evolution of the Cherenkov band is presented in figure 7.4 as a function of the charge velocity.

For charge velocity $v = 0.15c$, the Cherenkov spectrum is given by the intersections of the band structure with the planes $m = -1$ and $m = -2$. The plane corresponding to $m = 0$ does not intersect the band structure of the crystal (Figs. 7.3, 7.4). For smaller charge velocities, more and more planes intersect the band structure and the Cherenkov spectrum is built from a number of discrete sub-bands. For even smaller charge velocities the spectral range of the first photonic band becomes densely filled with the discrete sub-bands (Fig. 7.4).

In the long wavelength limit the periodic medium is effectively homogeneous. For the considered PhC an effective refractive index is equal to $n_{\text{eff}} = \sqrt{\epsilon_{\text{eff}}} \approx 2.186$. Consequently, for $m = 0$ the relation (7.23) imposes the condition on a minimal charge velocity resulting in the Cherenkov radiation at small frequencies, namely $v_{\min} \geq c/n_{\text{eff}} \approx 0.457c$. For charge velocities larger than the threshold value the Cherenkov band covers the spectral range from zero to the maximum frequency, which is defined by the intersection of

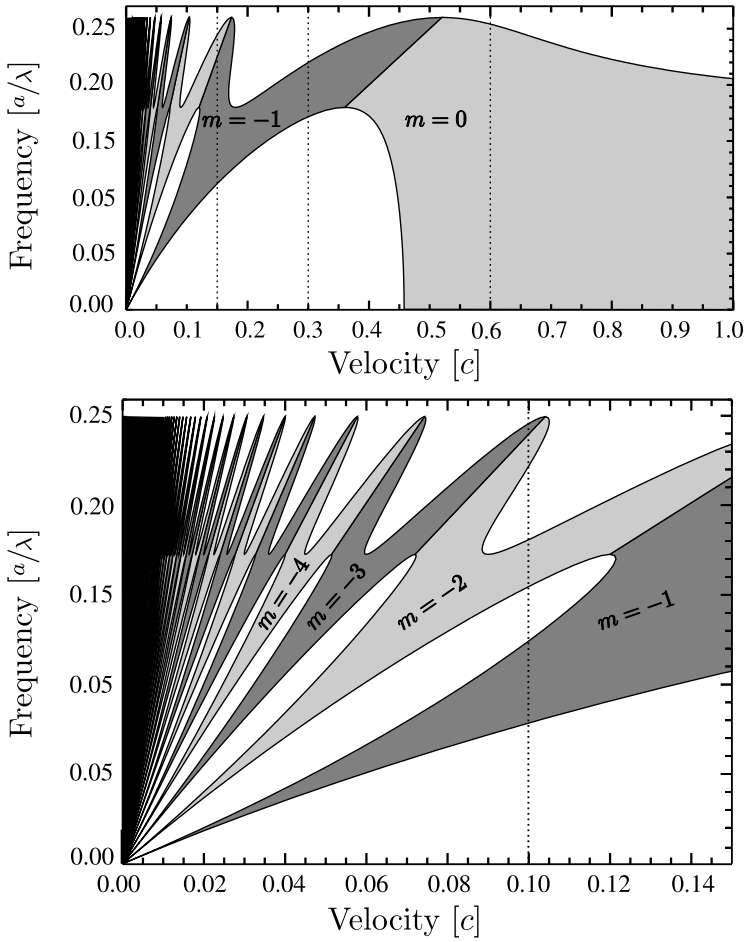

Figure 7.4: Cherenkov radiation band. Sub-bands defined by the intersections of the band structure with the planes corresponding to the different m's are shaded in light and dark gray. Vertical lines mark the charge velocities used in the further calculations, $v = 0.15c$, $v = 0.3c$ and $v = 0.6c$ in the top panel and $v = 0.1c$ in the bottom panels, respectively.

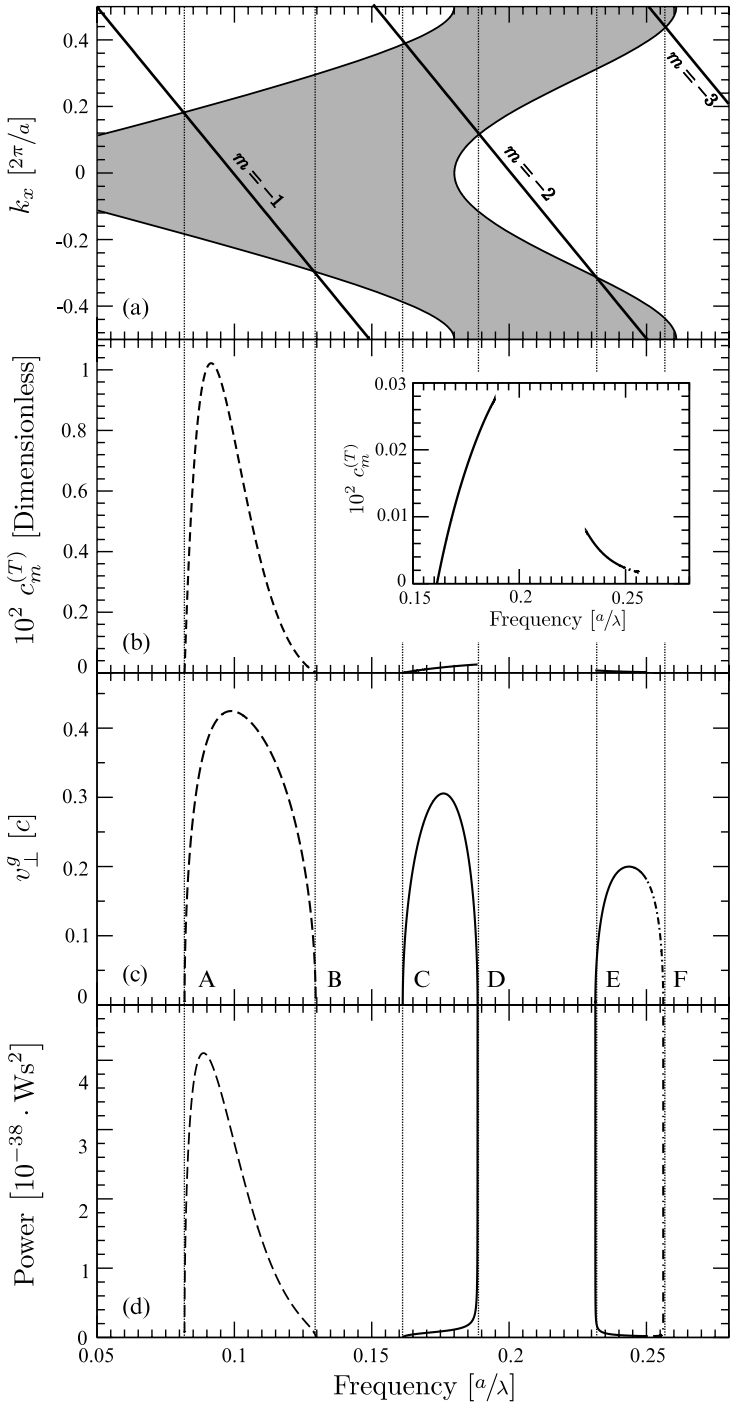

Figure 7.5: Cherenkov emission spectrum for the charge velocity $v = 0.1c$. Projections of the first band of the considered photonic crystal and the planes $m = -1$, $m = -2$ and $m = -3$ defining the Cherenkov band on the k_x-ω plane are shown (a). The Fourier coefficients, $c_m^{(T)}(\mathbf{k}; n)$, the orthogonal component of the group velocity, $v_\perp^g$, and the Cherenkov power spectrum are shown in panels (b), (c) and (d), respectively. Vertical lines mark the edges of the Cherenkov sub-bands. Contribution from the sub-bands corresponding to $m = -1$, $m = -2$ and $m = -3$ are shown as dashed, solid and dashed-dotted lines, respectively.

the band structure with the plane $m = 0$ at the first BZ boundary (Fig. 7.4).

To use further Eq. (7.22), one should calculate the Bloch modes along the charge trajectory, their Fourier transforms and corresponding group velocities for wave vectors belonging to the intersections defined by Eq. (7.23). The calculation of the Cherenkov spectrum is illustrated in figure 7.5 for a line charge ($q = 1.6 \times 10^{-19}\, C$) moving with the velocity $v = 0.1c$. To calculate Bloch modes and group velocities, the plane wave expansion method [32] and the Hellmann-Feynman theorem [8] were used, respectively. For the velocity $v = 0.1c$ the Cherenkov spectrum consists on three sub-bands defined by planes $m = -1$, $m = -2$ and $m = -3$ (Figs.7.4, 7.5), respectively. The Fourier coefficients, $c_m^{(T)}(\mathbf{k}; n)$, (Fig. 7.5-b) and the orthogonal component of the group velocity, $v_\perp^g$, (Fig. 7.5-c) are nonzero only within the sub-bands. Both Fourier coefficients and the orthogonal component of the group velocity approach zero at sub-band edges A, B and C. At the edges D, E, and F only the orthogonal component of the group velocity is zero, while the Fourier coefficients have finite nonzero value. Calculation of the Cherenkov radiated power at the band edges A, B and C leads to the indeterminate limits of the form 0/0, which can be evaluated using l'Hôpital's rule and is equal to zero. The Cherenkov power at the band edges D, E and F diverges and becomes infinite.

In figure 7.6 the Cherenkov radiated power spectra are shown for charge velocities $v = 0.15c$, $v = 0.3c$ and $v = 0.6c$. For charge velocities smaller than the threshold value $v_{\min} \approx 0.457c$ the Cherenkov radiation is nonzero only within single or multiple spectral bands. For velocities above the threshold, the radiated power is nonzero almost everywhere within the first band, approaching asymptotically the value of the Cherenkov radiated power in a homogeneous medium with $n = n_{\text{eff}}$ for small frequencies. The radiated power calculated using Eq. (7.26) for $v = 0.6c$ and $n_{\text{eff}} = 2.186$ is shown in figure 7.6 (bottom panel) as dotted line. The Cherenkov radiated power is enhanced near the frequencies where the group velocity component orthogonal to the charge trajectory vanishes, while the Fourier coefficients remain finite (Fig. 7.6).

To substantiate our analytical results the direct numerical integration of the Maxwell's equations has been performed using rigorous finite-difference time-domain (FDTD) method [28]. The simulated structure was a $10a \times Na$ lattice of air holes in a homogeneous medium with $\epsilon = 12.0$. The longitudinal dimension of the periodic structure was set to $N = 188$, $N = 376$ and $N = 752$ lattice constants for charge velocities $v = 0.15c$, $v = 0.3c$ and $v = 0.6c$, respectively. The lattice was surrounded by a $2a$ wide layer of homogeneous material. The simulation domain was discretized into squares with a side $\Delta = a/18$ and was surrounded by a 35-cell-wide perfectly matched layer (PML) [33]. An integration time step was set to the 98% of the Courant value. A moving point source (6.2) was

modeled as a current density source [28] with the Dirac delta function represented via an appropriately normalized Kronecker delta δ_{ij}/Δ^2. The charge moves in the longitudinal direction with the trajectory placed in the geometrical center of the crystal, exactly between the 5th and 6th row of holes.

To calculate the radiated power the electric and magnetic fields were stored at the detector and their Fourier transforms were found using discrete Fourier transform method. The longitudinal dimension of the structure was different for different charge velocities in order to keep the integration time at the detector and consequently the spectral resolution constant. The detector enclosing the crystal was situated in the close vicinity of the crystal boundary. The total radiated power per unit length was calculated as

$$\frac{dP}{dl} = \frac{1}{d}\frac{2}{\pi}\int_0^d dz\, \mathbf{S}(z,\omega)\cdot\hat{\mathbf{n}} \tag{7.27}$$

where $\mathbf{S}(z,\omega) = \frac{1}{2}\Re\{\mathbf{E}(z,\omega)\times\mathbf{H}^{\star}(z,\omega)\}$ is a time averaged Poynting vector, d is the length of the detector along the trajectory and $\hat{\mathbf{n}}$ is a unit vector orthogonal to the detector interface.

An overall very good agreement between the results of the analytical (Fig. 7.6, solid lines) and numerical calculations (Fig. 7.6, dashed lines) is obtained. Both the spectral range of a nonzero radiated power and its absolute value are well represented using the FDTD method. The main difference can be traced back to Fabry-Perot-like oscillations of the radiated power due to the finite-size effects in the FDTD calculations. In the finite structure, the Cherenkov radiated power stays considerably enhanced near the band edges having large but finite value. The total power oscillates around the analytical value becoming partially suppressed or enhanced for different frequencies. To confirm that these oscillations indeed result from the finite transverse dimension of the considered photonic crystal, we have performed simulations for the crystal with a double thickness ($20a \times 188a$) for the charge velocity $v = 0.15c$. Resulting radiated power spectrum is shown in the corresponding panel in figure 7.6 as a dashed-dotted curve. One can see twice as many oscillations as in the case of the thinner structure, which is a typical signature of the Fabry-Perot like phenomena. The further enhancement of the radiated power in comparison to the infinite structure can be associated with the longer interaction time of the charge at resonance frequencies with the effectively slow Fabry-Perot modes of a photonic crystal slab.

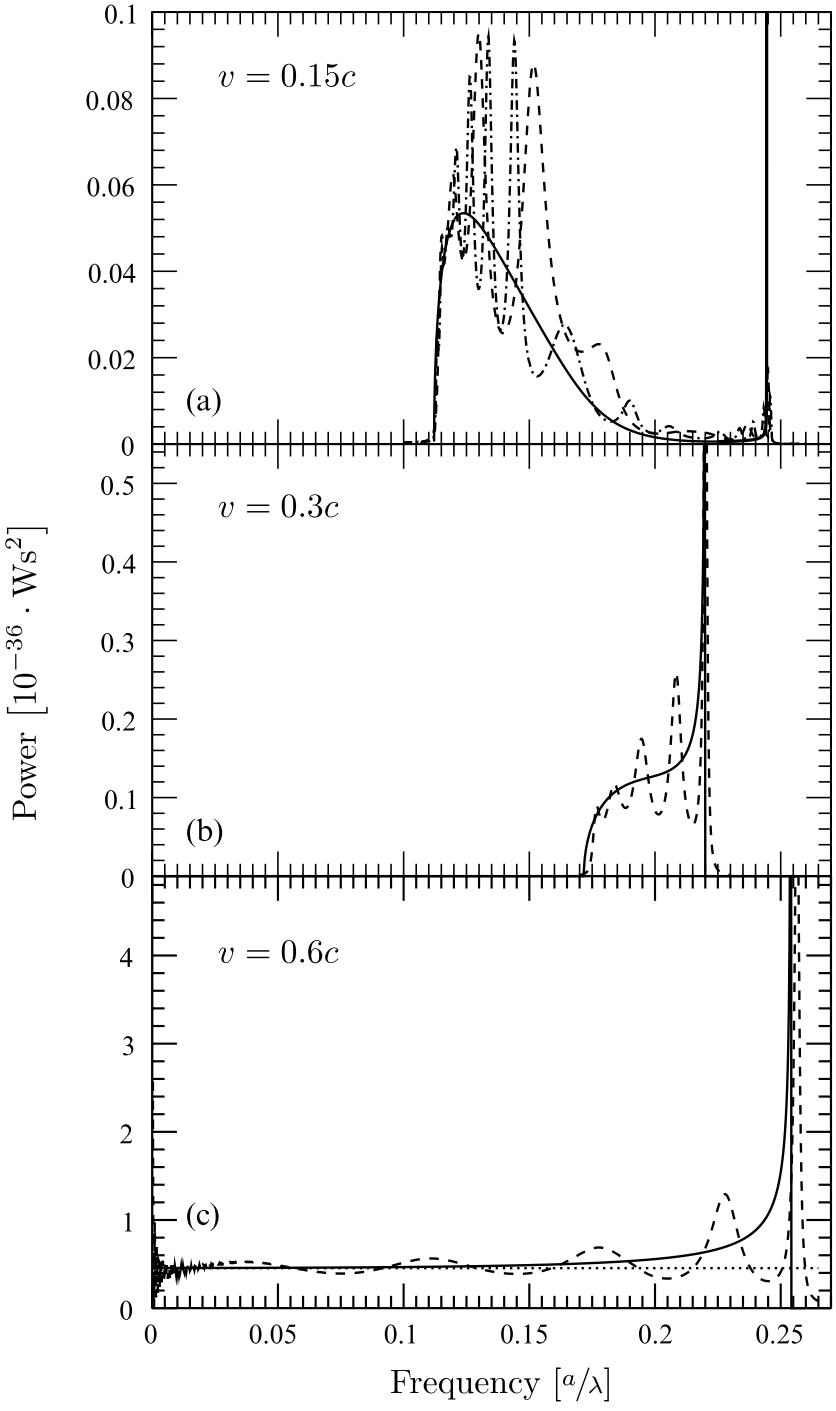

Figure 7.6: Cherenkov emission spectra for different charge velocities in a 2D photonic crystal. Solid lines correspond to the analytical results (7.22). Dotted line in the bottom panel ($v = 0.6c$) corresponds to the Cherenkov radiated power in the homogeneous medium with $n_{\mathrm{eff}} = 2.186$, Eq. (7.26). Radiated power spectra obtained using FDTD method are shown as dashed lines. For charge velocity $v = 0.15c$ radiated power spectra are show for both $10a \times 188a$ (dashed line) and $20a \times 188a$ (dashed-dotted line) structures.

7.4 Summary

In this chapter, an analytical expression for the Cherenkov power emitted per unit length of the charge trajectory in the case of a general 3D and 2D periodic dielectric medium has been derived. The obtained formula for the Cherenkov power involves the calculations of Bloch modes and corresponding group velocities at limited points of the reciprocal space only, making the application of the proposed method computationally not demanding. All calculations have been performed on a desktop PC and our method requires 5 to 10 times less CPU time then FDTD method. The analysis of the Cherenkov emission spectrum in the periodic medium reveals that the Cherenkov effect indeed exists for every electron velocity. Similar to the case of the modification of the dipole emission in a photonic crystal, the Cherenkov radiation can be suppressed if the coupling of the current density produced by a moving electron with a Bloch mode is poor. At the same time, an enhancement of the Cherenkov radiation is possible also if only the component of the group velocity orthogonal to the electron trajectory is small. We have illustrated the developed analytical method and its conclusions using a numerically rigorous finite-difference time-domain method in a special case of a 2D photonic crystal and demonstrated a reasonable agreement between numerical and analytical results.

8 Spatial Distribution[1]

The goal of this chapter is to develop an analytical theory of the Cherenkov radiation in far-field zone in order to provide a simple semi-analytical tool to study its spatial distribution peculiarities in general 3D and 2D periodic dielectric media. To achieve this goal we first derive an analytical expression for the electric far-field in terms of the Bloch mode expansion. Secondly we restrict the full k-space integration in the Bloch mode expansion of the field to a relatively simple surface (contour) integral in the first Brillouin zone of the 3D (2D) periodic medium. Thirdly, we restrict this integral further to a simple sum over a small number of Bloch eigenmodes. These derived formulas allow us to identify the main contribution to the spatial peculiarities of the Cherenkov radiation.

The chapter is organized as follows. In section (8.1) an analytical expression for the Cherenkov far-field is derived both for 3D and 2D photonic crystals. In section (8.2) we apply the developed theory to calculate the Cherenkov far-field in the particular case of a 2D photonic crystal. Predictions of the analytical theory are substantiated by numerically rigorous finite-difference time-domain (FDTD) [28] calculations.

8.1 Cherenkov Radiation in the Far-Zone

Combining the general solutions (4.60) and (4.68) in time space for the 3D case and the 2D case respectively and substituting (6.2) for the current density the Cherenkov field can be written

$$\mathbf{E}(\mathbf{r},t) = -\frac{q\,|\mathbf{v}|}{(2\pi)^d \epsilon_0} \sum_n \int_{BZ} d^d k \int_{-\infty}^{t} dt' \cos\left[\omega_{\mathbf{k}n}^{(T)}\left(t-t'\right)\right] \cdot \mathbf{E}_{\mathbf{k}n}^{(T)}(\mathbf{r}) \left(\mathbf{E}_{\mathbf{k}n}^{(T)\star}\left(\mathbf{v}t'\right)\cdot\hat{\mathbf{v}}\right) \quad (8.1)$$

where $d \in \{2,3\}$ denotes the dimensionality of the crystal and $\mathbf{E}_{\mathbf{k}n}^{(T)}(\mathbf{r})$ the quasi-transverse Bloch eigenmodes (Sec. 4.1 and 4.4) characterized by the band index n, the

[1] This chapter is based on: C. Kremers and D.N. Chigrin, "Spatial distribution of Cherenkov radiation in periodic dielectric media", *J. Opt. A.*, **11**(11)

wave vector $\mathbf{k}$ and the eigenfrequencies $\omega_{\mathbf{k}n}^{(T)}$. The longitudinal modes do not contribute to the radiation as was shown in the previous chapter. Therefore we skip the label (T) in the following discussion. Expressing the cosine function in Eq. (8.1) as a sum of two complex exponential functions and using Bloch's theorem $\mathbf{E}_{\mathbf{k}n}(\mathbf{r}) = \mathbf{e}_{\mathbf{k}n}(\mathbf{r}) \exp(i\mathbf{k}\cdot\mathbf{r})$, where $\mathbf{e}_{\mathbf{k}n}(\mathbf{r})$ is a lattice periodic function (Sec. 4.4), the Cherenkov field (8.1) becomes

$$\mathbf{E}(\mathbf{r},t) = -\frac{q\,|\mathbf{v}|}{2(2\pi)^d \epsilon_0} \sum_n (I_+ + I_-) \tag{8.2}$$

where $I_\pm$ is defined as

$$I_\pm = \int_{BZ} d^d k \int_{-\infty}^{t} dt'\, \mathbf{e}_{\mathbf{k}n}(\mathbf{r}) \left(\mathbf{e}^\star_{\mathbf{k}n}\left(\mathbf{v}t'\right)\cdot\hat{\mathbf{v}}\right) \mathcal{E}_\pm(\mathbf{k},t') \tag{8.3}$$

with

$$\mathcal{E}_\pm(\mathbf{k},t') = \exp\left\{i\left[\mathbf{k}\cdot\left(\mathbf{r}-\mathbf{v}t'\right) \pm \omega_{\mathbf{k}n}\left(t-t'\right)\right]\right\}. \tag{8.4}$$

Further taking into account the symmetries of the Bloch eigenmodes, $\mathbf{e}_{-\mathbf{k}n} = \mathbf{e}^\star_{\mathbf{k}n}$ and $\omega_{-\mathbf{k}n} = \omega_{\mathbf{k}n}$ (Sec. 4.4.4), the following relation for the integrals $I_\pm$ (8.3) holds

$$I_+ = I_-^\star = \int_{\mathrm{BZ}} d^d k \int_{-\infty}^{t} dt'\, \mathbf{e}_{-\mathbf{k}n}(\mathbf{r}) \left(\mathbf{e}^\star_{-\mathbf{k}n}\left(\mathbf{v}t'\right)\cdot\hat{\mathbf{v}}\right) \mathcal{E}_+(-\mathbf{k},t').$$

Therefore the radiated field (8.2) can be exclusively expressed in terms of the real part of the integral I_-

$$\mathbf{E}(\mathbf{r},t) = -\frac{q\,|\mathbf{v}|}{(2\pi)^d \epsilon_0} \sum_n \Re\,(I_-)\,. \tag{8.5}$$

To analyze further the Cherenkov field (8.5) we limit ourselves to charge trajectories which do not cut dielectric interfaces of the periodic medium. In this case "bremsstrahlung" radiation can be neglected and the trajectories themselves are necessarily oriented rationally with respect to the periodic lattice. In this case $\mathbf{e}^\star_{\mathbf{k}n}(\mathbf{v}t')\cdot\hat{\mathbf{v}}$ in (8.3) is a one-dimensional (1D) periodic function with a period $\mathfrak{a}$ defined by the orientation of the charge trajectory therefore one can Fourier expand it as follows

$$\mathbf{e}^\star_{\mathbf{k}n}(\mathbf{v}t')\cdot\hat{\mathbf{v}} = \sum_{m=-\infty}^{\infty} c_{nm}(\mathbf{k}) \exp\left(i\frac{2\pi|\mathbf{v}|}{\mathfrak{a}} m t'\right) \tag{8.6}$$

with Fourier coefficients

$$c_{nm}(\mathbf{k}) = \frac{1}{\mathfrak{a}} \int_0^{\mathfrak{a}} d\xi\ \left(\mathbf{e}^\star_{\mathbf{k}n}(\xi\hat{\mathbf{v}})\cdot\hat{\mathbf{v}}\right) \exp\left(-i\frac{2\pi}{\mathfrak{a}} m\xi\right). \tag{8.7}$$

This allows us to rewrite (8.3) in the form

$$I_- = \sum_{m=-\infty}^{\infty} \int_{BZ} d^d k \int_{-\infty}^{t} dt' \, \mathbf{e}_{\mathbf{k}n}(\mathbf{r}) \, c_{nm}(\mathbf{k}) \tilde{\mathcal{E}}_{nm}(\mathbf{k}, t') \tag{8.8}$$

where the function $\tilde{\mathcal{E}}_{nm}(\mathbf{k}, t')$ is given by

$$\begin{aligned} \tilde{\mathcal{E}}_{nm}(\mathbf{k}, t') &= \exp\left[i \left(\mathbf{k} \cdot \left(\mathbf{r} - \mathbf{v}t' \right) - \omega_{\mathbf{k}n} \left(t - t' \right) + \frac{2\pi |\mathbf{v}|}{\mathfrak{a}} m t' \right) \right] \\ &= \exp\left[i f_{nm}(\mathbf{k}, t') \right]. \end{aligned} \tag{8.9}$$

We are interested in the field far away from the trajectory of the charge. In the far-field zone the following relation $|\mathbf{r} - \mathbf{v}t'| \gg \lambda$ holds for all moments of time $t' < t$. If this condition is fulfilled a small variation of the wave vector $\mathbf{k}$ results in rapid oscillations of the exponential function $\tilde{\mathcal{E}}_{nm}(\mathbf{k}, t')$. Taking into account that the function $\mathbf{e}_{\mathbf{k}n}(\mathbf{r}) \, c_{nm}(\mathbf{k})$ is a slowly varying function of the wave vector, the main contribution to the integral I_- in the far-field zone comes from the neighborhood of k-points where the variation of the phase $f_{nm}(\mathbf{k}, t')$ is minimal. Such stationary k-points are defined by the relation

$$\nabla_{\mathbf{k}} f_{nm}(\mathbf{k}, t') = 0, \tag{8.10}$$

which explicitly reads as

$$\mathbf{v}_{\mathrm{g}}(\mathbf{k}) = \nabla_{\mathbf{k}} \omega_n(\mathbf{k}) = \frac{\mathbf{r} - \mathbf{v}t'}{t - t'}. \tag{8.11}$$

Where $\mathbf{v}_g(\mathbf{k})$ is the group velocity of the Bloch eigenmode. Relation (8.11) can be written in the equivalent form

$$\left(\mathbf{v}_{\mathrm{g}}(\mathbf{k}) - \mathbf{v} \right) \cdot \left(\mathbf{r} - \mathbf{v}t \right) = \frac{|\mathbf{r} - \mathbf{v}t|^2}{t - t'}, \tag{8.12}$$

with its right hand side being positive for all moments of time $t' < t$. Taking that into account, the integration in (8.8) can be restricted to the part of the Brillouin zone, BZ_1, containing all wave vectors whose group velocities fulfill the relation

$$\left(\mathbf{v}_{\mathrm{g}}(\mathbf{k}) - \mathbf{v} \right) \cdot \left(\mathbf{r} - \mathbf{v}t \right) > 0. \tag{8.13}$$

Further, noting that in BZ_1 there does not exist any stationary points for $t' > t$, the t'-integration in (8.8) can be extended to the whole real axis without severe error. With

a good accuracy the integral I_- can be approximated by

$$I_- \approx \sum_{m=-\infty}^{\infty} \int_{\mathrm{BZ}_1} d^d k \int_{-\infty}^{\infty} dt' \, \mathbf{e}_{\mathbf{k}n}(\mathbf{r}) \, c_{nm}(\mathbf{k}) \tilde{\mathcal{E}}_{nm}(\mathbf{k}, t').$$

Using the integral expression of the Dirac delta function

$$\delta(\omega) = \frac{1}{2\pi} \int_{-\infty}^{\infty} dt \, e^{i\omega t}, \tag{8.14}$$

the t'-integration can be easily performed resulting in

$$I_- \approx 2\pi \sum_{m=-\infty}^{\infty} \int_{\mathrm{BZ}_1} d^d k \left\{ \mathbf{e}_{\mathbf{k}n}(\mathbf{r}) c_{nm}(\mathbf{k}) \exp\left[i\left(\mathbf{k}\cdot\mathbf{r} - \omega_{\mathbf{k}n} t\right)\right] \delta\left(\omega_{\mathbf{k}n} - \mathbf{k}\cdot\mathbf{v} + \frac{2\pi\,|\mathbf{v}|}{\mathfrak{a}} m\right) \right\}. \tag{8.15}$$

Furthermore, using the integral relation (7.18)

$$\int_V d^d r \, f(\mathbf{r}) \delta\left(g\left(\mathbf{r}\right)\right) = \int_{\partial V} d^{d-1} r \, \frac{f(\mathbf{r})}{|\nabla g(\mathbf{r})|},$$

where ∂V is a surface defined by the equation $g\left(\mathbf{r}\right) = 0$, the d-dimensional integral in (8.15) can be reduced to the $(d-1)$-dimensional integral

$$I_- \approx 2\pi \sum_m \int_{\mathcal{C}_m} d^{d-1} k \, \frac{\mathbf{e}_{\mathbf{k}n}\left(\mathbf{r}\right) c_{nm}(\mathbf{k})}{|\mathbf{v}_{\mathrm{g}}(\mathbf{k}) - \mathbf{v}|} \exp\left[i\left(\mathbf{k}\cdot\mathbf{r} - \omega_{\mathbf{k}n} t\right)\right], \tag{8.16}$$

which finally gives the following expression for the Cherenkov far-field

$$\mathbf{E}(\mathbf{r}, t) = -\frac{q\,|\mathbf{v}|}{(2\pi)^{d-1}\epsilon_0} \sum_{n,m} \Re\left\{ \int_{\mathcal{C}_m} d^{d-1} k \, \frac{\mathbf{e}_{\mathbf{k}n}\left(\mathbf{r}\right) c_{nm}(\mathbf{k})}{|\mathbf{v}_g(\mathbf{k}) - \mathbf{v}|} \exp\left[i\left(\mathbf{k}\cdot\mathbf{r} - \omega_{\mathbf{k}n} t\right)\right] \right\}. \tag{8.17}$$

The integration is performed over the part of the Brillouin zone, BZ_1, defined by (8.13) and the integration surface (3D case) or contour (2D case) $\mathcal{C}_m$ is defined by the generalized Cherenkov condition (7.14)

$$\omega_{\mathbf{k}n} = \mathbf{k}\cdot\mathbf{v} - \frac{2\pi}{\mathfrak{a}} m\,|\mathbf{v}|, \tag{8.18}$$

where m is an integer. In what follows we will refer to the integration surface (contour)

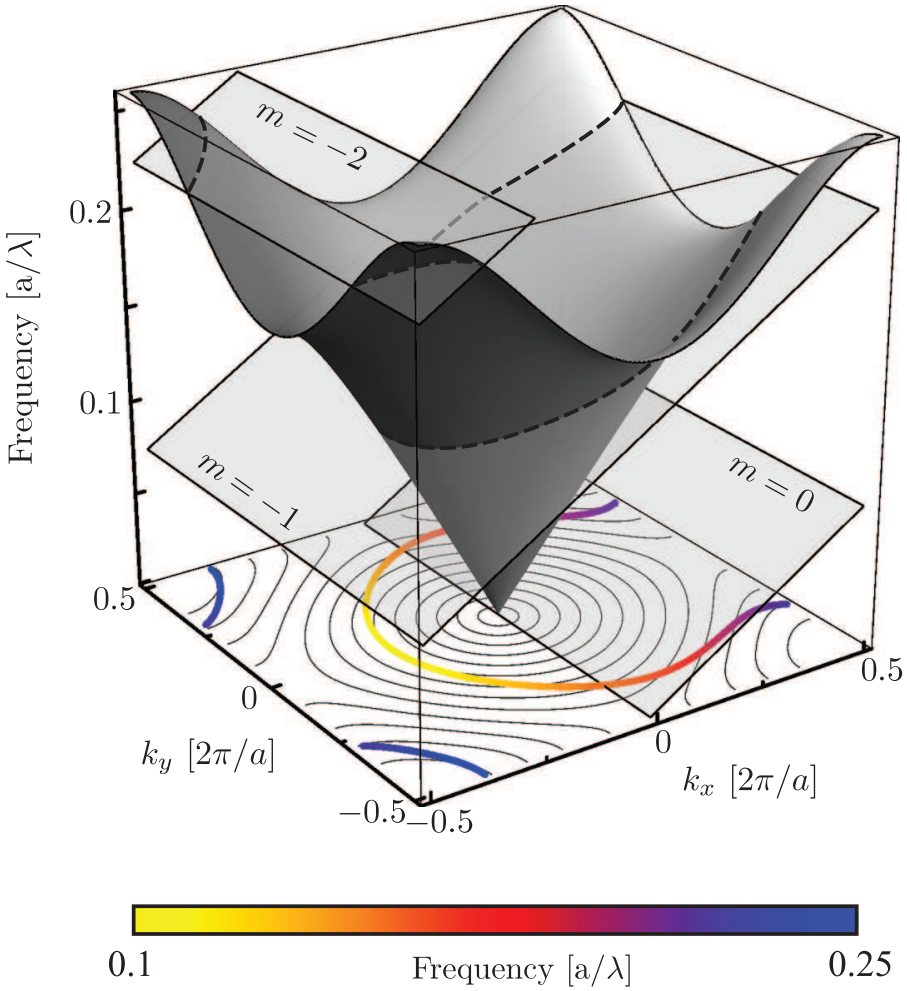

Figure 8.1: Diagram to illustrate the generalized Cherenkov condition. The band structure of the 2D photonic crystal (Fig: 8.1) for TE (transverse electric) polarization as well as the set of planes for $m = 0$, $m = -1$ and $m = -2$ and the charge velocity $\mathbf{v} = 0.15c\,\hat{\mathbf{x}}$ are shown. The intersections of the band structure with the planes define the integration contours $\mathcal{C}_m$ (dashed lines). Additionally a color coded projection of the contour on the first Brillouin zone is shown.

(8.18) as Cherenkov surface (contour).

Equation (8.17) is the main result of the present section. The main goal achieved until now is the restriction of the integration range from the whole Brillouin zone to the solutions of the generalized Cherenkov condition (8.18) in BZ_1 (8.13). A graphical illustration of the Cherenkov condition (8.18) is presented in figure 8.1. The band structure of an infinite square lattice photonic crystal is shown. The dielectric constant of the background medium is $\epsilon_r = 12$ and the radius of the air holes is $r = 0.4a$, where a is the lattice constant (Fig. 7.3-left). The manifold of the Cherenkov wave vectors (the integration contour $\mathcal{C}_m$) is given by the intersection of the band structure, $\omega_{\mathbf{k}n}$, with the set of planes $f(\mathbf{k}_\parallel) = |\mathbf{v}|\,\mathbf{k}_\parallel - |\mathbf{v}|\,\frac{2\pi}{\mathfrak{a}}m$ for different m. Here $\mathbf{k}_\parallel$ is the component of the wave vector parallel to the charge velocity. The slope of the planes is defined by the charge velocity, being $\mathbf{v} = 0.15c\,\hat{\mathbf{x}}$ in this example.

8.1.1 2D Photonic Crystal

To further simplify the integral (8.16) we can parameterize the contour $\mathcal{C}_m$ by its arc length s. Then the contour integral can be transformed into a 1D integral over s

$$I_- \approx 2\pi \sum_m \int ds\, \frac{\mathbf{e}_n\left(\mathbf{k}(s), \mathbf{r}\right) c_{nm}(\mathbf{k}(s))}{|\mathbf{v}_g(\mathbf{k}(s)) - \mathbf{v}|} \exp\left\{i\left[\mathbf{k}(s)\cdot\mathbf{r} - \omega_n(\mathbf{k}(s))t\right]\right\}, \tag{8.19}$$

where the wave vector $\mathbf{k}(s)$ belongs to the contour $\mathcal{C}_m$ defined by the generalized Cherenkov condition (8.18). The main contribution to the integral comes from the k-points $\mathbf{k}(s^\nu)$ in whose neighborhood the phase $h(s) = \mathbf{k}(s)\cdot\mathbf{r} - \omega_n(\mathbf{k}(s))t$ is stationary with respect to the variation of s

$$\begin{aligned} \frac{\partial}{\partial s}\left[\mathbf{k}(s)\cdot\mathbf{r} - \omega_n(\mathbf{k}(s))t\right]\Big|_{s=s^\nu} &= 0 \\ (\mathbf{r} - \mathbf{v}t)\cdot\frac{\partial \mathbf{k}^\nu}{\partial s} &= 0. \end{aligned} \tag{8.20}$$

The second equality holds as the derivative of the Cherenkov condition (8.18) with respect to the arc length s results in

$$\left(\mathbf{v}_\mathrm{g}(\mathbf{k}(s)) - \mathbf{v}\right)\cdot\frac{\partial \mathbf{k}}{\partial s} = 0. \tag{8.21}$$

Combining the stationary phase condition (8.20) with relation (8.21) and taking into account the definition of BZ_1 (8.13), one can see that for stationary Bloch modes the vector $\mathbf{v}_\mathrm{g}(\mathbf{k}^\nu) - \mathbf{v}$ must be parallel to the vector $\mathbf{r} - \mathbf{v}t$. In other words, only the eigenmodes

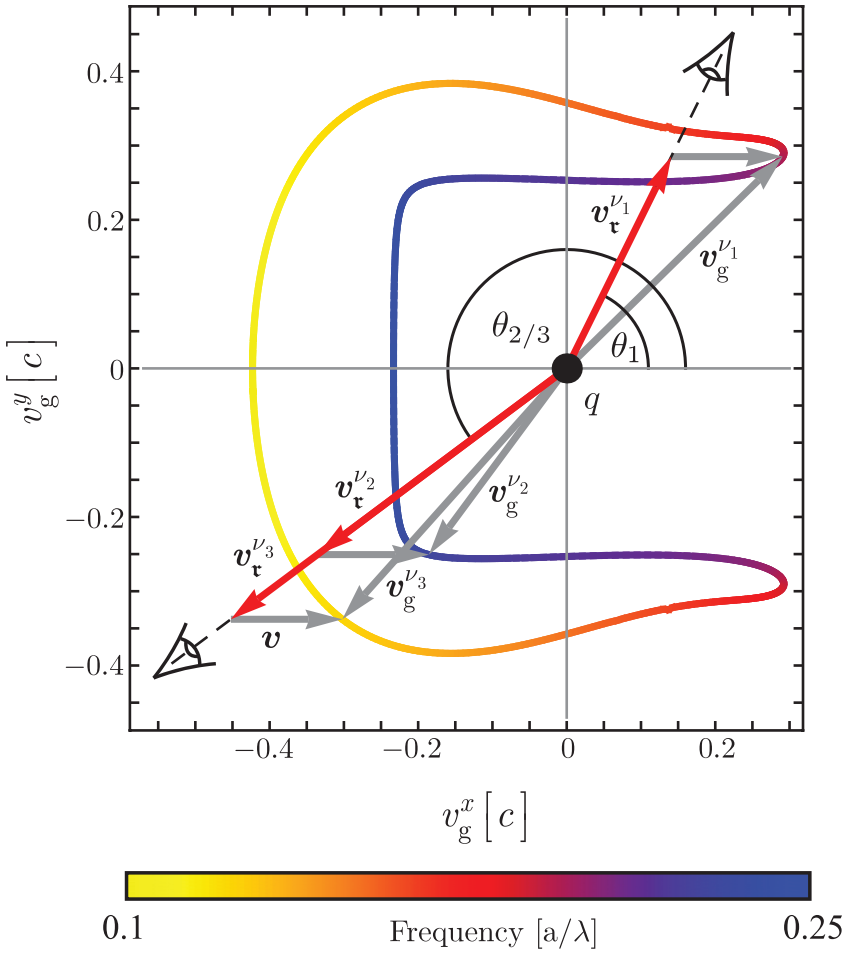

Figure 8.2: Group velocity contour corresponding to the integration contour $\mathcal{C}_m$. The main contribution to the Cherenkov radiation in the direction θ_1 ($\theta_{2/3}$) comes from the Bloch mode(s) with group velocity (velocities) $\mathbf{v}_{\mathrm{g}}^{\nu_1}$ ($\mathbf{v}_{\mathrm{g}}^{\nu_2}$ and $\mathbf{v}_{\mathrm{g}}^{\nu_3}$). The same color coding as in Fig. 8.1 is used.

whose group velocities are pointing towards an observation direction in the coordinate frame moving with the point (line) charge, contribute to the Cherenkov radiation in the far-field zone.

This statement is illustrated in figure 8.2. The group velocity contour corresponding to the integration contour $\mathcal{C}_m$ is shown. The color coding as in Fig. 8.1 is used, the same color corresponds to the same frequency and consequently to the same wave vector. Main contributions to the integral (8.19) for two different observation directions are depicted. For the direction θ_1 only one Bloch mode with group velocity $\mathbf{v}_{\mathrm{g}}^{\nu_1}$ satisfies the stationary phase condition $(\mathbf{v}_{\mathrm{g}}(\mathbf{k}^{\nu}) - \mathbf{v}) \uparrow\uparrow (\mathbf{r} - \mathbf{v}t)$, while for the direction $\theta_{2/3}$ there are two modes with group velocities $\mathbf{v}_{\mathrm{g}}^{\nu_2}$ and $\mathbf{v}_{\mathrm{g}}^{\nu_3}$ fulfilling the condition. There are no Bloch modes satisfying the stationary phase condition for forward observation directions characterized by angles smaller than θ_1.

The integral (8.19) can be further approximated by expanding the phase $h(s)$ near the stationary points $\mathbf{k}(s^\nu) = \mathbf{k}^\nu$ in a Taylor series up to quadratic order

$$h(s) \approx \mathbf{k}^\nu \cdot \mathbf{r} - \omega_n(\mathbf{k}^\nu)t + \frac{1}{2}(\mathbf{r} - \mathbf{v}t) \cdot \frac{\partial^2 \mathbf{k}^\nu}{\partial s^2}(s - s^\nu)^2 \tag{8.22}$$

and extending the integration range to the whole real axis

$$I_- \approx 2\pi \sum_\nu \frac{\mathbf{e}_n(\mathbf{k}^\nu, \mathbf{r})\, c_{nm}(\mathbf{k}^\nu)}{|\mathbf{v}_\mathrm{g}(\mathbf{k}^\nu) - \mathbf{v}|} \exp\{i[\mathbf{k}^\nu \cdot \mathbf{r} - \omega_n(\mathbf{k}^\nu)t]\} \cdot \int_{-\infty}^{\infty} ds\, \exp\left\{\frac{i}{2}\left[(\mathbf{r} - \mathbf{v}t) \cdot \frac{\partial^2 \mathbf{k}^\nu}{\partial s^2}\right](s - s^\nu)^2\right\}. \tag{8.23}$$

Here summation is taken over all possible stationary points ν. The resulting 1D integral can be evaluated analytically [30]

$$\int_{-\infty}^{\infty} dt\, e^{ibt^2} = \sqrt{\frac{\pi}{|b|}} \exp\left[i\frac{\pi}{4}\mathrm{sign}(b)\right], \tag{8.24}$$

which together with the relation

$$(\mathbf{r} - \mathbf{v}t) \cdot \frac{\partial^2 \mathbf{k}^\nu}{\partial s^2} = \mathrm{sign}\left((\mathbf{r} - \mathbf{v}t) \cdot \frac{\partial^2 \mathbf{k}^\nu}{\partial s^2}\right) |(\mathbf{r} - \mathbf{v}t)| \left|\frac{\partial^2 \mathbf{k}^\nu}{\partial s^2}\right| \tag{8.25}$$

results in the final expression for the Cherenkov electric field in far-field zone for a 2D medium

$$\mathbf{E}^{(2D)}(\mathbf{r}, t) \approx -\frac{q\,|\mathbf{v}|}{\epsilon_0 \sqrt{2\pi\,|\mathbf{r} - \mathbf{v}t|}} \sum_{n,\nu} \Re\left(\frac{\mathbf{e}_n(\mathbf{k}^\nu, \mathbf{r})\, c_{nm}(\mathbf{k}^\nu)}{|\mathbf{v}_\mathrm{g}(\mathbf{k}^\nu) - \mathbf{v}|\sqrt{\mathcal{K}^\nu}} \cdot \exp\{i[\mathbf{k}^\nu \cdot \mathbf{r} - \omega_n(\mathbf{k}^\nu)t]\} \exp\left\{i\left[\frac{\pi}{4}\mathrm{sign}\left((\mathbf{r} - \mathbf{v}t) \cdot \vec{\mathcal{K}}^\nu\right)\right]\right\}\right). \tag{8.26}$$

Here $\mathcal{K}^\nu = \left|\vec{\mathcal{K}}^\nu\right| = \left|\frac{\partial^2 \mathbf{k}^\nu}{\partial s^2}\right|$ is the curvature of the contour $\mathcal{C}_m$ at the stationary point $\mathbf{k}^\nu$. Relation (8.25) holds because of $\frac{\partial \mathbf{k}}{\partial s} \perp \frac{\partial^2 \mathbf{k}}{\partial s^2}$ and (8.20).

8.1.2 3D Photonic Crystals

By introducing a 2D coordinate system with unit vectors $\frac{\partial \mathbf{k}}{\partial s_1}$ and $\frac{\partial \mathbf{k}}{\partial s_2}$ tangential to the integration surface $\mathcal{C}_m$, the surface integral (8.16) can be expressed as

$$I_- \approx 2\pi \sum_m \int\int ds_1 ds_2 \left| \frac{\partial \mathbf{k}}{\partial s_1} \times \frac{\partial \mathbf{k}}{\partial s_2} \right| \frac{\mathbf{e}_n\left(\mathbf{k}(\mathbf{s}), \mathbf{r}\right) c_{nm}(\mathbf{k}(\mathbf{s}))}{|\mathbf{v}_\mathrm{g}(\mathbf{k}(\mathbf{s})) - \mathbf{v}|} \exp\left[i\left(\mathbf{k}(\mathbf{s}) \cdot \mathbf{r} - \omega_n(\mathbf{k}(\mathbf{s}))t\right)\right]. \quad (8.27)$$

where $\mathbf{s} \in \mathbb{R}^2$. Similar to the 2D case, the main contribution to the integral comes from the neighborhood of k-points $\mathbf{k}(\mathbf{s}^\nu) = \mathbf{k}^\nu$ where the phase $h\left(\mathbf{s}\right) = \mathbf{k}(\mathbf{s}) \cdot \mathbf{r} - \omega_n(\mathbf{k}(\mathbf{s}))t$ is stationary

$$(\mathbf{r} - \mathbf{v}t) \cdot \frac{\partial \mathbf{k}^\nu}{\partial s_i} = 0, \quad (8.28)$$

with $i \in \{1, 2\}$. Choosing a local coordinate system at the stationary point $\mathbf{k}^\nu$ with basis vectors $\frac{\partial \mathbf{k}}{\partial \xi_1}$ and $\frac{\partial \mathbf{k}}{\partial \xi_2}$ along the main directions of the surface curvatures the following form of the Taylor expansion of the phase $h\left(\mathbf{s}\right)$ can be used to evaluate the integral (8.27)

$$h\left(\xi_1, \xi_2\right) \approx \mathbf{k}^\nu \cdot \mathbf{r} - \omega_n(\mathbf{k}^\nu)t + \frac{1}{2}\left(\mathbf{r} - \mathbf{v}t\right) \cdot \left(\frac{\partial^2 \mathbf{k}^\nu}{\partial \xi_1^2}\left(\xi_1 - s_1^\nu\right)^2 + \frac{\partial^2 \mathbf{k}^\nu}{\partial \xi_2^2}\left(\xi_2 - s_2^\nu\right)^2 \right). \quad (8.29)$$

Here $\frac{\partial^2 \mathbf{k}^\nu}{\partial \xi_1^2}$ and $\frac{\partial^2 \mathbf{k}^\nu}{\partial \xi_2^2}$ are the main curvatures $\mathcal{K}_1^\nu$ and $\mathcal{K}_2^\nu$ of the integration surface $\mathcal{C}_m$. Then extending the integration limits to the whole real plane and using integral relation (8.24) the Cherenkov electric field in far-field zone for a 3D medium reads

$$\mathbf{E}^{(3D)}(\mathbf{r}, t) \approx -\frac{q\,|\mathbf{v}|}{2\pi\epsilon_0\,|\mathbf{r} - \mathbf{v}t|} \sum_{n,\nu} \Re\left(\frac{\mathbf{e}_n\left(\mathbf{k}^\nu, \mathbf{r}\right) c_{nm}(\mathbf{k}^\nu)}{|\mathbf{v}_\mathrm{g}(\mathbf{k}^\nu) - \mathbf{v}|\,\sqrt{\mathcal{K}_1^\nu \mathcal{K}_2^\nu}} \cdot \exp\left\{i\left[\mathbf{k}^\nu \cdot \mathbf{r} - \omega_n(\mathbf{k}^\nu)t\right]\right\} \exp\left\{ i\left[\frac{\pi}{4} \mathrm{sign}\left((\mathbf{r} - \mathbf{v}t) \cdot \vec{\mathcal{K}}_1^\nu \right) \right] \right\} \cdot \exp\left\{ i\left[\frac{\pi}{4} \mathrm{sign}\left((\mathbf{r} - \mathbf{v}t) \cdot \vec{\mathcal{K}}_2^\nu \right) \right] \right\} \right), \quad (8.30)$$

with the product of the main curvatures $\mathcal{K}_1^\nu \mathcal{K}_2^\nu$ being the Gaussian curvature of the surface $\mathcal{C}_m$ defined by the generalized Cherenkov condition (8.18) and $\vec{\mathcal{K}}_i = \frac{\partial^2 \mathbf{k}^\nu}{\partial \xi_i^2}$.

8.2 Numerical Example and Discussion

Formulas (8.17), (8.26) and (8.30) constitute the main result of the present work. In the far-field zone the electric field generated by a point (line) charge uniformly moving in a 3D (2D) periodic medium is dominated by a small number of Bloch eigenmodes of the medium. To calculate the far-field, these Bloch modes (their wave vectors) should be calculated as a solution of the generalized Cherenkov condition (8.18). In turn, the spatial variation of the Cherenkov radiation is dominated (i) by the interference of these Bloch modes at the observation point and (ii) by the topology of the dispersion relation at the Cherenkov surface (contour) in Eqs. (8.17) and (8.30) [Eqs. (8.17) and (8.26)].

In what follows, we apply formulas (8.17) and (8.26) to study spatial distribution of the Cherenkov radiation in the 2D periodic medium depicted in figure 7.3-left. The line charge oriented perpendicular to the periodicity plane of the crystal moves along the x-axis with a velocity $v = 0.15c$, staying always in the space between air holes. The corresponding current density (6.2) couples only to Bloch eigenmodes with an electric field in the periodicity plane, TE (transverse electric) polarization. The first TE photonic band of the considered crystal is presented in figure 8.1. The band structure as well as group velocities and Bloch eigenmodes were calculated using the plane wave expansion method [32].

In order to calculate both the electric field (8.17) and its approximation (8.26) the set of wave vectors contributing to the far-field should be calculated. This set can be found as a numerical solution of the generalized Cherenkov condition (dashed line in Fig. 8.1). In contrast to the homogeneous medium case, such a solution does exist for arbitrary (arbitrary small) charge velocity as was demonstrated in the previous chapter.

Having the set of wave vectors $\mathcal{C}_m$, the Bloch modes $\mathbf{e}_{\mathbf{k}n}$ and the Fourier coefficient $c_{nm}(\mathbf{k})$ should be calculated. The Fourier coefficients $c_{nm}(\mathbf{k})$ give the coupling strength between the current associated with the moving charge and the Bloch eigenmodes. As it can be seen from the definition (8.7) with increasing index $|m|$ the Fourier coefficients become smaller, reducing the contribution of the higher frequencies to the Cherenkov radiation in the far-field zone. Finally, the Cherenkov field (8.17) can be calculated by direct numerical integration.

To calculate the stationary phase approximation of the far-field (8.26), stationary wave vectors $\mathbf{k}^\nu$ should be calculated for a given observation direction $\mathbf{r} - \mathbf{v}t$. This can be done by parameterizing Cherenkov contour by the arc length s and looking for all Bloch modes whose group velocities (Fig. 8.2) satisfy the stationary phase condition $(\mathbf{v}_g(\mathbf{k}^\nu) - \mathbf{v}) \uparrow\uparrow (\mathbf{r} - \mathbf{v}t)$. Further the Bloch modes, the Fourier coefficient and curvature

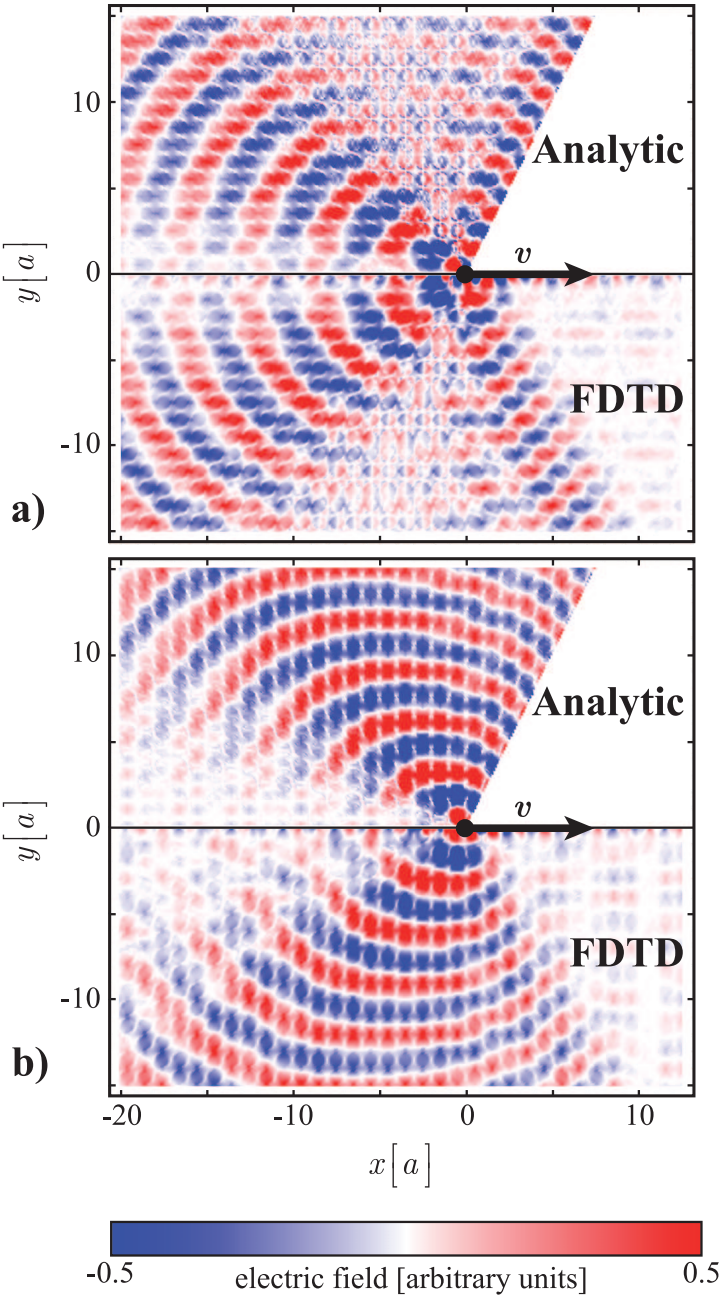

Figure 8.3: $E_x(\mathbf{r}, t = 0)$ (top panel) and $E_y(\mathbf{r}, t = 0)$ (bottom panel) components of the Cherenkov electric field for charge velocity $v = 0.15c$. The results of the stationary phase approximation (8.26) and direct numerical integration using FDTD methods are shown.

of the Cherenkov contour (see appendix E) should be calculated and summed for these stationary points only reducing the computational demands considerably.

In figure 8.3, a numerical calculations of the stationary phase approximation of the far-field is presented for $v = 0.15c$. The $E_x(\mathbf{r}, t = 0)$ and $E_y(\mathbf{r}, t = 0)$ components of the electric field are shown in the upper halves of the top and bottom panels, respectively. Only contributions from the first three sections of the Cherenkov contour corresponding to $m = 0, -1, -2$ have been analyzed. In the case of a homogeneous medium, the standard Cherenkov condition would impose a minimal charge velocity above which Cherenkov radiation is possible $v_{\min} \geq c/n_{\text{eff}} \approx 0.457c$. Here an effective refractive index of the considered periodic medium is asymptotically equal to $n_{\text{eff}} = \sqrt{\epsilon_{\text{eff}}} \approx 2.186$. Although the velocity of the line charge is considerable smaller than v_{min}, in the periodic medium the non-evanescent field can be clearly seen far apart from the charge trajectory (Fig. 8.3). Another characteristic feature of the spatial distribution of the Cherenkov radiation for $v = 0.15c$ is a backward-pointing radiation cone [27]. The field in the forward direction for the observation angles smaller than θ_1 is zero.

The zero field within the backward-pointing radiation cone should be associated with the absence of the stationary solutions for observation directions in the cone (Fig. 8.2). This is a direct consequence of the stationary phase approximation. In figure 8.4-top, the stationary phase approximation of the far-field 10 lattice constants apart from the trajectory is compared with the direct numerical integration of the integral representation of the field (8.17). An excellent agreement between these two solutions can be seen up to the Cherenkov cone θ_1, where the stationary phase approximation breaks down. The cone angle corresponds to the fold in the group velocity contour (Fig. 8.2). The curvature of the Cherenkov contour is zero at the corresponding wave vector and the Taylor expansion (8.22) fails to reproduce the contour accurately in the vicinity of this point. Zero curvature leads to the diverging field (Fig. 8.4-inset). The field calculated with Eq. (8.17) is small but final in the forward directions.

To substantiate our analytical calculations a direct numerical integration of Maxwell's equations using rigorous finite-differences time-domain (FDTD) method [28] has been performed. The corresponding FDTD field distributions are presented in the lower halves of the top and bottom panels of figure 8.3. $200a \times 70a$ lattice of holes with discretization $\Delta = a/18$ has been used for FDTD calculations. The simulation domain was surrounded by a $3a$-wide perfectly matched layer (PML). The integration time step was set to 98% of the Courant value. In order to describe a continuous movement of the charge, the source (6.2) was modeled by a discrete Gaussian in x-direction with a standard deviation $\sigma = 1\Delta$

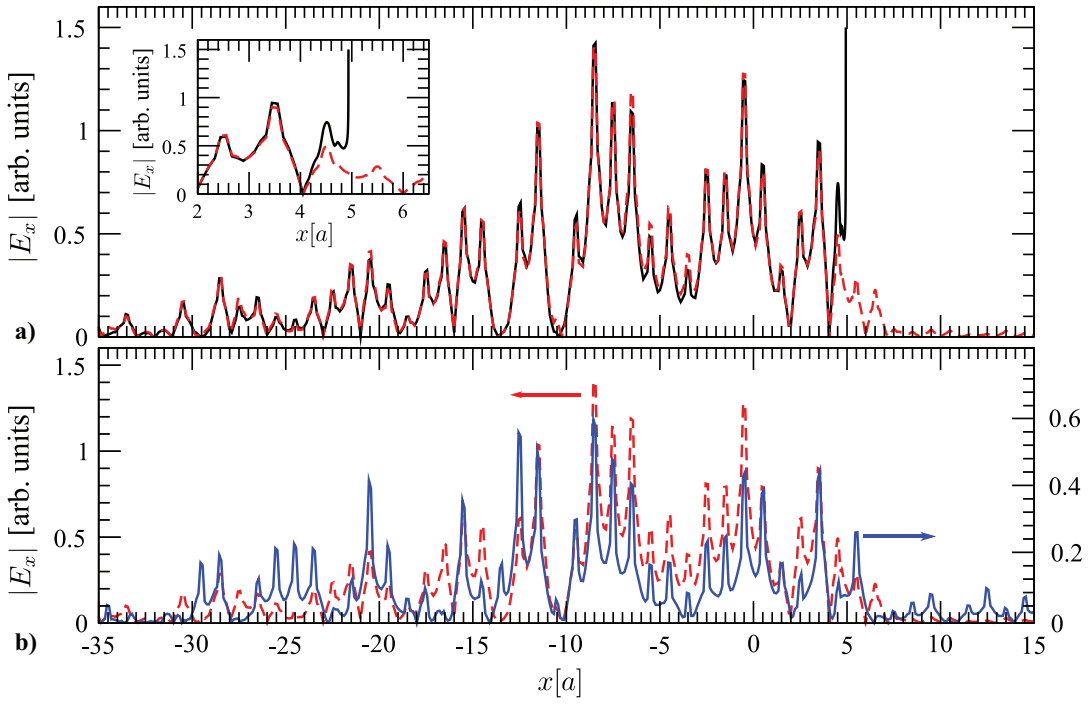

Figure 8.4: Comparison of the integral representation of the far-field (8.17) (dashed red line) with the stationary phase approximation (8.26) (black solid line) (top) and FDTD (blue solid line) (bottom) calculations. An absolute value of the horizontal component of the electric field is shown 10 lattice constants apart from the charge trajectory.

and by an appropriately normalized Kronecker delta in y-direction

$$j(x_i\Delta, y_j\Delta) = \frac{\delta_{jk}}{\sqrt{2\pi}\Delta^2} \exp\left[-\frac{(x_i\Delta - vt)^2}{2\Delta^2}\right]$$

where $y_k = 35a$ is the center of the crystal in vertical direction. In order to compare directly FDTD results with the predictions of formulas (8.17) and (8.26), the static contribution as well as the higher frequency contribution to the FDTD field have been filtered out. An overall good agreement between the results of the analytical and direct numerical calculations is obtained (Fig. 8.3 and 8.4). The FDTD calculations follow nicely the main characteristic of the analytically predicted field. The difference in the absolute values between FDTD and analytical calculations (Fig. 8.4) can be associated with the residual reflections from the perfectly matched layer.

8.3 Summary

In conclusion, we have developed an analytical theory of the Cherenkov radiation in the far-field zone. The field far apart from the charge trajectory can be calculated as a surface (contour) integral over a small fraction of the first Brillouin Zone in a 3D (2D) dielectric medium. We have shown that the main contribution to this integral comes from a small and discrete number of k-points. This opens the possibility to calculate the integral approximately, but with high accuracy. We have also shown, that the spatial variation of the Cherenkov radiation in the far-field is due to the interference of a few Bloch eigenmodes as well as the topological properties of the Cherenkov surface (contour). This has been defined as a manifold of all k-points contributing to the Cherenkov radiation for a given charge velocity. Simple formulas have been derived for the Cherenkov far-field both in 3D and 2D cases. We have compared the developed analytical theory with numerically rigorous FDTD calculations. A good agreement between these two methods has been demonstrated.

References

[1] P. Čerenkov. Visible Radiation Produced by Electrons Moving in a Medium with Velocities Exceeding that of Light. *Physical Review*, 52(4):378–379, August 1937.

[2] J. V. Jelley. *Čerenkov radiation, and its applications*. Pergamon Press, 1958.

[3] E. Fermi. The Ionization Loss of Energy in Gases and in Condensed Materials. *Physical Review*, 57(6):485–493, March 1940.

[4] G. N. Afanasiev, V. G. Kartavenko, and E. N. Magar. Vavilov Cherenkov radiation in dispersive medium. *Physica B*, 269:95–113, 1999.

[5] I. Carusotto, M. Artoni, G. La Rocca, and F. Bassani. Slow Group Velocity and Cherenkov Radiation. *Physical Review Letters*, 87(6), July 2001.

[6] M. Artoni, I. Carusotto, G. La Rocca, and F. Bassani. Vavilov-Cherenkov effect in a driven resonant medium. *Physical Review E*, 67(4), April 2003.

[7] I. M. Frank and I. E. Tamm. Coherent visible radiation of fast electrons passing through matter. *Dokl. Akad. Nauk SSSR*, 14(107), 1937.

[8] K. Sakoda. *Optical properties of photonic crystals*. Springer, 2005.

[9] J. D. Joannopoulos, S. G. Johnson, J. N. Winn, and R. D. Meade. *Photonic Crystals: Molding the Flow of Light*. Princeton University Press, 2008.

[10] V. P. Bykov. Spontaneous emission in a periodic structure. *Sov. Phys. JETP*, 35:269, 1972.

[11] E. Yablonovitch. Inhibited Spontaneous Emission in Solid-State Physics and Electronics. *Physical Review Letters*, 58(20):2059–2062, May 1987.

[12] S. John and J. Wang. Quantum electrodynamics near a photonic band gap: Photon bound states and dressed atoms. *Physical Review Letters*, 64(20):2418–2421, May 1990.

[13] P. S. J. Russell. Optics of Floquet-Bloch waves in dielectric gratings. *Applied Physics B Photophysics and Laser Chemistry*, 39(4):231–246, April 1986.

[14] R. Zengerle. Light Propagation in Singly and Doubly Periodic Planar Waveguides. *Journal of Modern Optics*, 34(12):1589–1617, December 1987.

[15] H. Kosaka, T. Kawashima, A. Tomita, M. Notomi, T. Tamamura, T. Sato, and S. Kawakami. Superprism phenomena in photonic crystals. *Physical Review B*, 58(16):R10096–R10099, October 1998.

[16] H. Kosaka, T. Kawashima, A. Tomita, M. Notomi, T. Tamamura, T. Sato, and S. Kawakami. Self-collimating phenomena in photonic crystals. *Applied Physics Letters*, 74(9):1212, 1999.

[17] P. Etchegoin and R. Phillips. Photon focusing, internal diffraction, and surface states in periodic dielectric structures. *Physical Review B*, 53(19):12674–12683, May 1996.

[18] D. N. Chigrin and C. M. Sotomayor Torres. Periodic thin-film interference filters as one-dimensional photonic crystals. *Optics and Spectroscopy*, 91(3):484–489, September 2001.

[19] D. N. Chigrin. Radiation pattern of a classical dipole in a photonic crystal: Photon focusing. *Physical Review E*, 70(5), November 2004.

[20] F. J. García De Abajo. Smith-Purcell radiation emission in aligned nanoparticles. *Physical Review E*, 61(5):5743–5752, May 2000.

[21] F. J. García De Abajo and L. A. Blanco. Electron energy loss and induced photon emission in photonic crystals. *Physical Review B*, 67(12), 2003.

[22] T. Ochiai and K. Ohtaka. Relativistic electron energy loss and induced radiation emission in two-dimensional metallic photonic crystals. I. Formalism and surface plasmon polariton. *Physical Review B*, 69(12), March 2004.

[23] T. Ochiai and K. Ohtaka. Relativistic electron energy loss and induced radiation emission in two-dimensional metallic photonic crystals. II. Photonic band effects. *Physical Review B*, 69(12), March 2004.

[24] K. Yamamoto, R. Sakakibara, S. Yano, Y. Segawa, Y. Shibata, K. Ishi, T. Ohsaka, T. Hara, Y. Kondo, H. Miyazaki, F. Hinode, T. Matsuyama, S. Yamaguti, and K. Ohtaka. Observation of millimeter-wave radiation generated by the interaction

between an electron beam and a photonic crystal. *Physical Review E*, 69(4):5–8, April 2004.

[25] T. Ochiai and K. Ohtaka. Theory of unconventional Smith-Purcell radiation in finite-size photonic crystals. *Optics Express*, 14(16):7378, 2006.

[26] F. J. García De Abajo, A. G. Pattantyus-Abraham, N. Zabala, A. Rivacoba, M. O. Wolf, and P. M. Echenique. Cherenkov Effect as a Probe of Photonic Nanostructures. *Physical Review Letters*, 91(14):1–4, September 2003.

[27] C. Luo, M. Ibanescu, S. G. Johnson, and J. D. Joannopoulos. Cerenkov radiation in photonic crystals. *Science (New York, N.Y.)*, 299(5605):368–71, January 2003.

[28] A. Taflove and S. C. Hagnes. *Computational Electrodynamics: The Finite-Difference Time-Domain Method.* Artech House, 2000.

[29] J. D. Jackson. *Classical Electrodynamics Third Edition.* Wiley, 1998.

[30] D. Zwillinger. *Table of Integrals, Series, and Products, Seventh Edition.* Academic Press, 2007.

[31] L. Hörmander. *The Analysis of Linear Partial Differential Operators I: Distribution Theory and Fourier Analysis (Classics in Mathematics) (Pt.1).* Springer, 2003.

[32] S. Johnson and J. Joannopoulos. Block-iterative frequency-domain methods for Maxwell's equations in a planewave basis. *Optics Express*, 8(3):173, January 2001.

[33] J. Berenger. A perfectly matched layer for the absorption of electromagnetic waves. *Journal of Computational Physics*, 114(2):185–200, October 1994.

9 Conclusion

Optical Antennas

The general three dimensional volume integral equation has been reduced in two alternative ways to a one dimensional integro-differential equation. In both ways the exact solution of the problem of plane wave scattering on infinite cylinder has be utilized but in different manner. In the derivation of the surface impedance integro-differential equation this solution is used to approximate the surface impedance of the antenna whereas the derivation of the volume current integro-differential equation use its separable nature and its radial dependence as ansatz for the current distribution inside the antenna. A regularization scheme is proposed in order to transform these integro-differential equations into solely integral equation so that the necessity to impose additional boundary conditions at the nanowire edges can be omitted. The integral equations are discretized within a method of moments (MoM) approach. To benchmark the proposed methods gold nanowires have been analyzed at optical and near-infrared spectral range. Both semi-analytical methods demonstrate good agreement and superior numerical performance in comparison with rigorous numerical methods. It has been demonstrated that the accuracy of the volume current integral equation (VC-IE) is slightly better in comparison with the surface impedance integral equation (SI-IE) especially for wires with a small aspect ratio.

Some interesting future project could involve (i) the application of the VC-IE to study the emission dynamic of quantum system in close vicinity to the plasmonic antenna, (ii) the study of coupled systems consisting of two or more nanoantennas and (iii) a formulation similar to the VC-IE but based on equivalent surface currents instead of volume currents.

Cherenkov Radiation in Photonic Crystals

Analytical expressions have been derived for the emission spectra as well as the electric field distribution in the far-field zone for radiation due to a uniformly moving charge (Cherenkov radiation) inside general three dimensional (3D) and two dimensional (2D)

periodic dielectric media.

The obtained formula for the emission spectrum (Cherenkov power emitted per unit length of the charge trajectory) involves the calculation of Bloch modes and corresponding group velocities at limited points of the reciprocal space only. It has been demonstrated that (i) the Cherenkov effect exists for every charge velocity (ii) the radiation can be suppressed if the coupling of the moving charge with a Bloch mode is poor and (iii) an enhancement of radiated energy is possible if the component of the group velocity orthogonal to the charge trajectory is small. The analytical expression derived for the field distribution has been discussed. Manifolds in k-space whose Bloch modes contribute most to the far-field have been illustrated and an intuitive condition for the existence of propagation in a given direction has been derived.

The derived analytical expressions have been used to calculate emission spectra and field distributions for different charge velocities in a two dimensional square lattice photonic crystal. For comparison the same calculations have been performed with rigorous numerical finite-difference time-domain method. Analytics and numerics have demonstrated good agreement.

An improvement of the theory could be done by taking into account the energy loss of the electron due to radiation. It could also be of interest to calculate Cherenkov radiation in a three dimensional photonic crystal structure of practical use to guide experimentalist in its observation. It is also of interest to study the potential of the Cherenkov effect to probe existing photonic crystal structures or building charged particle detectors. The advantage of photonic crystal Cherenkov detectors over conventional ones could be that there is (i) a strong dependence between radiation characteristic and charge velocity and (ii) that also slow particles could be detected.

Appendix

A Lee's Renormalization: Proof of Equation (2.37)

Here we want to give a proof of the Lee splitting Eq. (2.37) following closely the one using classical analysis published by Lee et al. in [9].

If one exclude the arbitrary shaped finite region $V^\star$ in which the singularity is located one can change the order of integration and differentiation, so

$$I_{ij} = A_{ij} + \frac{\partial^2}{\partial x_i \partial x_j} \lim_{\delta \to 0} \int_{V^\star - V_\delta} g(\mathbf{r}, \mathbf{r}') j(\mathbf{r}')\, d^3 r'. \tag{A.1}$$

Differentiating $g(\mathbf{r}, \mathbf{r}')$ once the singularity created is of the order $|\mathbf{r} - \mathbf{r}'|^{-2/3}$ which is still integrable [**?**]. So we can write

$$I_{ij} = A_{ij} - \frac{\partial}{\partial x_i} \lim_{\delta \to 0} \int_{V^\star - V_\delta} j(\mathbf{r}') \frac{\partial}{\partial x'_j} g(\mathbf{r}, \mathbf{r}')\, d^3 r'. \tag{A.2}$$

Substituting the integrand

$$j(\mathbf{r}') \frac{\partial}{\partial x'_j} g(\mathbf{r}, \mathbf{r}') = \nabla' \cdot \left[\hat{\mathbf{x}}_j j(\mathbf{r}') g(\mathbf{r}, \mathbf{r}') \right] - \left(\frac{\partial}{\partial x'_j} j(\mathbf{r}') \right) g(\mathbf{r}, \mathbf{r}')$$

and applying Gauss divergence theorem

$$\int_V \nabla \cdot \mathbf{F}(\mathbf{r}')\, d^3 r' = \oint_{\partial V} \mathbf{F}(\mathbf{r}') \cdot \hat{\mathbf{n}}\, d^2 r' \tag{A.3}$$

one yields

$$
\begin{aligned}
I_{ij} =& A_{ij} + \frac{\partial}{\partial x_i} \lim_{\delta \to 0} \Bigg\{ \int_{V^\star - V_\delta} \left(\frac{\partial}{\partial x'_j} j(\mathbf{r}') \right) g(\mathbf{r}, \mathbf{r}') \, d^3 r' \\
& - \oint_{\partial V^\star + \partial V_\delta} j(\mathbf{r}') g(\mathbf{r}, \mathbf{r}') \, (\hat{\mathbf{x}}_j \cdot \hat{\mathbf{n}}) \, d^2 r' \Bigg\} \\
=& A_{ij} - \lim_{\delta \to 0} \int_{V^\star - V_\delta} \left(\frac{\partial}{\partial x'_j} j(\mathbf{r}') \right) \frac{\partial}{\partial x'_i} g(\mathbf{r}, \mathbf{r}') \, d^3 r' \\
& + \oint_{\partial V^\star} j(\mathbf{r}') \frac{\partial}{\partial x'_i} g(\mathbf{r}, \mathbf{r}') \, (\hat{\mathbf{x}}_j \cdot \hat{\mathbf{n}}) \, d^2 r'
\end{aligned} \tag{A.4}
$$

where the second equality holds because (i) the same argument as above is applicable and (ii) the integral over ∂V_δ vanishes in the limit $\delta \to 0$ since the integrand is $\mathcal{O}(\delta^{-1})$ while the surface element is $\mathcal{O}(\delta^2)$. Next we can substitute

$$
\begin{aligned}
\left(\frac{\partial}{\partial x'_j} j(\mathbf{r}') \right) \frac{\partial}{\partial x'_i} g(\mathbf{r}, \mathbf{r}') =& \frac{\partial}{\partial x'_j} \left[j(\mathbf{r}') - j(\mathbf{r}) \right] \frac{\partial}{\partial x'_i} g(\mathbf{r}, \mathbf{r}') \\
=& \nabla' \cdot \left\{ \hat{\mathbf{x}}_j \left[j(\mathbf{r}') - j(\mathbf{r}) \right] \frac{\partial}{\partial x'_i} g(\mathbf{r}, \mathbf{r}') \right\} \\
& - \left[j(\mathbf{r}') - j(\mathbf{r}) \right] \frac{\partial^2}{\partial x'_j \partial x'_i} g(\mathbf{r}, \mathbf{r}')
\end{aligned} \tag{A.5}
$$

and by using Gauss theorem (A.3) a second time we yield

$$
\begin{aligned}
I_{ij} =& A_{ij} + \oint_{\partial V^\star} j(\mathbf{r}') \frac{\partial}{\partial x'_i} g(\mathbf{r}, \mathbf{r}') \, (\hat{\mathbf{x}}_j \cdot \hat{\mathbf{n}}) \, d^2 r' \\
& - \oint_{\partial V^\star} \left[j(\mathbf{r}') - j(\mathbf{r}) \right] \frac{\partial}{\partial x'_i} g(\mathbf{r}, \mathbf{r}') \, (\hat{\mathbf{x}}_j \cdot \hat{\mathbf{n}}) \, d^2 r' \\
& + \lim_{\delta \to 0} \int_{V^\star - V_\delta} \left[j(\mathbf{r}') - j(\mathbf{r}) \right] \frac{\partial^2}{\partial x'_j \partial x'_i} g(\mathbf{r}, \mathbf{r}') \, d^3 r' \\
=& A_{ij} + j(\mathbf{r}) \oint_{\partial V^\star} \frac{\partial}{\partial x'_i} g(\mathbf{r}, \mathbf{r}') \, (\hat{\mathbf{x}}_j \cdot \hat{\mathbf{n}}) \, d^2 r' \\
& + \lim_{\delta \to 0} \int_{V^\star - V_\delta} \left[j(\mathbf{r}') - j(\mathbf{r}) \right] \frac{\partial^2}{\partial x'_j \partial x'_i} g(\mathbf{r}, \mathbf{r}') \, d^3 r'.
\end{aligned} \tag{A.6}
$$

The last term can be rewritten as

$$\int_{V^\star} \left\{ j(\mathbf{r}') \frac{\partial^2}{\partial x'_j \partial x'_i} g(\mathbf{r}, \mathbf{r}') - j(\mathbf{r}) \frac{\partial^2}{\partial x'_j \partial x'_i} g_0(\mathbf{r}, \mathbf{r}') \right\} d^3r' \\ - j(\mathbf{r}) \int_{V^\star} d^3r' \, \frac{\partial^2}{\partial x'_j \partial x'_i} \left[g(\mathbf{r}, \mathbf{r}') - g_0(\mathbf{r}, \mathbf{r}') \right] \quad \text{(A.7)}$$

In this form the singularities no longer occur because g and g_0 behave identically for $\mathbf{r}' \to \mathbf{r}$ so one needs no longer a limiting procedure in order to define the integrals. Finally Gauss theorem can be used a third time to transform the last integral yielding Eq. (2.37)

$$\begin{aligned} I_{ij} &= A_{ij} + j(\mathbf{r}) \oint_{\partial V^\star} \frac{\partial}{\partial x'_i} g_0(\mathbf{r}, \mathbf{r}') \, (\hat{\mathbf{x}}_j \cdot \hat{\mathbf{n}}) \, d^2r' \\ &\quad + \int_{V^\star} \left\{ j(\mathbf{r}') \frac{\partial^2}{\partial x'_j \partial x'_i} g(\mathbf{r}, \mathbf{r}') - j(\mathbf{r}) \frac{\partial^2}{\partial x'_j \partial x'_i} g_0(\mathbf{r}, \mathbf{r}') \right\} \end{aligned} \quad \text{(A.8)}$$

B Scattering Cross Section, VC-IE and SI-IE

According to Eq. (3.39) the total scattering cross section σ_s is given by

$$\sigma_s = \frac{\oint_S d^2r \ |\mathbf{E}_s|^2}{|\mathbf{E}^{inc}|^2} \tag{B.1}$$

where the scattered electric field $\mathbf{E}_s$ is generated by the induced current density $\mathbf{j}$ and can be expressed as

$$\mathbf{E}_s(\mathbf{r}) = i\omega\mu_0 \int_V d^3r' \overleftrightarrow{\mathbf{G}}(\mathbf{r},\mathbf{r}')\mathbf{j}(\mathbf{r}') \tag{B.2}$$

with the dyadic free space Green's function $\overleftrightarrow{\mathbf{G}}$ (2.34). $\mathbf{E}^{inc}$ denotes the incident field. The spherical surface S lies at infinity. In the far field regime, i.e. $R = |\mathbf{r} - \mathbf{r}'| \gg 1$, only the order $\mathcal{O}\left[R^{-1}\right]$ term of the Green's function contributes and one can expand R for small r'/r up to first order yielding

$$\begin{aligned} R &= \sqrt{(\mathbf{r}-\mathbf{r}')\cdot(\mathbf{r}-\mathbf{r}')} \\ &= \sqrt{r^2 + r'^2 - 2rr'\cos\alpha} \\ &= r\sqrt{1 - 2\frac{r'}{r}\cos\alpha + \left(\frac{r'}{r}\right)^2} \\ &\approx r - r'\cos\alpha \\ &= r - \hat{\mathbf{r}}\cdot\mathbf{r}'. \end{aligned} \tag{B.3}$$

Here, α denotes the angle between $\mathbf{r}$ and $\mathbf{r}'$ and $\hat{\mathbf{r}}$ the unit vector in $\mathbf{r}$-direction. The term $\hat{\mathbf{r}}\cdot\mathbf{r}'$ influences the phase in the exponential function but can be safely ignored in the R^{-1} terms. So the dyadic Green's function in the far field regime is given by

$$\overleftrightarrow{\mathbf{G}}^{FF}(\mathbf{r},\mathbf{r}') = \frac{e^{ik(r-\hat{\mathbf{r}}\cdot\mathbf{r}')}}{4\pi r}\left\{\overleftrightarrow{\mathbf{I}} - \hat{\mathbf{r}}\otimes\hat{\mathbf{r}}\right\} \tag{B.4}$$

B.1 VC-IE

The induced current density needed in (B.2) is related to the resulting internal electric field of the VC-IE (5.38), which can be symbolically written as $\mathbf{E} = E_\rho(\rho, z)\hat{\boldsymbol{\rho}} + E_z(\rho, z)\hat{\mathbf{z}}$, by the volume equivalence theorem (3.6). Using (B.2) with the far field Green's function (B.4) we derive the scattering field in spherical coordinates (r, ϕ, θ)

$$\mathbf{E}_s(r,\phi,\theta) \approx k^2 \Delta\epsilon_r \frac{e^{ikr}}{4\pi r} \left\{ \overleftrightarrow{\mathbf{I}} - \hat{\mathbf{r}} \otimes \hat{\mathbf{r}} \right\} \int_V d^3r' \, e^{-ik\hat{\mathbf{r}}\cdot\mathbf{r}'} \left(E_\rho(\rho', z')\hat{\boldsymbol{\rho}}\left(\phi'\right) + E_z(\rho', z')\hat{\mathbf{z}} \right). \tag{B.5}$$

There is neither a ϕ-dependence nor a ϕ-component in the induced current and thus there are none in the scattering field either. Thus we can calculate the scattering field without loss of generality just in the incident plane, i.e. $\phi = 0$ and $\hat{\mathbf{r}} = \sin\theta\hat{\mathbf{x}} + \cos\theta\hat{\mathbf{z}}$. The r-component $(\mathbf{E}_s \cdot \hat{\boldsymbol{r}})$ has to be zero in the far zone because the field is transverse. So the problem reduces to the calculation of the θ-component

$$\begin{aligned}
E_{s\theta}(r,\theta,\phi) =& k^2\Delta\epsilon_r \frac{e^{ikr}}{4\pi r} \Bigg(\int_V d^3r' \, e^{-ik\hat{\mathbf{r}}\cdot\mathbf{r}'} E_\rho(\rho', z') \left[\left\{ \overleftrightarrow{\mathbf{I}} - \hat{\mathbf{r}} \otimes \hat{\mathbf{r}} \right\} \hat{\boldsymbol{\rho}} \right] \\
&+ \left[\left\{ \overleftrightarrow{\mathbf{I}} - \hat{\mathbf{r}} \otimes \hat{\mathbf{r}} \right\} \hat{\mathbf{z}} \right] \int_V d^3r' \, e^{-ik\hat{\mathbf{r}}\cdot\mathbf{r}'} E_z(\rho', z') \Bigg) \cdot \hat{\boldsymbol{\theta}} \\
=& k^2\Delta\epsilon_r \frac{e^{ikr}}{4\pi r} \Bigg(\int_V d^3r' \, e^{-ik\hat{\mathbf{r}}\cdot\mathbf{r}'} E_\rho(\rho', z') \left(\hat{\boldsymbol{\rho}} \cdot \hat{\boldsymbol{\theta}} \right) \\
&- \left(\hat{\mathbf{r}} \cdot \hat{\boldsymbol{\theta}} \right) \int_V d^3r' \, e^{-ik\hat{\mathbf{r}}\cdot\mathbf{r}'} E_\rho(\rho', z') \left(\hat{\mathbf{r}} \cdot \hat{\boldsymbol{\rho}} \right) \\
&+ \left[\hat{\mathbf{z}} - \hat{\mathbf{r}} \left(\hat{\mathbf{r}} \cdot \hat{\mathbf{z}} \right) \right] \cdot \hat{\boldsymbol{\theta}} \int_V d^3r' \, e^{-ik\hat{\mathbf{r}}\cdot\mathbf{r}'} E_z(\rho', z') \Bigg)
\end{aligned} \tag{B.6}$$

Here we used the vector identity $(\mathbf{a} \otimes \mathbf{b})\,\mathbf{c} = \mathbf{a}\,(\mathbf{b} \cdot \mathbf{c})$. By calculating the scalar products of the coordinate unit vectors, i.e. $\hat{\mathbf{r}} \cdot \hat{\boldsymbol{\theta}} = 0$, $\hat{\mathbf{z}} \cdot \hat{\boldsymbol{\theta}} = -\sin\theta$ and $\hat{\boldsymbol{\rho}} \cdot \hat{\boldsymbol{\theta}} = \cos\theta\cos\phi'$, (B.6) reduces to

$$\begin{aligned}
E_{s\theta}(r,\theta,\phi) =& k^2\Delta\epsilon_r \frac{e^{ikr}}{4\pi r} \Bigg(\cos\theta \int_V d^3r' \, e^{-ik\hat{\mathbf{r}}\cdot\mathbf{r}'} E_\rho(\rho', z') \cos\phi' \\
&- \sin\theta \int_V d^3r' \, e^{-ik\hat{\mathbf{r}}\cdot\mathbf{r}'} E_z(\rho', z') \Bigg).
\end{aligned} \tag{B.7}$$

Substituting $E_\rho = -k_\rho^{-1} J_1(k_\rho \rho) f'(z)$ and $E_z = J_0(k_\rho \rho) f(z)$ according to Eq. (5.38) the first integral in (B.7) becomes

$$\begin{aligned}\int_V d^3r'\, e^{-ik\hat{\mathbf{r}}\cdot\mathbf{r}'} E_\rho(\rho', z') \cos\phi' =& -\frac{1}{k_\rho} \int_{-\frac{l}{2}}^{\frac{l}{2}} dz' f'(z') \exp\left[-ik\cos\theta z'\right] \int_0^a \rho' d\rho' J_1\left(k_\rho \rho'\right) \\ & \cdot \int_0^{2\pi} d\phi' \cos\phi' \exp\left[-ik\sin\theta\rho'\cos\phi'\right] \\ =& -i\frac{4\pi a}{k_\rho} \frac{k_\rho J_0(k_\rho a) J_1(ak\sin\theta) - k\sin\theta J_1(k_\rho a) J_0(ak\sin\theta)}{k^2\cos(2\theta) - k^2 + 2k_\rho^2} \\ & \cdot \int_{-\frac{l}{2}}^{\frac{l}{2}} dz' f'(z') \exp\left[-ik\cos\theta z'\right] \\ =& \pi a^3 \left[\frac{i}{8} ka\sin\theta + \mathcal{O}\left(a^3k^3\right)\right] \int_{-\frac{l}{2}}^{\frac{l}{2}} dz' f'(z') \exp\left[-ik\cos\theta z'\right]\end{aligned} \tag{B.8}$$

and the second one

$$\begin{aligned}\int_V d^3r'\, e^{-ik\hat{\mathbf{r}}\cdot\mathbf{r}'} E_z(\rho', z') =& \int_{-\frac{l}{2}}^{\frac{l}{2}} dz' f(z') \exp\left[-ik\cos\theta z'\right] \int_0^a \rho' d\rho' J_0\left(k_\rho \rho'\right) \\ & \cdot \int_0^{2\pi} d\phi' \exp\left[-ik\sin\theta\rho'\cos\phi'\right] \\ =& \pi a^2 \left[1 - \frac{k^2a^2}{16}\left(1 + 2\left(\epsilon_r - \cos^2\xi\right) - \cos[2\theta]\right) + \mathcal{O}\left(a^4k^4\right)\right] \\ & \cdot \int_{-\frac{l}{2}}^{\frac{l}{2}} dz' f(z') \exp\left[-ik\cos\theta z'\right].\end{aligned} \tag{B.9}$$

In each of the above calculations of the integrals, we performed a series expansion with respect to small ak in the last step. A further simplification can be archived in (B.8) by integrating the residual integral by parts yielding

$$\begin{aligned}\int_{-\frac{l}{2}}^{\frac{l}{2}} dz' f'(z') \exp\left[-ik\cos\theta z'\right] =& f(z) \exp[-ik\cos\theta z]\Big|_{-\frac{l}{2}}^{\frac{l}{2}} \\ & + ik\cos\theta \int_{-\frac{l}{2}}^{\frac{l}{2}} dz' f(z') \exp\left[-ik\cos\theta z'\right]\end{aligned} \tag{B.10}$$

Taking into account that the field amplitude at the ends of the wire $f(-l/2)$ and $f(l/2)$ are generally very small so we can conclude that the contribution from (B.8) is of the order $\mathcal{O}\left(a^2k^2\right)$ which we can neglect for thin wires. Likewise we can neglect the terms

of order $\mathcal{O}\left(a^2k^2\right)$ in (B.9) except the term which involves ϵ_r because $|\epsilon_r|$ could be large for metals. So, we obtain finally

$$E_{s\theta}(r,\theta,\phi) = -\frac{k^2a^2\Delta\epsilon_r \sin\theta}{4}\frac{e^{ikr}}{r}\left(1-\frac{k^2a^2}{8}\epsilon_r\right)\int_{-\frac{l}{2}}^{\frac{l}{2}} dz' f(z')\exp\left[-ik\cos\theta z'\right]. \tag{B.11}$$

Plugging (B.11) in (B.1) we finally obtain the total scattering cross section

$$\sigma_s = \frac{\pi k^4a^4}{8\left|\mathbf{E}_i\right|^2}\left|\Delta\epsilon_r\left(1-\frac{k^2a^2}{8}\epsilon_r\right)\right|^2\int_0^\pi d\theta\,\sin^3\theta\left|\int_{-\frac{l}{2}}^{\frac{l}{2}} dz' f(z')\exp\left[-ik\cos\theta z'\right]\right|^2. \tag{B.12}$$

B.2 SI-IE

The induced current density in the surface impedance integral equation is expressed in terms of the resulting current $I(z)$ by Eq. (5.4) which leads under analog considerations as explained above to the scattering field in the far zone

$$\mathbf{E}_s = E_{s\theta}\hat{\boldsymbol{\theta}} \tag{B.13}$$

with

$$\begin{aligned}
E_{s\theta} =& i\omega\mu_0\frac{e^{ikr}}{4\pi r}\left[\left\{\overleftrightarrow{\mathbf{I}}-\hat{\mathbf{r}}\otimes\hat{\mathbf{r}}\right\}\int_V d^3r'\,e^{-ik\hat{\mathbf{r}}\cdot\mathbf{r}'}\left(I(z')\frac{\delta(\rho'-a)}{2\pi\rho'}\hat{\mathbf{z}}\right)\right]\cdot\hat{\boldsymbol{\theta}}\\
=& i\omega\mu_0\frac{e^{ikr}}{8\pi^2 r}\left[\left(\hat{\mathbf{z}}\cdot\hat{\boldsymbol{\theta}}\right)-\left(\hat{\mathbf{r}}\cdot\hat{\boldsymbol{\theta}}\right)\left(\hat{\mathbf{r}}\cdot\hat{\mathbf{z}}\right)\right]\int_{-\frac{l}{2}}^{\frac{l}{2}} dz' I(z')\exp\left[-ik\cos\theta z'\right]\\
&\cdot\int_0^{2\pi} d\phi'\exp\left[-ika\sin\theta\cos\phi'\right]\\
=& -i\omega\mu_0\frac{e^{ikr}}{4\pi r}\sin\theta J_0\left(ka\sin\theta\right)\int_{-\frac{l}{2}}^{\frac{l}{2}} dz' I(z')\exp\left[-ik\cos\theta z'\right]\\
=& -i\frac{\omega\mu_0\sin\theta}{4\pi}\frac{e^{ikr}}{r}\left(1+\mathcal{O}\left[k^2a^2\right]\right)\int_{-\frac{l}{2}}^{\frac{l}{2}} dz' I(z')\exp\left[-ik\cos\theta z'\right].
\end{aligned} \tag{B.14}$$

In the last step a series expansion of J_0 was performed neglecting terms of order $\mathcal{O}\left[k^2a^2\right]$. Plugging (B.14) into (B.1) we obtain the following expression for the scattering cross

section in terms of $I(z)$

$$\sigma_s = \frac{\omega^2 \mu_0^2}{8\pi} \int_0^{\pi} d\theta \, \sin^3\theta \left| \int_{-\frac{l}{2}}^{\frac{l}{2}} dz' I(z') \exp\left[-ik\cos\theta z'\right] \right|^2 . \tag{B.15}$$

C Derivation of Equation (7.6)

Using the Fourier representation (1.15) of a time dependent real function $\mathbf{F}(\mathbf{r},t)$,

$$\begin{aligned}\mathbf{F}(\mathbf{r},t) &= \Re\left\{\frac{1}{2\pi}\int_{-\infty}^{\infty} d\omega\, \mathbf{F}(\mathbf{r},\omega)\, \mathrm{e}^{-\mathrm{i}\omega t}\right\} \\ &= \frac{1}{4\pi}\int_{-\infty}^{\infty} d\omega\, \left(\mathbf{F}(\mathbf{r},\omega)\, \mathrm{e}^{-\mathrm{i}\omega t} + \mathbf{F}^{\star}(\mathbf{r},\omega)\, \mathrm{e}^{\mathrm{i}\omega t}\right),\end{aligned} \tag{C.1}$$

for the electric field $\mathbf{E}(\mathbf{r},t)$ and the current density $\mathbf{J}(\mathbf{r},t)$ in Eq. (7.4), the total radiated energy (7.5) can be written in the form

$$\begin{aligned}U = -\frac{2}{(4\pi)^2}\Re\Bigg\{\int_{V_0} d^d r \int_{-\infty}^{\infty} dt \int_{-\infty}^{\infty} d\omega \int_{-\infty}^{\infty} d\Omega \\ \left[\mathbf{J}(\mathbf{r},\omega)\cdot\mathbf{E}(\mathbf{r},\Omega)\, \mathrm{e}^{-\mathrm{i}(\omega+\Omega)t} + \mathbf{J}(\mathbf{r},\omega)\cdot\mathbf{E}^{\star}(\mathbf{r},\Omega)\, \mathrm{e}^{-\mathrm{i}(\omega-\Omega)t}\right]\Bigg\}.\end{aligned} \tag{C.2}$$

Changing the integration order and using the integral relation for the Dirac delta function

$$\delta(x) = \frac{1}{2\pi}\int_{-\infty}^{\infty} dy\, \mathrm{e}^{-\mathrm{i}xy} \tag{C.3}$$

we obtain for the total radiated energy

$$\begin{aligned}U &= -\frac{1}{4\pi}\Re\Bigg\{\int_{V_0} d^d r \int_{-\infty}^{\infty} d\omega \int_{-\infty}^{\infty} d\Omega \\ &\qquad \left[\mathbf{J}(\mathbf{r},\omega)\cdot\mathbf{E}(\mathbf{r},\Omega)\,\delta(\omega+\Omega) + \mathbf{J}(\mathbf{r},\omega)\cdot\mathbf{E}^{\star}(\mathbf{r},\Omega)\,\delta(\omega-\Omega)\right]\Bigg\}.\end{aligned} \tag{C.4}$$

Further, integrating over Ω and using the symmetry of the Fourier transform of the electric field, $\mathbf{E}(\mathbf{r},-\omega) = \mathbf{E}^{\star}(\mathbf{r},\omega)$, the total radiated energy can be written as an integral

over frequency (7.6)

$$U = -\frac{2}{\pi}\int_0^\infty d\omega\,\frac{1}{2}\Re\left\{\int_{V_0} d^d r\,\mathbf{J}\left(\mathbf{r},\omega\right)\cdot\mathbf{E}^\star\left(\mathbf{r},\omega\right)\right\}. \tag{C.5}$$

The integrand in Eq. (C.5) coincides with the time-averaged radiated power of the monochromatic source $\mathbf{J}\left(\mathbf{r},\omega\right)$ (1.38).

D Derivation of Equation (7.10)

Expanding a periodic function $\left(\mathbf{e}_{\mathbf{k}n}^{(\alpha)}\left(r_{\parallel}\right)\cdot\hat{\mathbf{r}}_{\parallel}\right)$ in the Fourier series

$$\left(\mathbf{e}_{\mathbf{k}n}^{(\alpha)}\left(r_{\parallel}\right)\cdot\hat{\mathbf{r}}_{\parallel}\right)=\sum_{m=-\infty}^{\infty}c_{m}^{(\alpha)}\left(\mathbf{k};n\right)\mathrm{e}^{\mathrm{i}\frac{2\pi}{a}mr_{\parallel}} \tag{D.1}$$

with coefficients $c_{m}^{(\alpha)}\left(\mathbf{k};n\right)$ defined in Eq. (7.11), integrals $I_{1}^{(\alpha)}$ and $I_{2}^{(\alpha)}$ in (7.9) can be transformed to

$$I_{1}^{(\alpha)}=\sum_{m=-\infty}^{\infty}c_{m}^{(\alpha)\star}\left(\mathbf{k};n\right)\int_{-\infty}^{\infty}dr_{\parallel}\,\mathrm{e}^{-\mathrm{i}\left(k_{\parallel}-\frac{\omega}{|\mathbf{v}|}-\frac{2\pi}{a}m\right)r_{\parallel}} \tag{D.2}$$

and

$$I_{2}^{(\alpha)}=\sum_{p=-\infty}^{\infty}c_{p}^{(\alpha)}\left(\mathbf{k};n\right)\frac{1}{l}\int_{-l/2}^{l/2}dr_{\parallel}\,\mathrm{e}^{\mathrm{i}\left(k_{\parallel}-\frac{\omega}{|\mathbf{v}|}-\frac{2\pi}{a}p\right)r_{\parallel}}, \tag{D.3}$$

respectively. In Eq. (D.2), integration over $r_{\parallel}$ immediately yields

$$I_{1}^{(\alpha)}=2\pi\sum_{m=-\infty}^{\infty}c_{m}^{(\alpha)\star}\left(\mathbf{k};n\right)\delta\left(k_{\parallel}-\frac{\omega}{|\mathbf{v}|}-\frac{2\pi}{a}m\right). \tag{D.4}$$

Integral in (D.3) is equal to l, if $k_{\parallel}-\frac{\omega}{|\mathbf{v}|}-\frac{2\pi}{a}p=0$. Otherwise it results in

$$\frac{\sin\left[\frac{l}{2}\left(k_{\parallel}-\frac{\omega}{|\mathbf{v}|}-\frac{2\pi}{a}p\right)\right]}{k_{\parallel}-\frac{\omega}{|\mathbf{v}|}-\frac{2\pi}{a}p}. \tag{D.5}$$

Then, in the limit $l\rightarrow\infty$, $I_{2}^{(\alpha)}$ vanishes for $k_{\parallel}-\frac{\omega}{|\mathbf{v}|}-\frac{2\pi}{a}p\neq0$, while is equal to $2\pi\sum_{p=-\infty}^{\infty}c_{p}^{(\alpha)}\left(\mathbf{k};n\right)$ for $k_{\parallel}-\frac{\omega}{|\mathbf{v}|}-\frac{2\pi}{a}p=0$. Finally, using the function

$$\widetilde{\delta}\left(x\right)=\begin{cases}1, & x=0\\ 0, & x\neq0\end{cases}, \tag{D.6}$$

relation (7.9) can be written in the form

$$I^{(\alpha)} = 2\pi \quad q^2 \sum_{m=-\infty}^{\infty} \sum_{p=-\infty}^{\infty} c_m^{(\alpha)\star}(\mathbf{k};n)\, c_p^{(\alpha)}(\mathbf{k};n) \times \tag{D.7}$$
$$\delta\left(k_\parallel - \frac{\omega}{|\mathbf{v}|} - \frac{2\pi}{a}m\right) \widetilde{\delta}\left(k_\parallel - \frac{\omega}{|\mathbf{v}|} - \frac{2\pi}{a}p\right),$$

which is non-zero only for $m = p$ yielding relation (7.10).

E The Curvature of the Cherenkov Contour

To calculate the curvature using its definition

$$\mathcal{K}(s) = \left| \frac{\partial^2 \mathbf{k}(s)}{\partial s^2} \right| \tag{E.1}$$

one should numerically evaluate the second derivative of the wave vector $\mathbf{k}(s)$ on the Cherenkov contour. This is typically associated with a large numerical error. In what follows we propose to use an alternative method to calculate the curvature which usually results in smaller numerical error and involves calculations of the first derivative of the wave vector on the contour and the second derivatives of the dispersion relation $\omega_n(\mathbf{k})$.

Taking the derivative of (8.21) with respect to s we obtain

$$\frac{\partial^2 \mathbf{k}}{\partial s^2} \cdot \left(\mathbf{v}_g \left(\mathbf{k}(s) \right) - \mathbf{v} \right) + \frac{\partial \mathbf{k}}{\partial s} \cdot \frac{\partial}{\partial s} \mathbf{v}_g \left(\mathbf{k}(s) \right) = 0 \tag{E.2}$$

The second term in (E.2) can be rewritten as

$$\begin{aligned} \frac{\partial \mathbf{k}}{\partial s} \cdot \frac{\partial}{\partial s} \mathbf{v}_g \left(\mathbf{k}(s) \right) &= \sum_i \frac{\partial k_i}{\partial s} \left[\frac{\partial}{\partial s} \frac{\partial}{\partial k_i} \omega_n(\mathbf{k}) \right] \\ &= \sum_{i,j} \frac{\partial k_i}{\partial s} \frac{\partial^2}{\partial k_j \partial k_i} \omega_n(\mathbf{k}) \frac{\partial k_j}{\partial s} \\ &= \left(\frac{\partial \mathbf{k}}{\partial s} \right)^T \mathcal{H}_{\omega_n}(\mathbf{k}) \frac{\partial \mathbf{k}}{\partial s} \qquad \text{(E.3)} \\ &\equiv \mathcal{M}, \qquad \text{(E.4)} \end{aligned}$$

where $\mathcal{H}_{\omega_n}(\mathbf{k})$ is the Hessian matrix of the dispersion relation $\omega_n(\mathbf{k})$. We can now rewrite (E.2) in the form

$$\frac{\partial^2 \mathbf{k}}{\partial s^2} \cdot \left(\mathbf{v}_g \left(\mathbf{k}(s) \right) - \mathbf{v} \right) = \mathcal{M} \tag{E.5}$$

or

$$\mathcal{K}\left|\mathbf{v}_g\left(\mathbf{k}(s)\right)-\mathbf{v}\right|\operatorname{sign}\left[\vec{\mathcal{K}}\cdot\left(\mathbf{v}_g\left(\mathbf{k}(s)\right)-\mathbf{v}\right)\right]=\mathcal{M} \tag{E.6}$$

with $\vec{\mathcal{K}}=\frac{\partial^2\mathbf{k}}{\partial s^2}$. Finally the following expression for the curvature is obtained

$$\mathcal{K}=\frac{|\mathcal{M}|}{\left|\mathbf{v}_g\left(\mathbf{k}(s)\right)-\mathbf{v}\right|}. \tag{E.7}$$

List of Publications

[1] *C. Kremers*, D. N. Chigrin and J. Kroha, *Theory of Cherenkov radiation in periodic dielectric media: Emission spectrum*, Phys. Rev. A, **79**(1):013829, 2009

[2] *C. Kremers*, D. N. Chigrin, *Spatial distribution of Cherenkov radiation in periodic dielectric media*, J. Opt. A, **11**(11):114008, 2009

[3] *C. Kremers*, D. N. Chigrin, *Light Scattering on Nanowire Antennas: A Semi-Analytical Approach*, to appear in Photonics Nanostruct. Fundam. and Appl., March 2011

[4] S. V. Zhukovsky, *C. Kremers* and D. N. Chigrin, *Plasmonic rod dimers as elementary planar chiral meta-atoms*, submitted to Opt. Lett., April 2011

[5] *C. Kremers*, D. N. Chigrin, *Light Scattering on Nanowire Antennas: A Semi-Analytical Approach*, AIP Conf. Proc., vol. 1291 (2010) pp. 64-66

[6] D. N. Chigrin, *C. Kremers*, S. V. Zhukovsky, *Metallic nanorods dimer: from optical nano-antennas to planar chiral metamaterials*, in the Proceedings of the international Workshop on Metamaterials, "Days on Diffraction" Conference, St. Petersburg, Russia, 2010, p. 100 (invited paper)

[7] *C. Kremers*, S. V. Zhukovsky, D. N. Chigrin, *Numerical time-domain simulation of planar chiral metamaterials*, AIP Conf. Proc., vol. 1176, (2009) pp. 118-120